Institut für Physik **Universität Potsdam**

Phase synchronization of chaotic systems: From theory to experimental applications

Habilitationsschrift

der Mathematisch-Naturwissenschaftlichen Fakultät
der Universität Potsdam

vorgelegt von

Michael Rosenblum

Potsdam, August 2002

Foreword

Synchronization is a fundamental nonlinear phenomenon, discovered at the beginning of the modern age of science by Christiaan Huygens [36]. In the classical sense, synchronization means adjustment of frequencies of periodic oscillators due to a weak interaction. This effect, observed in various physical and biological systems, is well studied and finds a lot of practical applications in electrical and mechanical engineering.

The first aim of this thesis is to extend the classical theory to cover the case of weakly coupled chaotic oscillators. This is achieved by introducing the notion of phase and mean frequency for autonomous time-continuous chaotic systems. It is demonstrated that for this class of objects one can observe such synchronization phenomena as entrainment by an external force, mutual synchronization of two systems, synchronization in spatially ordered and globally coupled oscillators. It is shown that synchronization of periodic, noisy and chaotic self-sustained oscillators can be considered within a unified framework, i.e., in terms of phase and frequency locking.

The second aim of the thesis is the development of data analysis tools, based on the ideas from the synchronization theory. In particular, two problems are considered: detection of weak interaction and determination of the direction of coupling from data. The techniques are exploited in analysis of experiments on cardiorespiratory interaction and pathological brain activity.

The first Chapter presents brief introduction to the classical synchronization theory; next, the notion of phase and phase dynamics of chaotic oscillators are discussed there; the Chapter is concluded by the description of synchronization of a chaotic oscillator by a periodic force. The second Chapter presents the effects of mutual synchronization of two systems, self-synchronization in ensembles of globally coupled oscillators and synchronization in lattices, as well as the discussion of synchronization transitions. Chapter 3 treats the case of oscillators which do not admit unambiguous definition of the phase (systems with ill-defined case). Chapter 4 is devoted to data analysis. It contains formulation of the synchronization approach to data analysis, discussion of the data analysis tools and experimental examples.

Presentation of results is mainly based on the papers [85, 86, 76, 88], the book chapter [91], and the book [70].

Acknowledgments

Results presented in this thesis were obtained during my work in the Max-Planck Arbeitsgruppe “Nichtlineare Dynamik” and in the Chair of Nonlinear Dynamics

at the University of Potsdam. I am much obliged to Jürgen Kurths who created friendly atmosphere in the group, enabling efficient research. I am grateful to my colleagues from the department for useful and friendly discussions. Especially, I highly appreciate intensive cooperation with Jürgen Kurths, Arkady Pikovsky, and Michael Zaks. My research was partly supported by Alexander von Humboldt Foundation and Max Planck Society.

Contents

Chapter 1

Phase synchronization of a periodically forced chaotic oscillator

1.1 Introduction

Synchronization, a basic nonlinear phenomenon, discovered at the beginning of the modern age of science by Huygens [36], is widely encountered in various fields of science, often observed in living nature [29, 28] and finds a lot of engineering applications [8, 9]. In the classical sense, synchronization means adjustment of frequencies of self-sustained oscillators due to a weak interaction. The phase of an oscillator may be locked by periodic external force; another situation is the locking of the phases of two interacting oscillators. Synchronization of periodic systems is pretty well understood [8, 2, 35, 45, 32], as well as the effects of noise on phase and frequency locking [106].

In the context of interacting *chaotic* oscillators, several effects are usually referred to as "synchronization". Due to a strong interaction of two (or a large number) of identical chaotic systems, their states can coincide, while the dynamics in time remains chaotic [25, 73]. This effect is called "complete synchronization" of chaotic oscillators. It can be generalized to the case of non-identical systems ("generalized synchronization") [93, 41, 63] or interacting subsystems ("master-slave synchronization") [64, 41, 63]. Another effect is the "chaos–destroying" synchronization, when a periodic external force acting on a chaotic system destroys chaos and a periodic regime appears [46], or, in the case of an irregular forcing, the driven system follows the behavior of the force [42]. This effect occurs for a relatively strong forcing as well. A characteristic feature of these phenomena is the existence of a threshold coupling value depending on the Lyapunov exponents of individual systems [25, 73, 7, 18].

The goal of the present work is to describe **weak** interaction of chaotic systems. In other words, we try to extend the classical synchronization theory to cover the case of chaotic systems. We denote the corresponding effects as "phase synchronization", to distinguish them from other forms of synchronization in chaotic systems. The phenomenon has been theoretically studied in [85, 74,

105, 69, 56, 71, 72, 87, 68, 86, 83, Appendices 1 and 2]. It has been observed in laboratory experiments with electronic generators, gas discharge, lasers, and electrodissolution of metals [62, 109, 113, 1, 38].

We mention also another direction in development of the classical synchronization theory, namely its extension to stochastic systems, see [54, 99, 3] and references therein.

We start with brief review of classical results on synchronization of periodic self-sustained oscillators in Section 1.1.1 and effects of noise in Section 1.1.2. The notion of phase and amplitude of chaotic systems is introduced and discussed in Section 1.2; We illustrate it taking as examples the famous Rössler and Lorenz models. We show that the dynamics of the phase in chaotic systems are similar to those in noisy periodic ones. Section 1.3 is devoted to effects of phase synchronization by periodic external force.

1.1.1 Periodic oscillations: locking of phases and frequencies

We remind basic facts on the synchronization of periodic oscillations (see, e.g., [58]). Stable periodic self-sustained oscillations are represented by a stable limit cycle in the phase space, and the dynamics of a phase point on this cycle can be described as

$$\frac{d\phi}{dt} = \omega_0 \ , \tag{1.1}$$

where $\omega_0 = 2\pi/T_0$, and T_0 is the period of the oscillation. It is important that starting from any monotonically growing variable θ on the limit cycle, one can introduce the phase satisfying Eq. (1.1). Indeed, an arbitrary θ obeys $\dot{\theta} = \nu(\theta)$ with a periodic $\nu(\theta + 2\pi) = \nu(\theta)$. A change of variables

$$\phi = \omega_0 \int_0^\theta [\nu(\theta)]^{-1} d\theta$$

gives the correct phase, where the frequency ω_0 is defined from the condition $2\pi = \omega_0 \int_0^{2\pi} [\nu(\theta)]^{-1} d\theta$. A similar approach leads to correct angle-action variables in Hamiltonian mechanics. From (1.1) it is evident that the phase corresponds to the zero Lyapunov exponent, while negative exponents correspond to the amplitude variables (not written in (1.1)).

If two oscillators are weakly coupled, then in the first approximation one can neglect variations of the amplitudes to obtain equations describing the phase dynamics. In general, these equations have the form

$$\frac{d\phi_1}{dt} = \omega_1 + \varepsilon g_1(\phi_1, \phi_2) \ , \qquad \frac{d\phi_2}{dt} = \omega_2 + \varepsilon g_2(\phi_2, \phi_1) \ , \tag{1.2}$$

where the coupling terms $g_{1,2}$ are 2π-periodic in both arguments, and ε is the coupling coefficient.

The phase space of Eqs. (1.2) is a 2-torus, and with the usual construction of the Poincaré map this system can be made equivalent to a circle map, with a well-known structure of phase-locking intervals (Arnold's tongues) [58]; each of the intervals corresponds to a $n : m$ synchronization region. This picture is universal and its qualitative features do not depend on the characteristics of

the oscillations and of the external force (e.g. nearly sinusoidal or relaxational), and on the relation between amplitudes.

Analytically, one can proceed as follows. The interaction between the oscillators essentially effects the evolution of their phases if the frequencies $\omega_{1,2}$ are in resonance, i.e., if for some integers n, m we have

$$n\omega_1 \approx m\omega_2 \ .$$

Then, in the first approximation, the Fourier expansion of the functions $g_{1,2}$ contains slowly varying terms $\sim n\phi_1 - m\phi_2$. This suggests to introduce the *generalized phase difference*,

$$\varphi_{n,m}(t) = n\phi_1(t) - m\phi_2(t) \ . \tag{1.3}$$

Subtracting the equations (1.2) and keeping only the resonance terms, we get

$$\frac{d\varphi_{n,m}}{dt} = n\omega_1 - m\omega_2 + \varepsilon G(\varphi_{n,m}) \ , \tag{1.4}$$

where $G(\cdot)$ is 2π-periodic. This is a one-dimensional ODE that admits solutions of two kinds: fixed points or periodic rotations of $\varphi_{n,m}$. The stable fixed point corresponds to perfect phase locking $\varphi_{n,m} = const$; periodic rotations describe quasiperiodic motion with two incommensurate frequencies in the system (1.2).

In the analytical treatment of the Eqs. (1.2) we have neglected nonresonant terms, what is justified for small coupling. With nonresonant terms, the condition of synchronization for periodic oscillators should be generally written as a phase locking condition

$$|n\phi_1(t) - m\phi_2(t) - \delta| < \text{const} \ , \tag{1.5}$$

where δ is some (average) phase shift, or as a frequency entrainment condition

$$n\Omega_1 = m\Omega_2 \ , \tag{1.6}$$

where $\Omega_{1,2} = \langle\dot{\phi}_{1,2}\rangle$ are observed frequencies. We emphasize, that in the synchronized state the phase difference is generally not constant but oscillates around δ. These oscillations vanish in the limit of very small coupling (correspondingly, the frequency mismatch $n\omega_1 - m\omega_2$ must be also small), or if the coupling depends only on the relative phase: $g_{1,2} = g_{1,2}(n\phi_1 - m\phi_2)$.

1.1.2 Synchronization in the presence of noise

In general, both properties of phase and frequency locking (Eqs. (1.5,1.6)) are destroyed in the presence of noise $\xi(t)$ when instead of (1.4) one has

$$\frac{d\varphi_{n,m}}{dt} = n\omega_1 - m\omega_2 + \varepsilon G(\varphi_{n,m}) + \xi(t) \ . \tag{1.7}$$

For small noise the stable phase dynamics is only slightly perturbed. Thus the relative phase $\varphi_{n,m}$ mainly fluctuates around some constant level (former fixed point). These nearly stationary fluctuations may be interrupted by phase slips, where the relative phase changes relatively rapidly by $\pm 2\pi$. Thus, strictly

speaking, the phase difference is unbounded and condition (1.5) is not valid anymore. Nevertheless, the distribution of the *cyclic relative phase*

$$\Psi_{n,m} = \varphi_{n,m} \bmod 2\pi \tag{1.8}$$

has a dominating peak around the value corresponding to the stable fixed point [106]. Presence of this peak can be understood as the phase locking in a statistical sense.

If the noise is weak and *bounded*, then there exists a range of frequency mismatch $n\omega_1 - m\omega_2$, where the phase slips are impossible and the averaged condition of frequency locking (1.6) is fulfilled. Near the boundaries of the Arnold tongue the noise causes phase slips and the transition out of the synchronous regime is now smeared. If the noise is unbounded, e.g., Gaussian, the probability of a slip to occur is nonzero even for $n\omega_1 - m\omega_2 = 0$, so that strictly speaking the region of frequency locking shrinks to a point. As this probability is (exponentially) small for weak noise, practically the synchronization region appears as an interval of $n\omega_1 - m\omega_2$, where $n\Omega_1 \approx m\Omega_2$. Within this region, the distribution of the cyclic relative phase is not uniform, so that one can speak of phase locking.

In the case of strong noise, the phase slips in both directions occur very frequently, so that the segments of nearly constant relative phase are very short and time course of $\varphi_{n,m}(t)$ looks like a random walk, that is unbiased in the very center of the synchronization region and biased otherwise. The synchronization transition is now completely smeared and, hence, synchronization appears only as a weakly seen tendency.

1.2 Phase of a chaotic oscillator

1.2.1 Definition and estimation of the phase

The first problem in extending the basic notions from periodic to chaotic oscillations is to introduce the notion of phase. There seems to be no unambiguous and general definition of phase applicable to an arbitrary chaotic process. Roughly speaking, we want to define phase as a variable which is related to the zero Lyapunov exponent of a continuous-time dynamical system with chaotic behavior. Moreover, we want this phase to correspond to the phase of periodic oscillations satisfying (1.1).

Suppose we can define a Poincaré map for our autonomous continuous-time system. Then, for each piece of a trajectory between two cross-sections with the Poincaré surface we define the phase just proportional to time, so that the phase increment is 2π at each rotation:

$$\phi(t) = 2\pi \frac{t - t_n}{t_{n+1} - t_n} + 2\pi n, \qquad t_n \le t < t_{n+1}. \tag{1.9}$$

Here t_n is the time of the n-th crossing of the secant surface. Note that for periodic oscillations corresponding to a fixed point of the Poincaré map, this definition gives the correct phase satisfying Eq. (1.1). For periodic orbits having many rotations (i.e., corresponding to periodic points of the map) we get a piecewise-linear function of time, moreover, the phase grows by a multiple of 2π during the period. The second property is in fact useful, as it represents

the organization of periodic orbits inside the chaos in a proper way. The first property demonstrates that the phase of a chaotic system cannot be defined as unambiguously as for periodic oscillations. In particular, the phase crucially depends on the choice of the Poincaré surface.

Nevertheless, defined in this way, the phase has a physically important property: its perturbations neither grow nor decay in time, so it does correspond to the direction with the zero Lyapunov exponent in the phase space. We note also, that this definition of the phase directly corresponds to the special flow construction which is used in the ergodic theory to describe autonomous continuous-time systems [15].

To be not too abstract, we illustrate a general approach on the well-known Rössler system [92]

$$\begin{aligned} \dot{x} &= -y - z \ , \\ \dot{y} &= x + 0.15y \ , \\ \dot{z} &= 0.4 + z(x - 8.5) \ . \end{aligned} \tag{1.10}$$

This attractor has a sharp peak in the power spectrum and a rather simple form (Fig. 1.1). Here the Poincaré map can be easily constructed, a proper choice of the Poincaré surface may be the half-plane $y = 0,\ x < 0$. The phase computed according to Eq. 1.9 is also shown in Fig. 1.1. The phase grows nearly uniformly: the phase diffusion constant is extremely small ($D_p < 10^{-4}$), what corresponds to an extremely sharp peak in the power spectrum; due to the this reason the attractor is called phase-coherent.

For the Rössler attractor, as well as for many other systems a specially chosen projection of the phase portrait (x–y for this case) looks like rotations around a point that can be taken as the origin. Hence, we can also introduce a phase variable as the angle between the projection of the phase point on the plane and a given direction on the plane (see also [69, 30, Appendix 2]):

$$\phi_P = \arctan(y/x) \ . \tag{1.11}$$

We can consider the variable ϕ_P as an easily computable estimate of the phase ϕ (for simplicity we often call ϕ_P simply phase). Note that although the two phases ϕ and ϕ_P do not coincide microscopically, i.e., on a time scale less than the average period of oscillation, they have equal average growth rates. In other words, the mean frequency defined as the average of $\dot{\phi}_P$ over large period of time coincides with a straightforward definition of the mean frequency via the average number of crossings of the Poincaré surface per unit time.

Finally, we mention one more approach to phase estimation, that is particularly useful in experimental applications. It exploits a well-known tool in signal processing, the analytic signal concept [60]. This general approach, based on the Hilbert transform and originally introduced by Gabor [27], unambiguously gives the instantaneous phase and amplitude for an arbitrary scalar signal $s(t)$. The analytic signal $\zeta(t)$ is a complex function of time defined as

$$\zeta(t) = s(t) + i\tilde{s}(t) = A(t)e^{i\phi_H(t)} \ , \tag{1.12}$$

where the function $\tilde{s}(t)$ is the Hilbert transform of $s(t)$

$$\tilde{s}(t) = \pi^{-1}\mathrm{P.V.}\int_{-\infty}^{\infty} \frac{s(\tau)}{t-\tau} d\tau \tag{1.13}$$

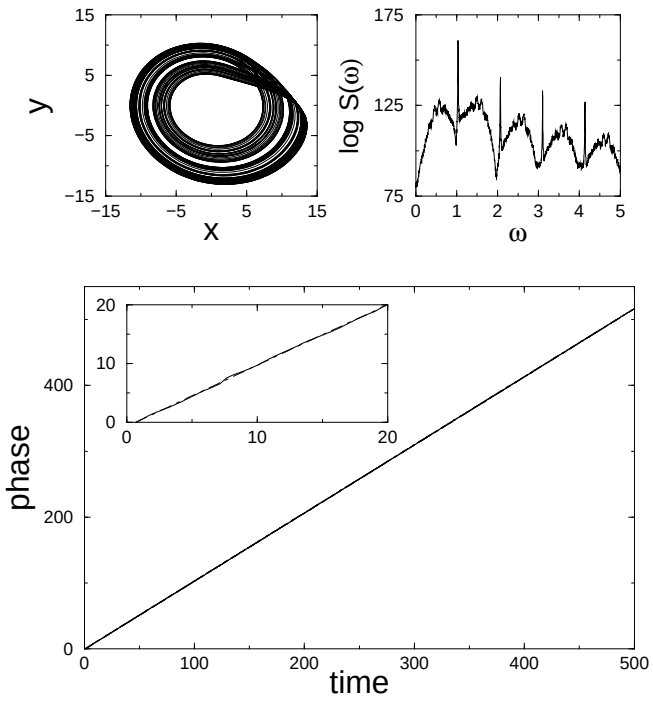

Figure 1.1: The phase portrait in the coordinates (x, y), the power spectrum of $x(t)$, and the time evolution of the phases for the phase-coherent Rössler oscillator. Dot-dashed line: the phase ϕ (see Eq. 1.9); solid line: the phase variable ϕ_P (Eq. 1.11); dashed line: the Hilbert-transform phase ϕ_H (Eq. 1.12). Three phase estimates practically coincide.

(where P.V. means that the integral is taken in the sense of the Cauchy principal value). The instantaneous amplitude $A(t)$ and the instantaneous phase $\phi_H(t)$ of the signal $s(t)$ are thus uniquely defined from (1.12).

For the example considered all three phase estimates give similar results (Fig. 1.1). In fact, we have found that the difference between ϕ, ϕ_P and ϕ_H is negligible.

1.2.2 A nontrivial example: the Lorenz system

Strange attractor of the Lorenz system

$$\begin{aligned} \dot{x} &= 10(y - x) \ , \\ \dot{y} &= 28x - y - xz \ , \\ \dot{z} &= -8/3 \cdot z + xy \ , \end{aligned} \tag{1.14}$$

is topologically different from the Rössler one. The variable $z(t)$ demonstrates characteristic chaotically modulated oscillations, but the processes $x(t), y(t)$ show additionally switchings due to evident symmetry $(x, y) \to (-x, -y)$ of

the Lorenz equations. While the oscillations of z are rather regular, the switchings are not. To overcome the complications due to this mixture of oscillations and switchings, we introduce a symmetrized observable $u(t) = \sqrt{x^2 + y^2}$ and project the phase portrait on the plane (u, z), see Fig. 1.2. In this projection the phase portrait resembles that of the Rössler attractor, and the phase can be introduced in a similar way. A possible Poincaré section is, e.g., $z = 27,\ u > 12$. Alternatively, one can define an angle variable $\phi_P(t)$ choosing the point $u_0 = 12,\ z_0 = 27$ as the origin and calculating

$$\phi_P = \arctan((z - z_0)/(u - u_0)) \ . \tag{1.15}$$

Again, this angle variable gives the same mean frequency as the phase based on the Poincaré map.

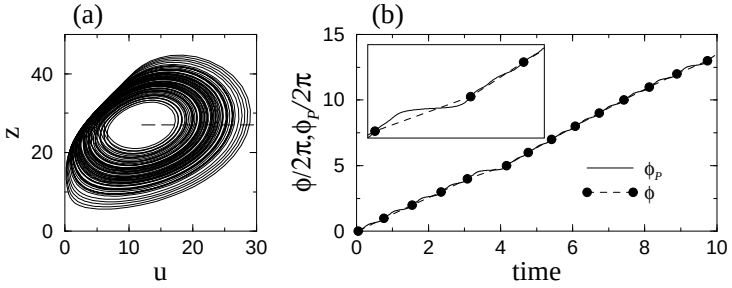

Figure 1.2: (a) The dynamics of the Lorenz system in the variables u, z looks like a smeared limit cycle with rotations around the unstable fixed point of the system. The dashed line shows the surface of section $z = 27, u > 12$. (b) The evolution of the phase ϕ based on the Poincaré map (Eq. 1.9), dashed line) and the angle variable ϕ_P (Eq. (1.15), solid line). They coincide at the points (filled circles) where the Poincaré surface is crossed, and differ slightly on the time scale smaller than a characteristic return time (see inlet in (b)).

1.2.3 Phase dynamics of a chaotic oscillator

In contrast to the dynamics of the phase of periodic oscillations, the growth of the phase in the chaotic case cannot generally be expected to be uniform. Instead, the instantaneous frequency depends in general on the amplitude. Let us hold to the phase definition based on the Poincaré map, so that one can represent the dynamics as (cf. [74])

$$A_{n+1} = M(A_n) \ , \tag{1.16}$$

$$\frac{d\phi}{dt} = \omega(A_n) \equiv \omega_0 + F(A_n) \ . \tag{1.17}$$

As the amplitude A we take the set of coordinates for the point on the secant surface; it does not change during the growth of the phase from 0 to 2π and can be considered as a discrete variable; the transformation M defines the Poincaré map. The phase evolves according to (1.17), where the "instantaneous" frequency $\omega = 2\pi/(t_{n+1} - t_n)$ depends in general on the amplitude. Assuming the

chaotic behavior of the amplitudes, we can consider the term $\omega(A_n)$ as a sum of the averaged frequency ω_0 and of some effective noise $F(A)$; in exceptional cases $F(A)$ may vanish. For the Rössler attractor the "period" of the rotations (i.e., the function $2\pi/\omega(A_n)$) is shown in Fig. 1.3a. This period is not constant, so that the function $F(A)$ does not vanish, but the variations of the period are relatively small.

Equation (1.17) is similar to the equation describing the evolution of phase of periodic oscillator in the presence of external noise. Thus, the dynamics of the phase is generally diffusive: for large t one expects

$$< (\phi(t) - \phi(0) - \omega_0 t)^2 > \propto D_p t \ ,$$

where the diffusion constant D_p determines the phase coherence of the chaotic oscillations. Roughly speaking, the diffusion constant is proportional to the width of the spectral peak calculated for the chaotic observable [22].

Generalizing Eq. (1.17) in the spirit of the theory of periodic oscillations to the case of periodic external force, we can write for the phase

$$\frac{d\phi}{dt} = \omega_0 + \varepsilon G(\phi, \psi) + F(A_n) \ , \qquad \frac{d\psi}{dt} = \nu \ , \tag{1.18}$$

where ψ, ν are the phase and frequency of the forcing. Here we assume that the force is small (of order of ε) so that it affects only the phase, and the amplitude obeys therefore the unperturbed mapping M. This equation is similar to Eq. (1.7), with the amplitude-depending part of the instantaneous frequency playing the role of noise. Thus, we expect that in general the synchronization phenomena for periodically forced chaotic system are similar to those in noisy driven periodic oscillations. One should be aware, however, that the "noisy" term $F(A)$ can be hardly explicitly calculated, and for sure cannot be considered as a Gaussian δ-correlated noise as is commonly assumed in the statistical approaches [106, 82].

We illustrate the coherence properties of the Rössler and Lorenz attractors in Fig. 1.3, where we show the return times T_n, or the "periods" of rotation. For the Rössler oscillator, the variation of T_n is comparatively small, while for the Lorenz oscillator the return time T_n can be arbitrary large (this corresponds to the slow motion in the vicinity of the saddle at $x = y = z = 0$). As we show below, this feature determines essentially different synchronization properties of these two systems.

In conclusion, we expect that the synchronization phenomena for chaotic systems are similar to those in noisy periodic oscillations. We support this conclusion by simulation results presented in the next Section.

1.3 Phase synchronization by external force

In this Section we consider periodically forced chaotic oscillators with well-defined phase. It means that here we restrict ourselves to the cases when the attractors have "good" topological structure, like attractors of the Lorenz and the Rössler systems. The case of ill-defined phase will be treated separately.

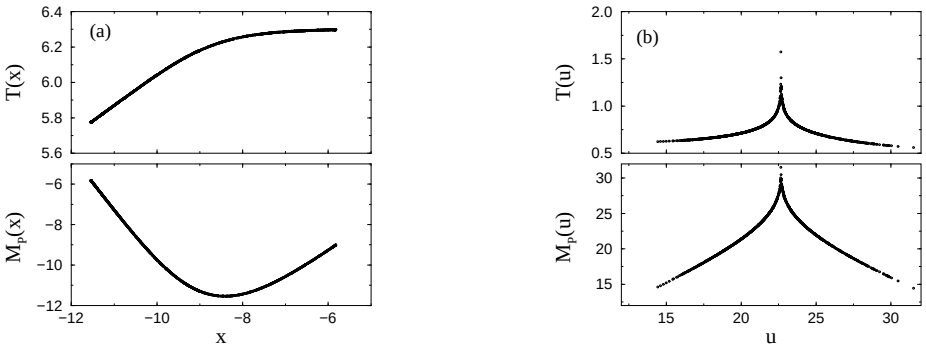

Figure 1.3: The return times and the Poincaré maps for the attractors of the Rössler (a) and the Lorenz (b) systems. The return time of the Lorenz system has a logarithmic singularity at $u \approx 23$.

1.3.1 Synchronization region

We add periodic forcing to two prototypic models of nonlinear dynamics: the Lorenz

$$\begin{aligned} \dot{x} &= 10(y-x), \\ \dot{y} &= 28x - y - xz, \\ \dot{z} &= -8/3 \cdot z + xy + E\cos\nu t. \end{aligned} \tag{1.19}$$

and the Rössler

$$\begin{aligned} \dot{x} &= -y - z + E\cos\nu t\ , \\ \dot{y} &= x + 0.15y\ , \\ \dot{z} &= 0.4 + z(x - 8.5)\ . \end{aligned} \tag{1.20}$$

oscillators. In the absence of forcing, both are 3-dimensional dissipative systems which admit a straightforward construction of the Poincaré maps. The mean rotation frequency can be thus directly calculated as

$$\Omega = \lim_{t\to\infty} 2\pi\frac{N_t}{t}\ , \tag{1.21}$$

where N_t is the number of crossings of the Poincaré section during observation time t. This method can be straightforwardly applied to the observed time series, in the simplest case one can, e.g., take for N_t the number of maxima (of $x(t)$ for the Rössler system and of $z(t)$ for the Lorenz one). Alternatively, we can compute the phase of the driven systems according to (1.11) or (1.15) and compute the observed frequencies as $\Omega = \langle\dot{\phi}_P\rangle$.

Dependence of the frequency Ω on the amplitude and frequency of the external force is shown in Fig. 1.4. Synchronization here corresponds to the plateau $\Omega = \nu$. One can see that the synchronization properties of these two systems differ essentially. For the Rössler system there exists a well-expressed region where the systems are perfectly locked. Moreover, it is seen that the amplitude threshold of synchronization is very small, almost negligible. Thus, the phase locking properties of the Rössler system are practically the same as for a periodic oscillator; in particular, one can also observe high order $(n:m)$ locking [71]. On the contrary, for the Lorenz system we observe the frequency locking only as a tendency seen at relatively large forcing amplitudes, as this should be expected

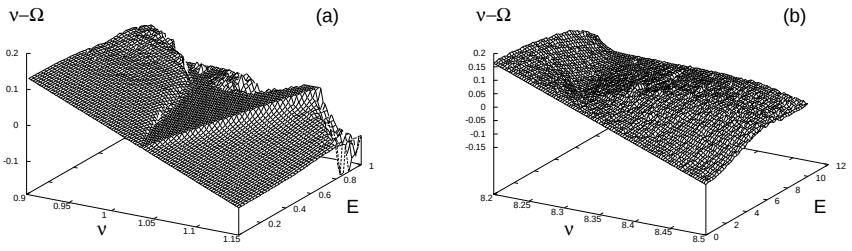

Figure 1.4: The phase synchronization regions for the Rössler (a) and the Lorenz (b) systems.

for oscillators subject to a rather strong noise. In this respect, the difference between Rössler and Lorenz systems can be described in terms of phase diffusion properties. Indeed, the phase diffusion coefficient for autonomous Rössler system is extremely small $D_p < 10^{-4}$, whereas for the Lorenz system it is several oder of magnitude larger, $D_p \approx 0.2$. This difference in the coherence of the phase of autonomous oscillations implies different response to periodic forcing.

1.3.2 Statistical approach

We characterize now phase synchronization considering the distribution of phases. The invariant measure of an autonomous chaotic system gives a nearly uniform distribution of the phases.[1] With a periodic external force, the measure is explicitly time-dependent. Phase synchronization means that for each time the distribution density of the phases is non-uniform (there is a time-dependent preferable value of the phase), where the sharpness of the peak characterizes the level of synchronization. This peak in the phase distribution rotates with the phase of the external force. The distribution of the amplitudes remains, however, broad. Due to ergodicity, the probability distribution can be obtained also from one chaotic trajectory, if it is observed stroboscopically in the proper phase of external force.

As an example we consider again the Rössler system. Let us observe the oscillator stroboscopically, at the moments corresponding to some phase ψ_0 of the external force. In the synchronous state the probability distribution of the oscillator phase is localized near some preferable value (which of course depends on the choice of ψ_0). In the non-synchronous state the phase is spread along the attractor (Fig. 1.5). One can say that synchronization means localization of the probability density near some preferable time-periodic state. In other words, this means appearance of the long-range correlation in time and of the significant discrete component in the power spectrum of oscillations.

The main advantage of the statistical approach is that it provides characterization of synchronization without explicit computation of phase. This becomes especially important in case of attractors with "bad" topology, i.e., when the phase is not well-defined (see Chapter 3).

[1] Phases here are taken modulo 2π.

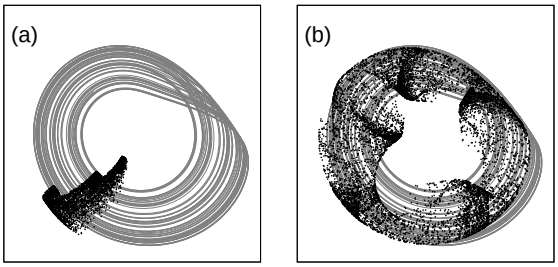

Figure 1.5: Distribution inside (a) and outside (b) the synchronization region for the Rössler system, shown with black dots. The autonomous Rössler attractor is shown with gray.

1.3.3 Interpretation through embedded periodic orbits

In order to understand structural metamorphoses of attracting chaotic sets under the action of the synchronizing force, it is convenient to look at the properties of individual periodic orbits embedded into the strange attractors. Unstable periodic orbits (UPOs) are known to build a kind of "skeletons" for chaotic sets [58]; in particular, each of the systems (1.19) and (1.20) in the absence of forcing possesses infinite number of periodic solutions with two-dimensional unstable manifolds. Let us pick up one of these solutions and consider the influence of a small periodic force on it. With the exception that the cycle is now unstable, we come to a standard problem of periodically forced periodic oscillator. Hence, for a particular orbit one can determine the corresponding Arnold tongue.

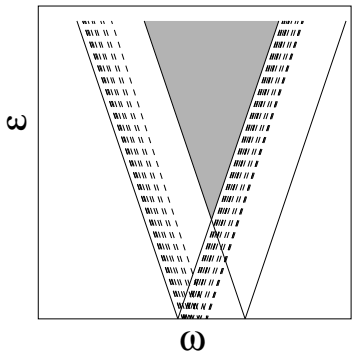

Figure 1.6: A schematic view of the Arnold tongues for an unstable periodic orbits in a chaotic system. Generally, the autonomous orbits have different frequencies $\omega_0^{(i)}$; therefore the tongues tip the ω-axis in different points. The rightmost and the leftmost tongues corresponding to the orbits with the minimal and maximal $\omega_0^{(i)}$ are shown by solid lines. In the shadowed region all the cycles are synchronized and the mean frequency of oscillations virtually coincides with the forcing frequency.

If we plot the Arnold tongues for the set of UPOs (Fig. 1.6), then generally the tongues touch the ω-axis in different points ω_i, where $\omega_0^{(i)}$ is the mean

frequency of the i-th autonomous orbit. The frequencies $\omega_0^{(i)}$ can be close to each other or widespread, depending on the properties of the return times. If the frequencies $\omega_0^{(i)}$ are not very different, the Arnold tongues overlap and one can find a parameter region where the motion along all periodic orbits is locked by the external force. If the forcing remains moderate, this is the overlapping region for the leftmost and the rightmost Arnold tongues, which correspond to the periodic orbits of the autonomous system with the smallest and the largest values of $\omega_0^{(i)}$, respectively. Inside this region, the chaotic trajectories repeatedly visit the neighborhoods of different UPOs; but, as all UPOs are locked, the overall motion remains locked to the external force as well. Outside the region where all the tongues overlap, synchronization cannot be perfect: for some time intervals a trajectory follows the locked cycles and the phase follows the external force, but for other time epochs the trajectory comes close to non-locked cycles what results in a phase slip (see details in [118, 61]).

Chapter 2

Phase synchronization in coupled systems

In this Chapter we demonstrate the effects of phase synchronization in coupled chaotic oscillators. We start with the simplest case of two interacting systems, and then briefly discuss globally coupled systems and oscillator lattices.

2.1 Synchronization of two interacting oscillators

We consider here two *non-identical* coupled Rössler systems

$$\begin{aligned} \dot{x}_{1,2} &= -\omega_{1,2} y_{1,2} - z_{1,2} + \varepsilon(x_{2,1} - x_{1,2}), \\ \dot{y}_{1,2} &= \omega_{1,2} x_{1,2} + 0.15 y_{1,2}, \\ \dot{z}_{1,2} &= 0.2 + z_{1,2}(x_{1,2} - 10). \end{aligned} \tag{2.1}$$

The parameters $\omega_{1,2} = 1 \pm \nu$ and ε determine the mismatch of natural frequencies and the coupling, respectively.

Again, like in the case of periodic forcing, we can define the mean frequencies $\Omega_{1,2}$ of oscillations of each system, and study the dependence of the frequency mismatch $\Omega_2 - \Omega_1$ on the parameters ν and ε. This dependence shown in Fig. 2.1 gives a typical picture of the synchronization region. The phase diagram of different regimes (in dependence on the coupling ε and the frequency mismatch $\omega_2 - \omega_1$) exhibits three regions of qualitatively different behavior:

(I) The synchronization region, where the frequencies are locked, $\Omega_1 = \Omega_2$. It is important to note that there is almost no threshold of synchronization; this is a particular feature of the phase-coherent Rössler attractor.

(II) The region of non-synchronized oscillations, where $|\Omega_1 - \Omega_2| = |\Omega_b| > 0$. In analogy to the case of periodic oscillators, this frequency Ω_b can be considered as the "beat frequency".

(III) In this region oscillations in both systems disappear, due to diffusive coupling. This effect is known for periodic systems as oscillation death, or quenching.

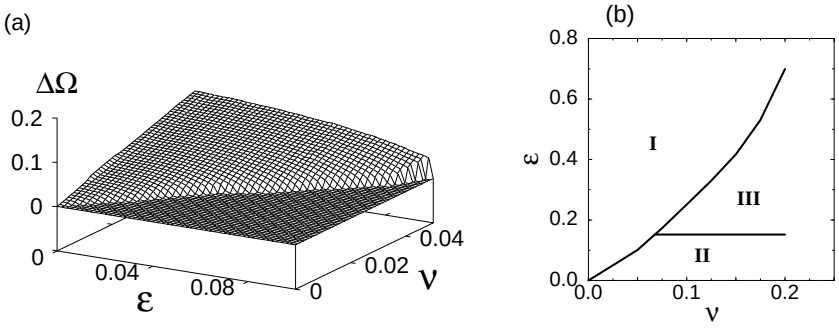

Figure 2.1: (a) The synchronization region for two coupled Rössler oscillators (2.1): the plot of the difference in observed frequencies $\Delta\Omega = \langle\dot{\phi}_1 - \dot{\phi}_2\rangle$ in dependence on the coupling ε and mismatch ν exhibits a domain where $\Delta\Omega$ vanishes. (b) A schematic diagram showing the regions of non-synchronous (II) and synchronous (I) motion, and of the oscillations death (III). The diagram is approximate, the windows of periodic behavior in regions I and II are not shown.

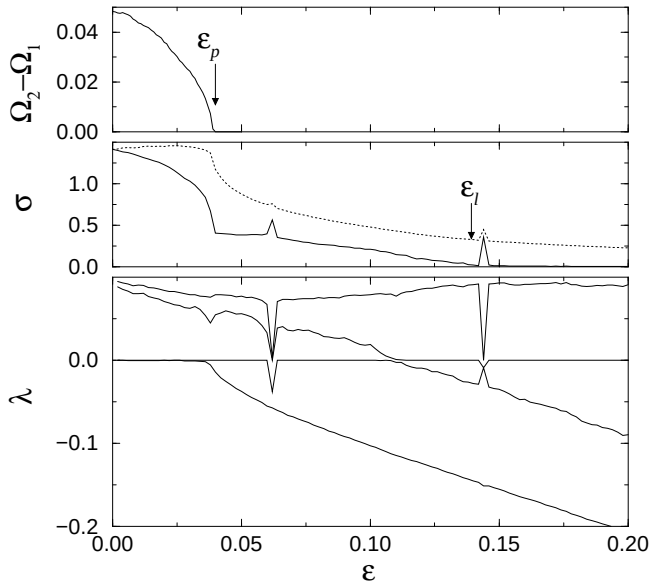

Figure 2.2: The 4 largest Lyapunov exponents and the frequency difference vs. coupling ε in the coupled Rössler oscillators (2.1); $\nu = 0.015$. For small couplings there are two positive and two nearly zero Lyapunov exponents. Transition to the phase synchronization occurs at $\varepsilon \approx 0.028$, at this value of the coupling one of zero Lyapunov exponents becomes negative.

It is instructive to characterize the synchronization transition by means of the Lyapunov exponents (LE). The 6-order dynamical system (2.1) has 6 LEs (see Fig. 2.2). For zero coupling we have a degenerate situation of two independent systems, each of them has one positive, one zero, and one negative

exponent. The two zero exponents correspond to the two independent phases. With coupling, the phases become dependent and the degeneracy must be removed: only one LE should remain exactly zero. We observe, however, that for small coupling also the second zero Lyapunov exponent remains extremely small (in fact, numerically indistinguishable from zero). Only at relatively stronger coupling, when the synchronization sets on, the second LE becomes negative: now the phases are dependent and a relation between them is stable. Note that the two positive exponents remain positive which means that the amplitudes remain chaotic and independent: the coupled system remains in the state of hyperchaos.

2.2 Population of globally coupled chaotic oscillators

A number of physical, chemical and biological systems can be viewed at as large populations of weakly interacting non-identical oscillators [45]. One of the most popular models here is an ensemble of globally coupled nonlinear oscillators (often called "mean-field coupling"). A nontrivial transition to self-synchronization in a population of periodic oscillators with different natural frequencies coupled through a mean field has been described by Kuramoto [45, 44]. In this system, as the coupling parameter increases, a sharp transition is observed for which the mean field intensity serves as an order parameter [32]. This transition owes to a mutual synchronization of the periodic oscillators, so that their fields become coherent (i.e. their phases are locked), thus producing a macroscopic mean field. In its turn, this field acts on the individual oscillators, locking their phases, so that the synchronous state is self-sustained. Different aspects of this transition have been studied in [94, 16, 17], where also an analogy with the second–order phase transition has been exploited.

A similar effect can be observed in a population of *non-identical chaotic* systems, e.g., the Rössler oscillators [69, Appendix 2]

$$\begin{aligned} \dot{x}_i &= -\omega_i y_i - z_i + \varepsilon X, \\ \dot{y}_i &= \omega_i x_i + a y_i, \\ \dot{z}_i &= 0.4 + z_i(x_i - 8.5), \end{aligned} \tag{2.2}$$

coupled via the mean field $X = N^{-1}\sum_1^N x_i$. Here N is the number of elements in the ensemble, ε is the coupling constant, a and ω_i are parameters of the Rössler oscillators. The parameter ω_i governs the natural frequency of an individual system. We take a set of frequencies ω_i which are Gaussian-distributed around the mean value ω_0 with variance $(\Delta\omega)^2$. The Rössler system typically shows windows of periodic behavior as the parameter ω is changed; therefore we usually choose a mean frequency ω_0 in a way that we avoid large periodic windows. In our computer simulations we solve numerically Eqs. (2.2) for rather large ensembles $N = 3000 \div 5000$.

With an increase of the coupling strength ε, the appearance of a non-zero macroscopic mean field X is observed [69, Appendix 2]. This indicates the phase synchronization of the Rössler oscillators that arises due to their interaction via mean field. This mean field is large, if the attractors of individual systems are phase-coherent (parameter $a = 0.15$) and the phase is well-defined. On the

contrary, in the case of the funnel attractor, $a = 0.25$, when the oscillations look wild, and the imaging point makes large and small loops around the origin, the field is rather small, and there seems to be no way to choose the Poincaré section unambiguously. Nevertheless, in both cases synchronization transition is clearly indicated by the onset of the mean field, without computation of the phases themselves.

Our numerical results are confirmed by recent experiments with globally coupled chaotic chemical oscillators [39, 40].

2.3 Lattice of chaotic oscillators

Here we consider the case when chaotic oscillators are ordered in space and form a lattice with nearest neighbor interaction. Such a situation is relevant, e.g., for modeling chemical systems, where homogeneous oscillations are chaotic, and the diffusive interaction can be model-led with dissipative nearest neighbors coupling [12, 30]. One can expect to observe complex spatio-temporal synchronization in such a lattice.

Our model is a 1-dimensional lattice of Rössler oscillators with local dissipative coupling:

$$\begin{aligned} \dot{x}_j &= -\omega_j y_j - z_j, \\ \dot{y}_j &= \omega_j x_j + a y_j + \varepsilon(y_{j+1} - 2y_j + y_{j-1}), \\ \dot{z}_j &= 0.4 + (x_j - 8.5) z_j. \end{aligned} \tag{2.3}$$

Here the index $j = 1, \ldots, N$ counts the oscillators in the lattice and ε is the coupling coefficient. To study synchronization in a lattice of non-identical oscillators, we introduce a linear distribution of natural frequencies ω_j

$$\omega_j = \omega_1 + \delta(j-1), \tag{2.4}$$

where δ is the frequency mismatch between neighboring sites. Depending on the values of δ we observed two scenarios of transition to synchronization [56]. For small δ, the transition occurs smoothly, i.e., all the elements along the chain gradually adjust their frequencies. If the frequency mismatch is larger, clustering is observed: the oscillators build phase-synchronized groups having different mean frequencies. At the borders between clusters phase slips occur; this can be considered as appearance of defects in the spatio-temporal representation. Both regular and irregular patterns of defects can be found. Synchronization was observed not only for the systems with simple attractor ($a = 0.15$), but also for the systems with the funnel attractor ($a = 0.25$) [56].

2.4 Synchronization transitions

In this Section we describe synchronization transitions. First, we discuss intermittency at the threshold of phase synchronization. Next, we follow what happens if the coupling strength is increased further, and describe the effect of *lag synchronization* [87, Appendix 3].

2.4.1 Intermittency at the synchronization transition

An interesting feature is the appearance of intermittency at the onset of phase synchronization. Consider again two coupled Rössler oscillators (Eqs. (2.1)). As one can see from Fig. 2.3a, at the border of the region of complete phase locking, the phases are almost locked. It means that from time to time phase slips occur, where during a rather small interval of time the phase difference changes by 2π. The time intervals between these slips are irregular, as one can see from their distribution (Fig. 2.4a). The slips are exponentially rare, and the dependence of the number of phase slips per constant time N_s on the coupling strength obeys a relation $N_s \sim \exp(-|\varepsilon - \varepsilon_c|^{-1/2})$ [86] (Fig. 2.4b).

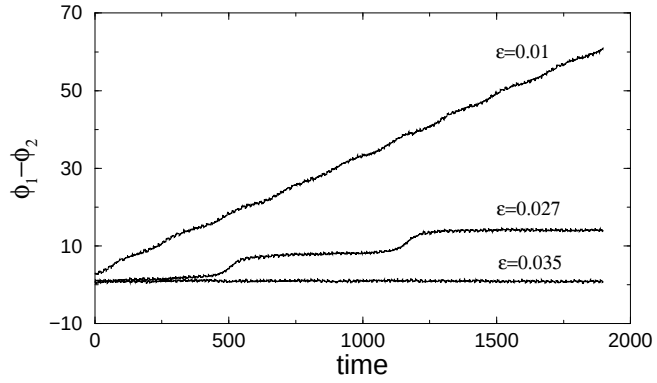

Figure 2.3: Phase difference of two coupled Rössler systems (Eq. (2.1)) vs. time for non–synchronous, ($\varepsilon = 0.01$), nearly synchronous, or intermittent, ($\varepsilon = 0.027$) and synchronous ($\varepsilon = 0.035$) states. In the last case the amplitudes $A_{1,2}$ remain chaotic, their cross-correlation is less than 0.2. The frequency mismatch is $\nu = 0.015$.

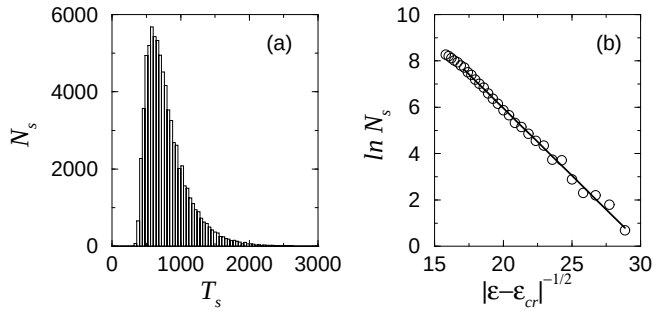

Figure 2.4: (a): The distribution of the number of phase slips N_s with the interval between slips T_s for $\varepsilon = 0.027$; it demonstrates that the slips occur irregularly. (b) The number of phase slips per constant time N_s vs. the coupling strength in the vicinity of the transition point. The slips are exponentially rare.

2.4.2 Lag synchronization

If the coupling between two chaotic oscillators is sufficiently strong, then one can observe the onset of phase synchronization. We discuss what happens in the system of two symmetrically coupled *non–identical* oscillators with the further increase of coupling. We demonstrate that for larger couplings a new regime which we call lag synchronization (LS) sets in. LS appears as almost perfect coincidence of *shifted in time* states of two systems, $\mathbf{x}_1(t+\tau_0) \approx \mathbf{x}_2(t)$. Finally, with further increase of coupling, the time shift decreases and this regime tends to complete synchronization. We show that these transitions are related to the changes in the spectrum of Lyapunov exponents (LE). For this purpose, we take our basic model, two coupled Rössler systems

$$\begin{array}{rcl} \dot{x}_{1,2} &=& -\omega_{1,2} y_{1,2} - z_{1,2} + \varepsilon(x_{2,1} - x_{1,2}), \\ \dot{y}_{1,2} &=& \omega_{1,2} x_{1,2} + a y_{1,2}, \\ \dot{z}_{1,2} &=& f + z_{1,2}(x_{1,2} - c), \end{array} \tag{2.5}$$

where $a = 0.165$, $f = 0.2$, $c = 10$. The parameters $\omega_{1,2} = 0.97 \pm 0.02$ and ε determine the mismatch of natural frequencies and the coupling, respectively. The parameters are chosen by trial in such a way that appearance of large windows of periodic behavior is avoided.

To characterize LS, we introduce a similarity function S as a time averaged difference between the variables x_1 and x_2 (with mean values being subtracted) taken with the time shift τ

$$S^2(\tau) = \frac{\left\langle (x_2(t+\tau) - x_1(t))^2 \right\rangle}{(< x_1^2(t) >< x_2^2(t) >)^{1/2}} \ , \tag{2.6}$$

and search for its minimum $\sigma = \min_\tau S(\tau)$. If the signals x_1 and x_2 are independent, the difference between them is of the same order as the signals themselves; respectively $S(\tau) \sim 1$ for all τ. If $x_1(t) = x_2(t)$, as in the case of complete synchronization, $S(\tau)$ reaches its minimum $\sigma = 0$ for $\tau = 0$. Here we demonstrate a nontrivial case, when the similarity function $S(\tau)$ has a minimum for non-zero time shift τ, meaning the existence of a time lag between the two processes.

Computation of the observed frequencies $\Omega_{1,2}$ allows us to follow the transition to the frequency entrainment $\Omega_1 = \Omega_2 = \Omega$; it takes place at $\varepsilon = \varepsilon_p \approx 0.036$ (see Fig. 2.5). For stronger coupling $\varepsilon = \varepsilon_l \approx 0.14$ we observe a new transition to lag synchronization (see the σ vs ε curve in Fig. 2.5). In Fig. 2.6 we show numerically obtained similarity functions in system (2.5) for relatively weak, intermediate and strong coupling. For weak coupling $\varepsilon < \varepsilon_p$ (curves 1,2), $S \sim 1$ and practically does not depend on τ, as can be expected for independent signals. For intermediate coupling strength $\varepsilon_p < \varepsilon < \varepsilon_l$, a minimum of $S(\tau)$ appears (curves 3,4) indicating the existence of some characteristic time shift τ_0 between x_1 and x_2. This shift is related to the phase difference as $\tau_0 = \delta\phi/\Omega$. Note that in this regime the amplitudes are uncorrelated, so the value of $S(\tau_0)$ is relatively large. Further increase of coupling makes at $\varepsilon \approx \varepsilon_l$ this minimum very sharp (curves 5,6) and practically equal to zero. It means that the states of the systems become identical, but shifted in time with respect to each other. The regime of LS can be easily demonstrated by plotting $x_1(t+\tau_0)$ vs $x_2(t)$. It is important that calculations of $S(0)$, i.e., the comparison of x_1 and x_2 without time shift, reveal no transition at $\varepsilon = \varepsilon_l$. For larger couplings $\varepsilon > \varepsilon_l$, the time lag τ_0 continuously decreases, but no qualitative transitions are observed.

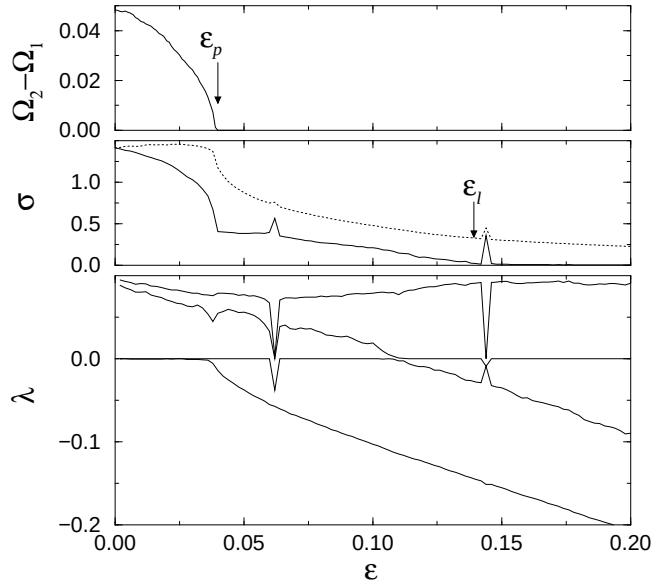

Figure 2.5: The frequency difference $\Omega_1 - \Omega_2$, the minimum of the similarity function σ and the four largest Lyapunov exponents λ of two coupled Rössler oscillators vs. the coupling ε. Three different regions are clearly seen on σ vs ε plot correspondent to non–synchronous state, phase and lag synchronization respectively. The transitions between these regimes are reflected in the spectrum of Lyapunov exponents: at the first transition one of the zero LE becomes negative, while the second transition corresponds to the zero crossing of one of the positive LE. The dashed line shows dependence of $S(0)$ on the coupling; from this plot one can see that comparison of states of interacting systems without time shift does not reveal the transition to LS. Two "outbursts" on σ vs ε plot at $\varepsilon \approx 0.06$ and $\varepsilon \approx 0.145$ correspond to period 3 windows.

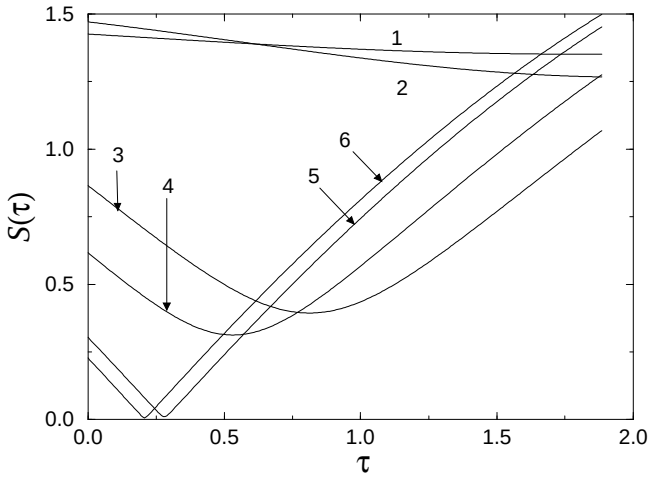

Figure 2.6: Similarity function $S(\tau)$ for different values of coupling strength ε (1: $\varepsilon = 0.01$, 2: $\varepsilon = 0.015$, 3: $\varepsilon = 0.05$, 4: $\varepsilon = 0.075$, 5: $\varepsilon = 0.15$, 6: $\varepsilon = 0.2$). With the increase of coupling a minimum appears indicating the existence of a certain phase shift between interacting systems (curves 3 and 4). In the regime of lag synchronization (curves 5 and 6) the minimum is extremely small.

The transitions between different types of synchronization can be related to the changes in the Lyapunov spectrum (see Fig. 2.5). For small coupling $\varepsilon < \varepsilon_p$ there are two positive LE (corresponding to chaotic amplitudes) and two nearly zero LE (corresponding to independently rotating phases). At the phase locking transition at $\varepsilon \approx \varepsilon_p$, one of the zero LEs becomes negative, corresponding to a definite stable relation between phases (one zero LE, corresponding to a simultaneous phase shift of both Rössler oscillators, remains for all couplings, as it should be in an autonomous system). The second transition to LS corresponds to the change of the sign by the second positive LE, but does not exactly coincide with it due to intermittency discussed below. This means that the relation appears not only between the phases, but also between the amplitudes. The phase shift remains, and therefore a time lag between the signals x_1 and x_2 is observed.

Chapter 3

Systems with ill-defined phase

In this Chapter we treat the case when a chaotic system has no well-defined phase. It means that we are not able to find a projection of the strange attractor that looks like smeared rotations around some center and, hence, we are not able to choose unambiguously the Poncaré section. However, synchronization can be characterized in this case as well. We consider two approaches to the problem.

3.1 Statistical approach

3.1.1 An example: Rössler system with funnel attractor

Now we consider the Rössler system for parameters slightly different from those in (1.20): instead of the term $0.15y$ take $0.25y$ in the second equation. This change leads to the appearance of the so-called funnel attractor, shown in Fig. 3.1. The Rössler system with the funnel attractor serves as an example of the system with ill-defined phase. The topological structure is now complex: there are small and large loops on the x, y plane, and it is not clear which phase shift (π or 2π) should be attributed to these loops. Respectively, different definitions of the phase give different results (Fig. 3.1).

3.1.2 Indirect characterization of synchronization

An important consequence of the statistical approach described in Section 1.3.2 is that the phase synchronization can be characterized without explicit computation of the phase and/or the mean frequency: it can be indicated implicitly by the appearance of a macroscopic mean field in the ensemble of oscillators, or by the appearance of the large discrete component in the spectrum. Although there may be other mechanisms leading to the appearance of macroscopic order, the phase synchronization appears to be the mostly common ones.

We use this approach to look for possible effects of phase synchronization in the Rössler system with the funnel attractor. Because the phase itself is ill-defined, we considered only implicit characteristics of synchronization. Namely, we take a large ensemble of identical copies of the chaotic oscillator which differ

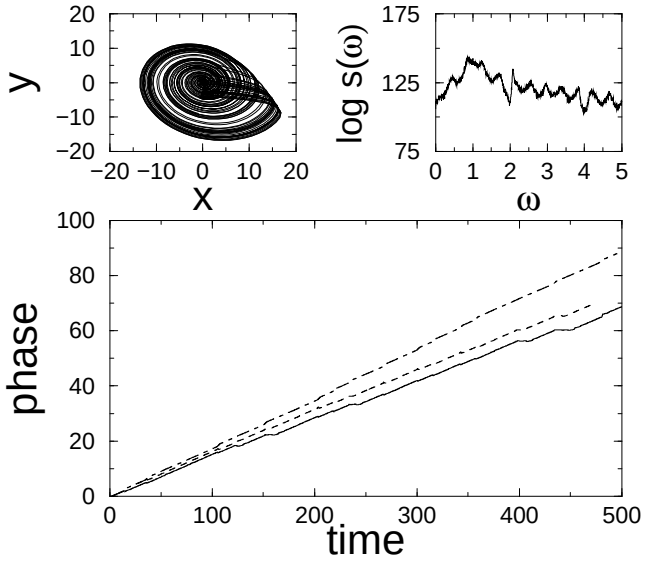

Figure 3.1: Rössler oscillator with the funnel attractor is an example of the system with ill-defined phase. Here different approaches to phase estimations provide different results. Dot-dashed line: the phase ϕ, solid line: the phase variable ϕ_P, dashed line: the Hilbert-transform phase ϕ_H.

only by their initial states, and let them evolve under the same periodic forcing. After the transient, the projections of the phase state of each oscillator onto the plane x, y form the cloud that exactly corresponds to the probability density. Let us now consider the ensemble average of some observable, e.g., $x(t)$. Without synchronization the cloud is spread over the projection of the attractor, and the average is small: no significant average field is observed. In the synchronous state the probability is localized, so the average is close to some middle point of the cloud; this point rotates with the frequency of the force and one observes large regular oscillations of the average field.

Hence, the synchronization can be easily indicated through the appearance of a large (macroscopic) mean field in the ensemble. Physically, this effect is rather clear: unforced chaotic oscillators are not coherent due to internal chaos, thus the summation of their fields yields a small quantity. Being synchronized, the oscillators become coherent with the external force and thereby with each other, so the coherent summation of their fields produces a large mean field.

3.2 Locking-based frequency measurement

In this Section we discuss a method that allows one to reveal synchronization of systems with ill-defined phases, estimating the average frequency $\langle\dot{\phi}\rangle$ of individual oscillators from observed signals. This method, based on the use of *auxiliary limit cycle oscillators*, can characterize synchronization of two or many coupled systems; unlike the above described statistical approach it does not require ensemble averaging.

3.2.1 Idea of the method

Let us consider an ensemble of *uncoupled* limit cycle oscillators with natural frequencies ω_k distributed in an interval $[\omega_{min}, \omega_{max}]$. Let each oscillator of this ensemble be driven by a common periodic force of a frequency ν. It is well-known that the force synchronizes those elements of the ensemble which have frequencies close to $n\nu/m$, where n, m are integers. This can be demonstrated by plotting the frequencies of the driven limit cycle oscillators Ω_k, called hereafter the observed frequencies, vs. the natural frequencies ω_k: the synchronization manifests itself in the appearance of horizontal plateaus (more precisely, one expects to observe a devil's staircase structure with infinitely many plateaus whose widths depend on the amplitude of the forcing). This means that the frequencies of entrained elements corresponding to a particular plateau are in exact $n : m$ relation to the frequency of the forcing. Hence, an *unknown* frequency of the drive can be revealed by the analysis of the Ω_k vs. ω_k plot. The idea of our approach is to use the ensemble of auxiliary oscillators as a *device for measuring the frequency of complex signals*.

A simple implementation of the method is to drive the array of Poincaré oscillators with a signal $X(t)$

$$\dot{A}_k = (1 + i\omega_k)A_k - |A_k|^2 A_k + \varepsilon X(t) \; . \tag{3.1}$$

Separating the real amplitude R and the phase ϕ from the complex amplitude

$A = Re^{i\phi}$ we can rewrite (3.1) as

$$\begin{aligned} \dot{R}_k &= R_k - R_k^3 + \varepsilon X(t)\cos\phi_k \ , \\ \dot{\phi}_k &= \omega_k - R_k^{-1}\varepsilon X(t)\sin\phi_k \ . \end{aligned} \tag{3.2}$$

Noting that for small ε the amplitude R is close to unity, and neglecting its fluctuations, we can write equations for our measuring oscillators as pure phase equations:

$$\dot{\phi}_k = \omega_k - \varepsilon X(t)\sin\phi_k \ , \tag{3.3}$$

and the observed frequencies are $\Omega_k = \langle\dot{\phi}_k\rangle$. Note that Eqs. (3.3) become exact if one writes a higher order nonlinearity $|A|^p A$ in (3.1) and considers the limit $p \to \infty$. Practically, in calculations below we normalize the signal $X(t)$ to have zero mean and unit variance so that the coupling constant ε is the only parameter of the method.[1]

3.2.2 Synchronization of chaotic oscillators with complex dynamics

Driven systems

First we consider the Rössler system with a funnel attractor (Fig. 3.1):

$$\begin{aligned} \dot{x} &= -y - z \ , \\ \dot{y} &= x + 0.4y \ , \\ \dot{z} &= 0.25 + z(x - 8.5) \ . \end{aligned} \tag{3.4}$$

Clearly we cannot find an origin that is revolved by all trajectories. Due to this, there is no direct way to introduce the phase for this system and to characterize its synchronization. Therefore we use the (normalized) signal $x(t)$ to drive system (3.3) with $\varepsilon = 0.5$. The frequencies of the oscillators in the measuring device driven by $X(t) = x(t)$ are shown in the solid curve denoted by $E = 0$ as functions of the natural frequencies in Fig. 3.2. The resulting plateau in the Ω_k vs. ω_k plot gives $\Omega^p \approx 0.94$, where "p" stands for "plateau". Thus an estimate of the characteristic frequency of the signal $x(t)$ is $\Omega^p = 0.94$. One can see that this characteristic frequency cannot be directly associated with a peak in the power spectrum (Fig. 3.1). We also see that Fig. 3.2 does not show the devil's staircase structure, but only one, smeared plateau. This is due to the chaotic nature of the process $x(t)$, so that, similar to the case of narrow-band noisy signals, the high-order phase-locked regions are not observed [47, 70].

Next we study a synchronization of the system (3.4) by a periodic forcing. The first equation of (3.4) now reads as $\dot{x} = -y - z + E\sin(\nu t)$. Performing measurements with "device" (3.3) for different values of the forcing amplitude E, we see that the measured frequency Ω^p approaches the external frequency ν, giving a clear picture of frequency entrainment (Fig. 3.2). Note also that the plateau becomes wider: this can be interpreted as an indication that the external force brings order in the Rössler system. It is important to mention that the shift of the plateau is due to the entrainment of the chaotic oscillations and is not an effect of the presence of a periodic component in the signal $x(t)$. This was checked by using a mixture of an unforced oscillation $x(t)$ and a periodic

[1] The mean value can slightly influence the result.

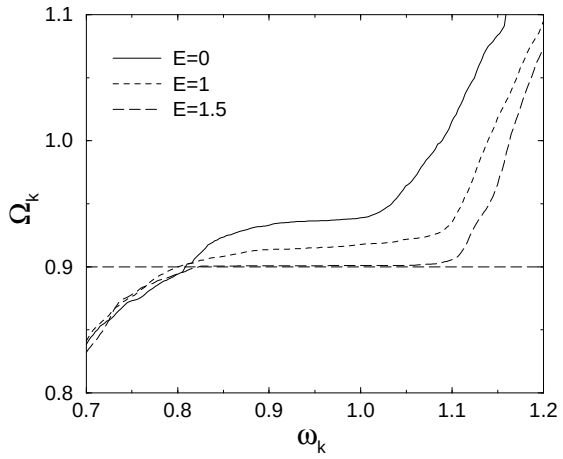

Figure 3.2: Output of the frequency measuring "device" (3.3) as a function of the natural frequencies of auxiliary systems ω_k for the driven Rössler oscillator at three forcing amplitudes (results for (3.1) practically coincide with them). Bold curve shows the frequencies of an ensemble of uncoupled limit cycle oscillators driven by the system (3.4). The height of the plateau determines the characteristic frequency of this chaotic drive $\Omega^{(p)} = 0.94$. Two other curves are obtained for the forced (with the amplitude E) Rössler system, and demonstrate shift of the characteristic frequency towards the frequency of the forcing $\nu = 0.9$ (horizontal line), thus indicating synchronization.

force $E\sin(\nu t)$ for $X(t)$ in (3.3); in this case no shift of the plateau has been observed.

The described method has been also applied to experimental data obtained from the ensemble of 64 globally coupled chaotic electrochemical oscillators [116, 38]. (See [116] for the details of the experiment). The oscillators have been subjected to a mutual coupling stronger than that required for phase synchronization but weaker than that necessary for complete synchronization. The array was forced periodically and the oscillations have been recorded for several values of the forcing amplitude. Because of the coupling, several of the oscillators in this parameter range demonstrate complex patterns of oscillations so that it was impossible to define the phase with the Hilbert Transform method. Nevertheless, with applying our method we were able, without any special adjustment, to determine the frequencies of all oscillators in the array and to show that with increasing of the forcing amplitude they become phase synchronized with the external force.

Coupled oscillators

Our next application is the analysis of two coupled oscillators with ill-defined phases. The scalar signals $x_{1,2}$ from these systems are used as inputs for two measuring devices, i.e., $x_{1,2}$ drive two identical ensembles (3.1) or (3.3). The outputs of the devices are two frequencies $\Omega^p_{1,2}$; for uncoupled systems we expect that they differ due to a detuning. The onset of the equality $\Omega^p_1 = \Omega^p_2$ with the increase of coupling will reflect the synchronization of the complex systems

under consideration. As a particular example we consider two weakly coupled Rössler systems with funnel attractors:

$$\begin{aligned} \dot{x}_{1,2} &= -\omega_{1,2} y_{1,2} - z_{1,2} + \eta(x_{2,1} - x_{1,2}) \,, \\ \dot{y}_{1,2} &= \omega_{1,2} x_{1,2} + 0.22 y_{1,2} + \eta(y_{2,1} - y_{1,2}) \,, \\ \dot{z}_{1,2} &= 0.1 + z_{1,2}(x_{1,2} - 8.5), \end{aligned} \tag{3.5}$$

where $\omega_1 = 0.98$, $\omega_2 = 1.03$. Application of the method (Fig. 3.3) reveals synchronization for coupling parameter $\eta \gtrsim 0.05$. The particular parameter values in (3.5) give us a possibility to compare our approach with direct phase measurements. Indeed, for most η the trajectory in the coordinates $(\dot{x}, \dot{y})$ rotates around the origin and the phase $\phi = \arctan(\dot{y}/\dot{x})$ is well-defined; this does not hold for coupling $0.04 \gtrsim \eta \gtrsim 0.03$, when some trajectories do not wrap the origin (although these events are relatively rare).[2] Thus the onset of synchronization in system (3.5) can be traced in a straightforward way, by plotting the phase difference that becomes bounded with increase of coupling (for $\eta \gtrsim 0.05$).

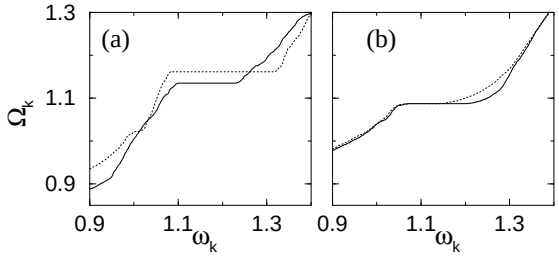

Figure 3.3: Output of the frequency measuring "device" for two Rössler systems (2.5). (a) no coupling, (b) coupling, $\eta = 0.05$. For zero coupling (a) the characteristic frequencies $\Omega_{1,2}^{(p)}$ are different (plateaus have different height); for coupling (b) these frequencies coincide, i.e. synchronization sets in. Solid and dotted lines correspond to first and second oscillator, respectively. Note that the common frequency in (b) lies below both frequencies in (a); such a frequency shift is usual for diffusive coupling, it appears due to dependence of the frequency on the amplitudes, the latter being reduced due to coupling.

Discussion of the method

We expect that for chaotic systems with very complicated topology of the phase space the plateau may be not seen at all and hence the frequency may be not found. This limitation of the presented method is due to the principal fact that systems with strong effective noise do not have a characteristic frequency and are not capable of synchronization. Like noisy systems, chaotic oscillators with ill-defined phase do not allow an unambiguous definition of synchronization; therefore the distinction between the systems that can and cannot synchronize is smeared. Note also, that with our method we define frequency of a signal,

[2] It is easy to see that the transformation to the coordinates $(\dot{x}, \dot{y})$ proposed in Chen *et al.* Phys. Rev. E. **64**, 016212 (2001), is not of general use. So, it also fails for the driven system (3.4) and another parameter choice in (3.5), whereas our technique reveals phase synchronization in these cases as well.

not of an oscillator. In particular, frequencies for different observables from one system can differ.

In a general context, we can interpret the ensemble of uncoupled oscillators with a common input (Eqs. (3.1) or (3.3)) as a nonlinear filter that picks up a certain frequency from a broad-band input. Indeed, the average velocity of the phase point rotation around the limit cycle in a single oscillator (3.1) is determined by some average properties of the aperiodic driving force. In particular, the system filters out the action when the signal $X(t)$ is nearly zero (and therefore the phase is ill-defined), because the point of the oscillator continues to rotate (with the natural frequency). In this respect our device is similar to the well-known technical system, the phase locked loop [6]. The latter provides a phase of an input even during epochs when the amplitude of the input is small (say, of the same order as the underlying noise). In particular, taking the natural frequency in (3.3) in the middle of the plateau, one can use the corresponding phase $\phi_k(t)$ as an "estimate" to the signal's phase. It is essential to use nonlinear self-sustained oscillators and not linear resonators, in the latter case simply the power spectrum of the process would be measured, while in our case a single frequency is extracted.

Chapter 4

Synchronization approach to bivariate data analysis

In this Chapter we use the idea of phase synchronization for experimental applications. The problems we consider can be formulated as follows. Suppose we observe two systems that are possibly coupled. We do not have access to the parameters of these systems but just can measure the signals at their outputs. Out goal is to analyze these bivariate data in order to find out whether these systems interact. If they do, the natural problems are:

1. to quantify the strength of interaction;

2. to quantify the asymmetry in interaction (coupling direction).

We discuss methods of data analysis giving answers to the above questions and illustrate them by experimental examples. The relation of the developed and traditional techniques is also discussed.

Our approach is especially important for applications in medicine and biology. Indeed, in experiments with live systems a researcher usually cannot perform an active experiment, i.e., to change the parameters of systems and/or coupling and to look for the response in the dynamics of the systems. Quite often one can perform only passive experiments, i.e., to measure the signals from biological systems under free-running conditions and analyze them.

4.1 Introduction

Remarkably, the properties of phase synchronization in chaotic systems are similar to those of synchronization in periodic *noisy* oscillators (see the discussion in Section 1.2.3. This allows one to describe both effects within a common framework. Moreover, from the experimentalist's point of view, one can use the same methods in order to detect synchronization both in chaotic and noisy systems. Therefore, describing particular experiments and searching for phase relations, we will not be interested in the question, whether the observed oscillations are chaotic or noisy: the approach we present below is equally applicable in both these cases.

Synchronization phenomena are often encountered in living nature. Indeed, the concept of synchronization is widely used in experimental studies and in the modeling of interaction between different physiological (sub)systems demonstrating oscillating behavior. The examples range from the modeling of the heart in the pioneering paper of van der Pol and van der Mark [114] to investigation of the circadian rhythm [5, 29], phase locking of respiration with a mechanical ventilator [67] or with locomotory rhythms [10], coordinated movement [29] and animal gaits [14], phase locking of chicken embrion heart cells with external stimuli and interaction of sinus node with ectopic pacemakers [29], synchronization of oscillations of human insulin secretion and glucose infusion [107], locking of spiking from electroreceptors of a paddlefish to weak external electromagnetic field [53], and synchronization of heart rate by external audio or visual stimuli [4].

The notion of synchronization is also related to several central issues of neuroscience (see, e.g., [103, 33, 34]). For instance, synchronization seems to be a central mechanism for neuronal information processing within a brain area as well as for communication between different brain areas. Another evidence is that synchronization of the oscillatory activity in the sensorimotor cortex may serve for the integration and coordination of information underlying motor control [50]. On the other hand, synchronization plays an important role in several neurological diseases like epilepsies [20] and pathological tremors [23, 19]. Correspondingly, it is important to analyze such synchronization processes to achieve a better understanding of physiological brain functioning as well as disease mechanisms.

4.1.1 Synchronization and analysis of bivariate data

Synchronization phenomena are abundant in the real world and biological systems, in particular. Thus, detection of synchronization from experimental data appears to be an important problem, that can be formulated as follows: Suppose we can obtain several signals coming from different simultaneous measurements (e.g., an electrocardiogram and respiratory movements, multichannel electro- or magnetoencephalography data, records of muscle activity, etc.). Usually it is known how to attribute these signals to different oscillating objects. The question is whether there are states (or epochs) where these objects oscillate in synchrony. Unfortunately, typically observed oscillations are highly irregular, especially in live systems, and therefore possible synchronization phenomena are masked by strong noise and/or chaos, as well as by nonstationarity.

This task is similar to a well-known problem in time series analysis: how to reveal the presence of an interdependence between two (or more) signals. The analysis of such bivariate data is traditionally done by means of linear cross-correlation (cross-spectrum) techniques [78] or nonlinear statistical measures like mutual information or maximal correlation [81, 77, 115].

Recently, different synchronization concepts of nonlinear dynamics have been used in studies of bivariate data. Schiff et al. [98] used the notion of dynamical interdependence [65] and applied the mutual prediction technique to verify the assumption that measured bivariate data originate from two synchronized systems, where synchronization was understood as the existence of a functional relationship between the states of two systems, called generalized synchronization. In our previous works [86, 90, 89, 111, 95, Appendices 4 and 5], we

proposed an ansatz based on the notion of phase synchronization; this implies existence of a relationship between phases of two weakly interacting systems, whereas the amplitudes may remain uncorrelated [85, 71, Appendix 1]. In our approach we assume that the measured bivariate data originate from two interacting self-oscillatory systems which may either be phase locked or oscillate independently.

Generally, we try to access the following problem: suppose we observe a system with a complex structure that is not known exactly, and measure two time series at its outputs (Fig. 4.1). Our goal is not only to find out whether these signals are dependent or not - this can be done by means of traditional statistical techniques - but to extract additional information on the interaction of some subsystems within the system. Obviously, we cannot consider the system under study as a "black box", but need some additional knowledge to support the assumption that the content of this "box" is complex, and we indeed encounter several subsystems, that generate their own rhythms, but are, probably, weakly coupled.

An advantage of our approach is that it allows to address rather weak interaction between the two oscillatory subsystems. Indeed, the notion of phase synchronization implies only some interdependence between phases, whereas the irregular amplitudes may remain uncorrelated. The irregularity of amplitudes can mask the phase locking so that traditional techniques treating not the phases but the signals themselves may be less sensitive in the detection of the systems' interrelation [86, 89].

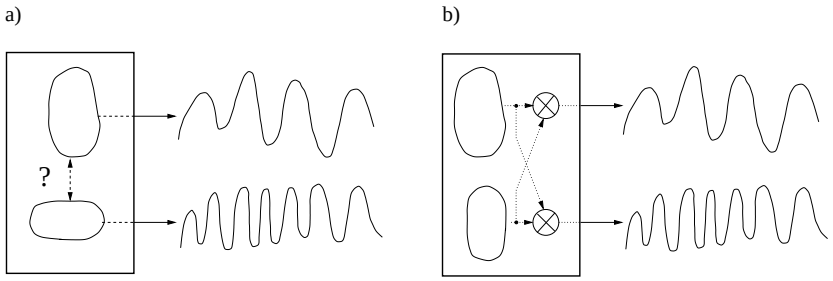

Figure 4.1: Illustration of the synchronization approach to analysis of bivariate data. The goal of the analysis is to reveal the presence of a weak interaction between two subsystems from the signals at their outputs only. The assumption made is that the data are generated by two oscillators having their own rhythms (a). An alternative hypothesis is a mixture of signals generated by two uncoupled systems (b).

To conclude this Section, we stress that the appearance of synchronization entails some relations between phases and frequencies of oscillators, but the inverse statement is strictly speaking not correct. Indeed, if a system is outside the synchronization region, but close to its border, then the distribution of the cyclic relative phase $\Psi_{n,m}(t)$ is also non-uniform, and the frequencies of oscillators are closer than those for non-interacting systems. Thus, the presence of a peak in the distribution of $\Psi_{n,m}(t)$ generally indicates the presence of some interaction only, but does not necessarily mean that the systems are synchronized. As we are not interested in determination of the borders of a synchronization

region, but are only searching for the presence of coupling, this fact does not influence interpretation of our results. We emphasize that interdependence of phases can results not only from coupling of self-sustained oscillators, capable to synchronize, but also due to such effects as modulation or stochastic resonance [51]. Hence, the interpretation of passive experiments must be made very carefully.

4.2 Estimating phases from data

Before we can analyze the relations between the phases of two oscillators, we have to estimate these phases from scalar signals. We have shown above how to define the phase for a periodic self-sustained system and for chaotic oscillations. Quite often, the phase of an oscillator can be determined if one can find a suitable projection of the phase space ensuring that all the trajectories rotate around some point that is taken as the origin. From this projection, the phase can be identified with the angle (with respect to an arbitrary direction) of the vector drawn from the origin to the corresponding point on the trajectory. Note that in this way we obtain a some non-uniformly rotating phase, what can essentially complicate the analysis. Another possibility is to construct a Poincaré map (stroboscopic map) and to define the phase according to (1.9).

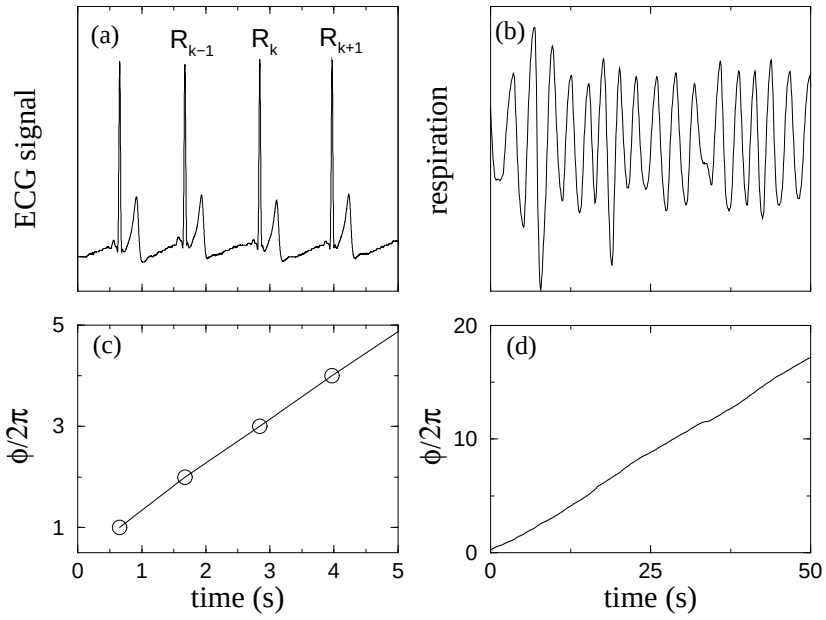

Figure 4.2: Short segments of (a) an electrocardiogram (ECG) with R-peaks marked and (b) of a respiratory signal; both signals are shown in arbitrary units. (c) Phase of the ECG computed according to Eq. (4.1) is a piece-wise linear function of time; the instants when the R-peaks occur are shown by circles. (d) Phase of respiration obtained via the Hilbert transform (Eq. (1.13)).

These two methods can be adapted for estimation of phases from experimental data. To explain the details, we consider a human electrocardiogram

(ECG) and a respiratory signal (air flow measured at the nose of the subject) as examples. An essential feature of the ECG is that every (normal) cardiocycle contains a well-pronounced sharp peak that can be with high precision localized in time; traditionally it is denoted as R-peak (Fig. 4.2a). The series of R-peaks can be considered as a sequence of point events taking place at times t_k, $k = 1, 2, \ldots$. Phase of such a process can be easily obtained. Indeed, the time interval between two R-peaks corresponds to one complete cardiocycle; therefore the phase increase during this time interval is exactly 2π. Hence, we can assign to the times t_k the values of phase $\phi(t_k) = 2\pi k$, and for arbitrary instant of time $t_k < t < t_{k+1}$

$$\phi(t) = 2\pi k + 2\pi \frac{t - t_k}{t_{k+1} - t_k} \ . \tag{4.1}$$

This method (see also [99]) can be applied to any process that contains distinct marker events and can therefore be reduced to the spike train. Determination of the phase via marker events in time series can be considered as the analogy to the technique of Poincaré section, although we do not need to assume that the system under study is a dynamical one.

Now we consider the respiratory signal (Fig. 4.2b); it reminds a sine-wave with slowly varying frequency and amplitude. Phase of such a signal can be effectively obtained by means of the *analytic signal concept*, see Section 1.2. Discussion of properties and practical implementation of the Hilbert Transform and analytic signal are given in Appendices to [91, 70].

An important practical question is: Which method should be chosen for analysis of particular experimental data? To address this problem we make the following remarks:

- If we define the phase of a system in order to characterize its frequency locking properties, then different methods (via the Poincaré section, from the two-dimensional projection of the phase space or from an oscillatory observable by means of the Hilbert transform) give similar results, at least if the system is a "good" one [71]. Although these phases vary microscopically, i.e., on the time scale less than one (quasi)period, the average frequencies obtained from these phases coincide, and it is exactly the frequencies what is primarily important for the description of synchronization. Therefore, theoretically all the definitions of the phase are equivalent. That is rarely the case in an experimental situation, where we have to estimate the phases from short, noisy and nonstationary records, so that numerical problems become a decisive factor.

- If the signal has very well-defined marker events, like the ECG, the Poincaré-map-technique is the best choice. It could be also applied to an "oscillatory" signal, like the respiratory one: here it is also possible to define the "events" (e.g., as the times of zero crossing) and to compute the phase according to Eq. (4.1). However, we do not recommend to do this: the drawback is that the determination of an event from the slowly varying signal is strongly influenced by noise and trends in the signal. Besides, we get only one event per quasiperiod, and if the record is short, then the statistics is poor. In such case the technique based on the Hilbert transform is much more effective because it provides the phase for every

point of the time series, so that we have a lot of points per quasiperiod and can therefore smooth out the influence of noise and obtain sufficient statistics for the determination of phase relationships.

Another important point is that even if we can unambiguously compute the phase of a signal, we cannot avoid the uncertainty in the determination of the phase of an oscillator.[1] The latter depends on the observable used; "good" observables provide equivalent phases (i.e., the average frequencies defined from these observables coincide). In an experiment we are rarely free in the choice of an observable. Therefore, one should always be very careful in formal application of the presented methods and in the interpretation of the results.

We emphasize, that even if the observable is good enough, the distribution of the *estimated* cyclic relative phase can essentially differ from that obtained from the distribution of the correct phase satisfying Eq. (1.9).

4.3 Detection of weak interaction: techniques and experimental examples

In this Section we on elaborate the techniques of phase relationship analysis and illustrate them by several examples. These techniques are based on the idea of synchronization and, therefore, we use the corresponding vocabulary, although generally speaking we can reveal only the presence of some interaction.

4.3.1 Straightforward analysis of phase difference: Application to posture control in humans

The simplest approach to look for synchronization is to plot the phase difference versus time and look for horizontal plateaus in this presentation. Generally, we have to plot the *generalized phase difference*

$$\varphi_{n,m} = n\phi_1 - m\phi_2 \ . \tag{4.2}$$

This straightforward method turned out to be quite effective in the analysis of model systems and some experimental data sets.

To illustrate this, we describe the results of experiments on posture control in humans [89]. During these tests a subject is asked to stay quietly on a special rigid force plate equipped with four tensoelectric transducers. The output of the setup provides current coordinates (x, y) of the center of pressure under the feet of the standing subject. These bivariate data are called stabilograms; they are known to contain rich information on the state of the central nervous system [31, 13, 26, 49]. Every subject was asked to perform three tests of quiet upright standing (3 minutes) with (i) eyes opened and stationary visual surrounding (EO); (ii) eyes closed (EC); (iii) eyes opened and additional video–feedback (AF). 132 bivariate records obtained from 3 groups of subjects (17 healthy persons, 11 subjects with an organic pathology and 17 subjects with a psychogenic pathology) were analyzed by means of cross-spectra and generalized

[1] We remind that although one can compute several phases from different observables of the same oscillator, there exist only one phase of that system corresponding to its zero Lyapunov exponent.

mutual information. It is important that interrelation between the body sway in anterior–posterior and lateral directions was found in pathological cases only. Another observation is that stabilograms can be qualitatively rated into two groups: noisy and oscillatory patterns. The latter appear considerably less frequently — only a few per cent of the records can be identified as oscillatory — and only in the case of pathology.

The appearance of oscillatory regimes in stabilograms suggests the excitation of self-sustained oscillations in the control system responsible for the maintenance of the constant upright posture; this system is known to contain several nonlinear feedback loops with time delay. From the other hand, the independence of the body sway in two perpendicular directions for all healthy subjects and many cases of pathology suggests that two separate subsystems are involved in the regulation of the upright stance. A plausible hypothesis is that when self-sustained oscillations are excited in both these subsystems, synchronization may take place. To test whether the interdependence of two components of a stabilogram may be due to a relation between their phases, we have performed the analysis of the phase difference.

Here we present the results for one trial (female subject, 39 years old, functional ataxia). We can see that in the EO and EC tests the stabilograms are clearly oscillatory (Figs. 4.3 and 4.4). The difference between these two records is that with eyes opened the oscillations in two directions are not synchronous during approximately the first 110 sec, but exhibit strong interrelation between phases during the last 50 sec. In the EC test, the phases of oscillations nearly coincide during all the time. The behavior is essentially different in the AF test; stabilograms represent noisy patterns, and no phase relation is observed. We emphasize, that the traditional techniques are not efficient to detect the cross-dependence of these signals because of the non-stationarity and insufficient length of the time series.

Remarks on the method

An important advantage of the straightforward phase analysis is that by means of $\varphi_{n,m}(t)$ plots one can trace transitions between qualitatively different regimes that are due to nonstationarity of parameters of interacting systems and/or coupling (Fig. 4.3). Noteworthy, this is possible even for very short records. Indeed, two different regimes that can be distinguished in Fig. 4.3 contain only about ten characteristic periods, i.e., these epochs are too short for reliable application of conventional methods of time series analysis.

A disadvantage of the method is that synchronous regimes of the order different from $n : m$, e.g., synchronization of order $n : (m + 1)$, appear in this presentation as nonsynchronous epochs. Besides, there exist no regular methods to pick up the integers n and m, so that they are usually found by trial and error. Respectively, in order to reveal all the regimes, one has to analyze a number of plots. In practice, the possible values of n and m can be estimated from the power spectra of the signals, or by computation of the frequencies along the recommendations given in the previous Section, and are often restricted due to some additional knowledge on the system under study.

Another drawback of this technique is that if noise is relatively strong, this method becomes ineffective and may be even misleading. Indeed, frequent phase slips mask the presence of plateaus and synchronization can be revealed only by

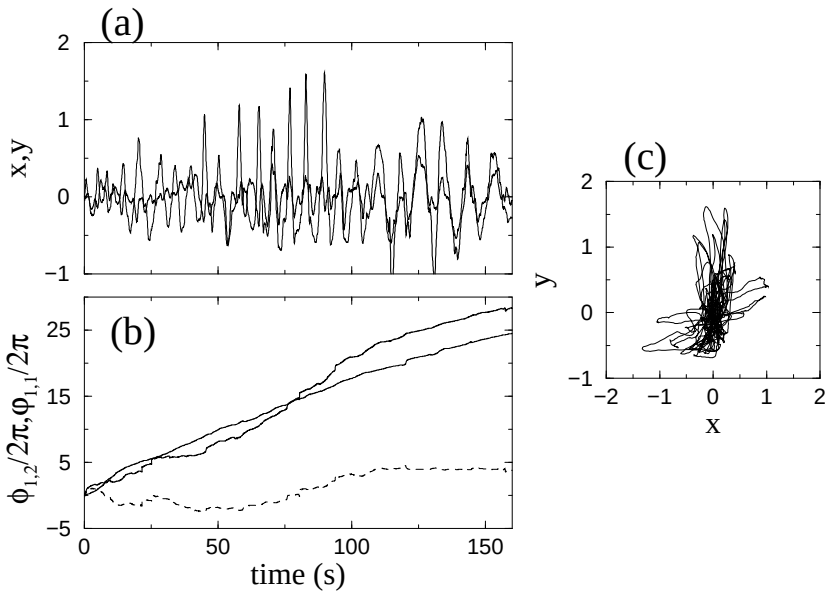

Figure 4.3: Stabilogram of a neurological patient. x (bold line) and y (solid line) represent the body sway while quiet stance with open eyes in anterior-posterior and lateral directions, respectively (a). The phases of these signals, and the phase difference are shown in (b) by bold, solid and dashed lines, respectively. The transition to a regime where the phase difference fluctuates around a constant is clearly seen at ≈ 110 sec. A typical plot of y vs. x shows no structure that could indicate the interrelation between the signals (c).

a statistical approach, e.g., by analysis of the distribution of the cyclic relative phase to be defined below.

4.3.2 Statistical analysis of phase difference: Application to brain activity

If the interacting oscillators are quasilinear then we can estimate the strength of the $n : m$ phase locking by comparing the distribution of the cyclic relative phase $\Psi_{n,m}(t) = (n\phi_1 - m\phi_2) \bmod 2\pi$ with the uniform distribution. For a single record this can be done by visual inspection, but in order to perform automatic analysis for large data sets or in order to trace the variation of the strength of interaction with variation of some parameter, we need quantitative criteria of synchronization. Quantitative characterization is also required for significance tests. To this end we introduce three $n : m$ *synchronization indices*:

(I) The synchronization index based on the Shannon entropy S of the phase difference distribution [111, Appendix 5]. Having an estimate p_k of the distribution of $\Psi_{n,m}$, we define the index ρ as

$$\rho_{n,m} = \frac{S_{max} - S}{S_{max}} \,, \tag{4.3}$$

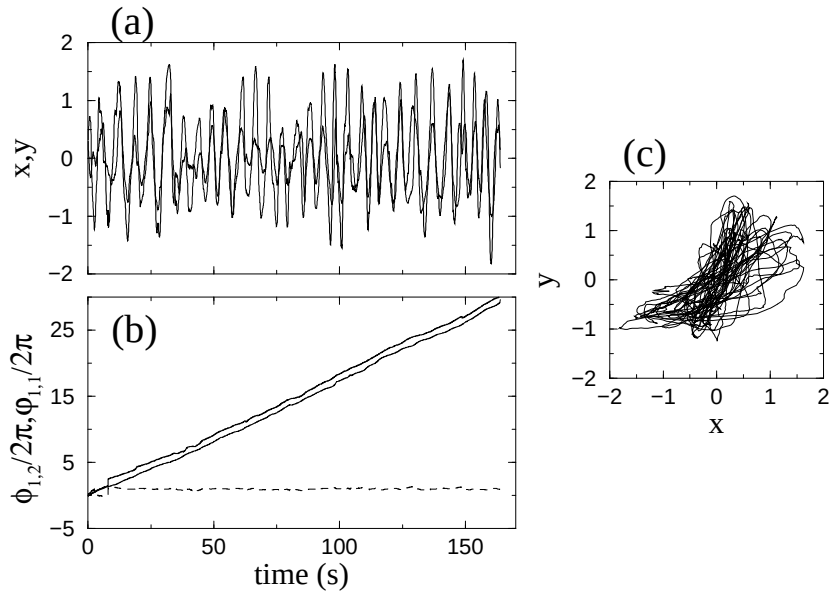

Figure 4.4: Stabilogram of the same patient as in the Fig. 4.3 obtained during the test with the eyes closed. All the notations are the same as in Fig. 4.3. From the phase difference one can see that the body sway in two directions are tightly related in phases within the whole test, although the amplitudes are irregular and essentially different.

where $S = -\sum_{k=1}^{N} p_k \ln p_k$, and the maximal entropy is given by $S_{max} = \ln N$; N is the number of bins and p_k is the relative frequency of finding $\Psi_{n,m}$ within the k-th bin.[2] Due to the normalization used,

$$0 \leq \rho_{n,m} \leq 1 \,, \tag{4.4}$$

whereas $\rho_{n,m} = 0$ corresponds to a uniform distribution (no synchronization) and $\rho_{n,m} = 1$ corresponds to a distribution localized in one point (δ-function). Such distribution can be observed only in the ideal case of phase locking of noise-free quasilinear oscillators.

(II) Intensity of the first Fourier mode of the distribution

$$\gamma^2_{n,m} = \langle \cos \Psi_{n,m}(t) \rangle^2 + \langle \sin \Psi_{n,m}(t) \rangle^2 \,, \tag{4.5}$$

where the brackets denote the average over time, can serve as the other measure of the synchronization strength; it also varies from 0 to 1. The advantage of this index is that its computation involves no parameters: we do not need to choose the number of bins as we do not calculate the distribution itself.

(III) If the oscillators are strongly nonlinear then the distribution of $\Psi_{n,m}(t)$ is non-uniform even in the absence of noise; this is essential if synchronization occurs via parametric action. In this case we need some other measure to

[2]The optimal number of bins can be estimated as $N = \exp[0.626 + 0.4 \ln(M-1)]$, where M is the number of samples [57].

characterize the strength of synchronization. For this purpose we recall the stroboscopic approach: we know that in the synchronous state the distribution of the stroboscopically observed phase is the δ-function; it is smeared in the presence of noise. Thus, for $n : m$ synchronization we have to characterize the distribution of

$$\eta = \phi_2 \bmod 2\pi n \,|_{\phi_1 \bmod 2\pi m = \theta} \ . \tag{4.6}$$

This means that we observe the phase of the second oscillator at the instants of time when the phase of the first one attains a fixed value θ (phase stroboscope). To account for the $n : m$ locking, the phases are wrapped into intervals $[0, 2\pi m]$ and $[0, 2\pi n]$, respectively. Repeating this procedure for all $0 \le \theta < 2\pi$ and averaging, we get a statistically significant synchronization index [111, Appendix 5].

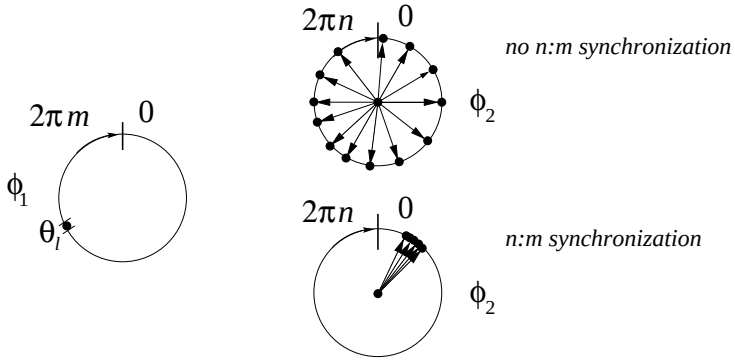

Figure 4.5: Synchronization index based on the conditional probability. Phase of the second oscillator ϕ_2 wrapped in the interval $[0, 2\pi n]$ is observed stroboscopically, i.e. when phase of the first oscillator ϕ_1 is found in the certain bin θ_l of the interval $[0, 2\pi m]$. If there is no synchronization then the stroboscopically observed ϕ_2 is scattered over the circle, otherwise it groups around some value. The sum of the vectors pointing to the position of the phase on the circle provides a quantitative measure of synchronization.

Practically, if we deal with the time series, we can introduce binning for the phase of the first oscillator, i.e. divide the interval $[0, 2\pi m]$ into N bins. Next, we denote the values of $\phi_1 \bmod 2\pi m$ falling into the l-th bin as θ_l and the number of points within this bin as M_l. Then, with the help of Eq. (4.6) we compute M_l corresponding values $\eta_{i,l}$, where $i = 1, \ldots, M_l$. If the oscillators are not synchronized, then we expect $\eta_{i,l}$ to be uniformly distributed on the interval $[0, 2\pi n]$, otherwise these quantities group around some value and their distribution is unimodal (Fig. 4.5). To quantify it, we compute

$$\Lambda_l = M_l^{-1} \sum_{i=1}^{M_l} \exp\left[\imath(\eta_{i,l}/n)\right] \ . \tag{4.7}$$

The case of complete dependence between both phases corresponds to $|\Lambda_l| = 1$, whereas $|\Lambda_l|$ vanishes if there is no dependence at all. To improve the statistics,

we average over all N bins and get the synchronization index

$$\lambda_{n,m} = N^{-1} \sum_{l=1}^{N} |\Lambda_l| \ . \tag{4.8}$$

According to the definition above $\lambda_{n,m}$ measures the conditional probability for ϕ_2 to have a certain value provided ϕ_1 is in a certain bin.

Comparison of these three indices using the simulated data was performed in [91]. We stress here two points. First, the indices are nonzero outside the synchronization region. It is not surprising: we have noted already that the distribution of the cyclic phase outside the region also has a peak. Thus, we can reveal the presence of interaction even if it is too weak to induce synchronization. Second, in case of frequency modulation in the signals, the conditional probability index is definitely superior over two other indices.

Human brain activity during pathological tremor

Here we briefly present the results of the investigation of phase synchronization between different brain areas, as well as between brain and muscle activity in Parkinsonian patients by means of noninvasive measurements [111, 110, Appendix 5]. The goal of the study was to find out whether synchronization between different cortical areas is involved in the generation of pathological tremor.

The neuronal activity of the human brain was noninvasively assessed by registering the magnetic field outside the scull by means of multichannel magnetoencephalography (MEG). In addition to the MEG, the electromyogram (EMG) from two antagonistic muscles exhibiting tremor activity, namely the right flexor digitorum superficialis muscle (RFM) and the right extensor indicis muscle (REM), was registered by standard techniques.

The phase analysis was performed in the following way. First, the instantaneous phases of signals were obtained by means of the Hilbert transform. Next, one signal was taken as the reference one, and phase locking between this channel and all others was studied in pairs. To cope with nonstationarity, a sliding window analysis was done and the distribution of $\Psi_{n,m}$ was computed for every time point t within the window $[t-T/2, t+T/2]$ and characterized by means of the synchronization indices ρ and λ.[3] The window length T was varied between 2 and 20 s; the results are robust with respect to this variation. In search of *corticomuscular* synchronization (CMS), an EMG signal was taken as a reference signal. Investigation of *cortico-cortical synchronization* (CCS) was done by choosing for reference one of the MEG channels over the left sensorimotor cortex.

It was found that tremor activity reflects the time course of cortico-cortical synchronization. Another important observation is that the onset of CCS precedes initiation of the tremor. Moreover, the phase analysis allows to localize the brain areas with MEG activity phase locked to tremor activity from noninvasive measurements (Fig. 4.6). The main focus of the $1:2$ synchronization is located over the contralateral sensorimotor cortex. Additionally, this type of locking is observed over premotor, frontal, contralateral parietal and contralateral temporal areas. In contrast to the $1:2$ locking, the $1:1$ synchronization is

[3] Computation of both indices gives consistent results.

much weaker, and is observed over contralateral sensorimotor, parieto-occipital and frontal areas. All areas which are $1:2$ locked with the tremor are also $1:1$ locked among each other.

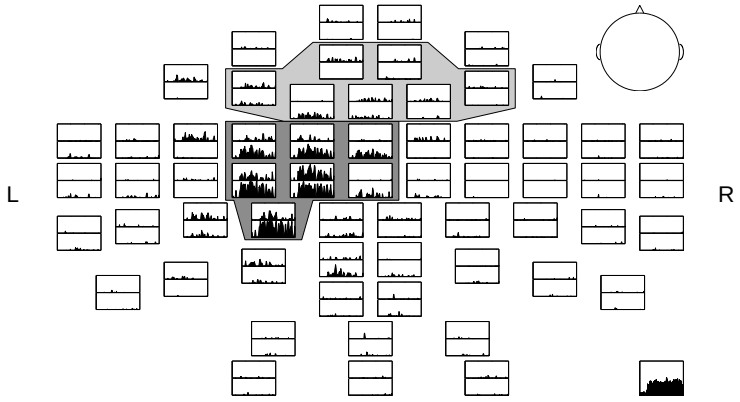

Figure 4.6: Time dependence of the synchronization index $\rho_{1,2}$ characterizing $1:2$ locking between the EMG of the right flexor muscle (reference channel, plotted in the lower right corner) and all MEG channels. Each rectangle corresponds to an MEG sensor; time axis spans 310 s and y-axis scales from 0 to 0.25. The head is viewed from above, 'L' and 'R' mean left and right (see the "head" in the upper right corner). The upper and lower gray regions corresponds to premotor and contralateral sensorimotor areas respectively. The results are similar for the extensor muscle.

4.3.3 Stroboscopic technique: Application to cardiorespiratory interaction

In this Section we present the synchronization analysis of cardiorespiratory interaction in humans. The data we analyze, namely electrocardiogram (ECG) and respiratory signal, were already introduced in Fig. 4.2. The complexity of this case is related to the following features:

- the time series have essentially different forms (respiration is a narrow-band signal, while ECG can be reduced to the spike train);
- the characteristic time scales of two signals are different (there are always several heartbeats per respiratory cycle) and vary essentially within one experimental record; therefore we expect (and we indeed observe it) synchronization of some high order $n:m$ and transitions between different synchronous states;
- synchronization is probably related to modulation of the heart rate by respiration, so that stroboscopic methods suitable for the detection of $n:m$ locking from nonstationary data are required.

These features make the problem a very useful example for comparison of different analysis techniques.

Phase stroboscope (Cardiorespiratory synchrogram)

First we present a graphic tool based on the stroboscopic technique. With this method, the phase of the driven oscillator is observed with the period of external force, $\phi_k = \phi(t_0 + k \cdot T)$, where $k = 1, 2, \ldots$ and t_0 is the (arbitrary) time of the first observation. If the oscillator is entrained, the distribution of the ϕ_k is a δ-function, if the oscillator is periodic, and it is narrow, if the oscillator is noisy or chaotic. Non-synchronous state implies that the stroboscopically observed phase attains an arbitrary value, and its distribution is therefore broad.

A simple generalization makes this technique a very effective tool of time series analysis. To this end, we consider two coupled oscillators and observe the phase of one oscillator not periodically in time, but periodically (with the period 2π) in phase of the other oscillator. In other words, we pick up ϕ_{1k} at the moments when $\phi_2(t) = \phi_0 + 2\pi \cdot k$. We refer to this technique as to the *phase stroboscope*. Obviously, if the second oscillator is periodic, the phase and the time stroboscopes are equivalent. Certainly, it does not matter which oscillator is taken as the reference one (second in our notation); the choice solely depends on the convenience of the phase determination. In the rest of this Section we explain and illustrate how the stroboscopic technique can be used for the detection of interaction (provided that we know that the signals originate from interacting self-sustained oscillators) in case when the frequencies of the signals obey $n\Omega_1 \approx m\Omega_2$, or, generally, for detection of complex relations between the phases of two signals.

Suppose first that we deal with two $n : 1$ synchronized oscillators that generate signals like shown in Fig. 4.2 and let n spikes[4] of the fastest signal occur within one cycle of the slow one, i.e., there is a $n : 1$ locking. Then we expect to find the spikes at n different values of the phase of the slow signal. A similar picture can be observed if there is no synchronization, but one process is modulated by the other one. Therefore, in a particular experiment, we can use this idea to reveal complex interaction, but cannot distinguish between synchronization and modulation.

It is natural to observe the phase of the slow signal at the times of spiking. Thus, we plot the stroboscopically observed cyclic phase $\psi(t_k) = (\phi_1(t_k) \bmod 2\pi)/2\pi$ versus time and call such a plot a *synchrogram*. Presence of interaction is reflected by the occurrence of n stripes in this presentation.

The final step is to extend the stroboscopic technique to the general case of $n : m$ locking. Suppose again that we observe one oscillator, whenever the phase of the second one is a multiple of 2π. Then, if interaction is present, we expect to make n observations within m cycles of the first oscillator. To construct a synchrogram we have to distinguish somehow the phases within m adjacent cycles. For this purpose we make use of the fact that phase can be defined either on a circle, i.e., from 0 to 2π, or on the real line. We often intermingled these two definitions, and the range of the phase variation was clear from the context. Now we perform the following trick: we take the unwrapped (i.e., infinitely growing) phase and wrap it on the cycle $[0, 2\pi m]$. In this way we consider m cycles as one cycle, and then proceed as before, plotting $\psi_m(t_k)$ versus time (Fig. 4.7); the index m indicates how the phase was wrapped. Note that only

[4] If there were no spikes, we can define the events as, say, zero crossing in one direction. In other words, we have to define the instants when the phase of the fastest oscillator attains some fixed value.

the value of m should be chosen by trial and error, and different epochs, say with approximate frequency ratios $n : m$ and $(n + 1) : m$, can be seen within one synchrogram.

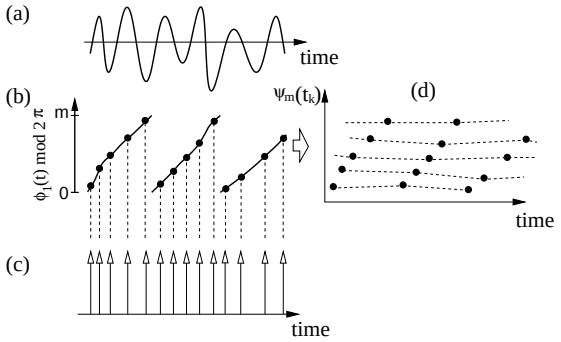

Figure 4.7: Principle of the phase stroboscope, or synchrogram. Here a slow signal (a) is observed in accordance with the phase of a fast signal (c). Measured at these instants, the phase ϕ_r of the slow signal wrapped modulo $2\pi m$, (i.e., m adjacent cycles are taken as a one longer cycle) is plotted in (d); here $m = 2$. In this presentation $n : m$ phase synchronization shows up as n nearly horizontal lines in (d); similar picture appears in the case of modulation.

Cardiorespiratory interaction

Interaction between human cardiovascular and respiratory systems was intensively studied. Although it is well-known that these systems do not act independently [43] and in spite of early communications in the medical literature (that often used different terminology) [108, 21, 66, 37, 79, 80], in the biological physics community these two systems were often considered to be not synchronized. So, an extensive review of previous studies of biological rhythms led to the conclusion that "there is comparatively weak coupling between respiration and the cardiac rhythm, and the resulting rhythms are generally not phase locked" (see [29], page 136). Recently, the interaction of these vital systems attracted attention of several physics groups, and synchronization during paced respiration [97, 102] was investigated. Here, as well as in Refs. [108, 66, 37, 97, 102] only synchronous states of orders $n : 1$ (n heartbeats within 1 respiratory cycle) were found due to limitation of the *ad hoc* methods used for the analysis of data. In our recent work [95, 96, 52, Appendices 4 and 6] we have reported on cardiorespiratory synchronization under free-running conditions in two groups of subjects: young athletes and healthy newborns. The proposed analysis technique allows to find out synchronous epochs of different orders $n : m$ by means of synchrograms (see an example in Fig. 4.8) as well as fully automatically, by means of stroboscopic synchronization index [52, Appendix 6]. Cardiorespiratory synchrogram was also used in [11, 104], where cardiorespiratory interaction in healthy relaxed subjects (non-athletes) and in rats during anesthesia was analyzed.

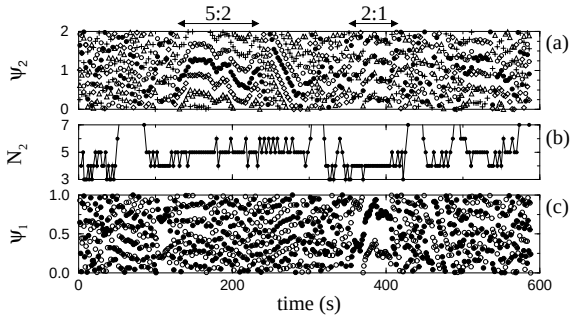

Figure 4.8: An example of alternation of interaction with approximate frequency relations $2:1$ and $5:2$ between heart rate and respiration of a healthy baby. (a) Two adjacent respiratory cycles are taken as one cycle. Therefore, epochs of $2:1$ and $5:2$ relation between phases appear as 4- and 5-lines patterns. (b) Plot of the number of heartbeats within two respiratory cycles N_2 also indicates epochs of interdependence. (c) If the respiratory phase is wrapped modulo 2π then only $2:1$ relation is seen. The data points are shown by different symbols in cyclic order (5 and 2 symbols in (a) and (c), respectively) for better visual impression.

4.3.4 Discussion

Is it really synchronization?

An important issue is interpretation of the results of the phase analysis. Here we have to be aware of two problems:

- Can we be sure that the patterns of the relative phase, described in the sections above, indeed indicate synchronization, and, respectively, underlying nonlinear dynamics?
- How reliable is this indication?

Before we address these questions, we remind that the synchronization transition in noisy systems is smeared. Next, as we already stressed, the relation between phases indicates, strictly speaking, the presence of interaction between systems, but not necessarily means that they are synchronized. Finally, our synchronization approach to data analysis is based on certain assumptions that might be not always fulfilled. All in all, we can never unambiguously state that we have observed synchronization; nevertheless, strong indications in favor of such a conclusion can be sometimes found.

As synchronization is not *a state, but a process* of adjustment of rhythms due to interaction, we cannot validate its existence if we do not have access to the system parameters and cannot check experimentally that the synchronous state is stable towards variation of the parameter mismatch within a certain range (i.e., if we cannot plot the frequency vs. detuning curve). If we are not able to do such experiments, but just have some data sets registered under free-running conditions, the only way to get some confirmation (but certainly not a proof) on the existence of synchronization is to make use of the fact that the data are nonstationary. Indeed, we can trace the variation of the

instantaneous frequencies of both signals and their relation with time. If we find some epochs, as in the case of cardiac and respiratory data, where both frequencies vary, but their relation remains stable (example of such epoch in context of cardiorespiratory interaction is given in [91]), this can be considered as a strong indication in favor of our conclusion.

Another indication that also can be obtained using the fact of nonstationarity of the data is the presence of several different $n : m$ epochs within one record. Indeed, one can argue that observed phase or frequency locking of, e.g. order $3 : 1$, could be due to the coincidence of frequencies of the uncoupled systems. Nevertheless, occasional coincidence of frequencies having the ratios exactly corresponding to neighboring Arnold tongues seems to be very unlikely.

If the data are rather stationary and we are not able to find such epochs, the situation is more difficult. Suppose that the distribution of the relative phase for such a bivariate record is non-uniform. Can it just happen due to an occasional coincidence of frequencies? From the theory and the simulation of model examples we know that even if the frequencies of uncoupled oscillators are equal, the distribution of $\Psi_{n,m}$, computed on a sufficiently long time scale, has to be nearly uniform due to the diffusion of the phase. Certainly, occasionally one can find short epochs where phases seem to be locked. How can we estimate what is "short" and "long" in this context?

From the first sight, a natural way to address this problem is to use the surrogate data techniques [59, 102]. However, we see some serious problems in this approach. The usual formulation of the null hypothesis that is used for nonlinearity tests is to consider a Gaussian linear process [112] with a power spectrum that is identical to that of the tested signal; more sophisticated methods [101] imply also preservation of the probability distribution. A modification of this null hypothesis for the tests for synchronization — a consideration of two surrogate signals that preserve the linear cross-correlation between the original data — seems to be not sufficient. Indeed, due to the definition of synchronization, we are interested in the relation between instantaneous phases, whereas the variations of amplitudes and their interrelation are of no importance. The usual way to construct surrogates (the randomization of Fourier phases) *mixes the phase and amplitude properties*, transforming the variation of instantaneous phase into the variation of instantaneous amplitude and vice versa. Moreover, the signals generated by self-sustained oscillators possess certain properties of the distribution of instantaneous amplitudes (see [48] and references therein), and this distribution is destroyed by the Fourier phase randomization.

Although we cannot give a general recipe how to estimate the reliability of phase analysis, some empirical methods can be used in particular experiments. So, in the above described MEG study [111, 110, Appendix 5] the surrogates were constructed by taking either white noise or empty room measurements (instrumental noise) and filtering them with the same band-pass filter as the data. The 95th percentile of the distribution of a synchronization index for surrogates was taken as the significance level. Afterwards, the synchronization indices were re-calculated in accordance to this level, e.g. $\rho_{n,m} \to \max\{\rho_{n,m} - \tilde{\rho}, 0\}$, where $\tilde{\rho}$ is the significance level.

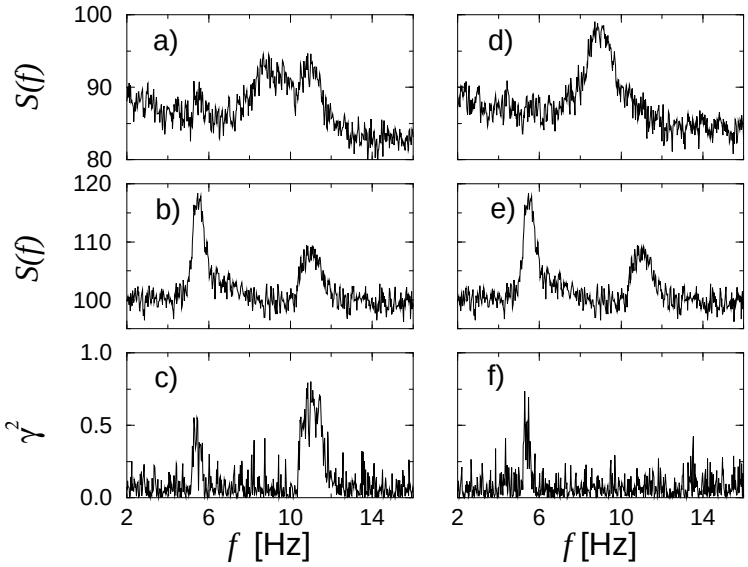

Figure 4.9: Results of the cross-spectral analysis of two pairs of signals. The autospectra of a channel characterizing the sensorimotor and muscle activities and the coherence function are shown in (a), (b), and (c), respectively. The same is shown in (d), (e) and (f) for a channel over the right temporal cortex. (The spectrum of the EMG is repeated in (e) for convenience). It is seen that both MEG channels are coherent with the muscle activity, whereas only one channel is synchronized with it.

Synchronization versus coherence

A very important problem is the difference between our synchronization approach and traditional correlation (coherence) analysis. Coherence is widely used in neuroscience as a standard tool for the detection of interaction [55]. However, since the coherence analysis does not separate the phase and amplitude dynamics but treats the signals themselves, it addresses different aspects of systems interaction as compared to the phase synchronization analysis. This is illustrated in Fig. 4.9.

4.4 Identification of coupling direction from data

In this Section we discuss experimental detection of directionality of weak coupling between two self-sustained oscillators from bivariate data [84, 88, Appendix 7]. The algorithms we present provide directionality index that shows whether the coupling between the oscillators is unidirectional or bidirectional and quantifies the asymmetry of bidirectional coupling. These techniques are applied to analysis of cardiorespiratory interaction in healthy infants. The results reveal that the direction of coupling between cardiovascular and respiratory systems varies with the age within the first 6 months of life: we find a tendency to change from nearly symmetric bidirectional interaction to nearly unidirectional one (from respiration to the cardiovascular system).

Estimation of interdependence between two time series is a traditional problem of signal processing. Widely used tools like cross-spectra [57], mutual information [77] or maximal correlation [115] provide *symmetric* measures and are therefore not suitable for evaluation of *causality* in interrelation. The latter issue was addressed in recent studies, where one can outline two main approaches. One approach, based on the information theory, used entropy measures [100]. A second approach, arising from studies of generalized synchronization, exploited the idea of mutual predictability: it quantified the ability to predict the state of the first system from the knowledge of the second one [98]. While both approaches are rather complicated to implement and interpret, neither requires any assumptions on the systems under investigation. On the contrary, the approach to analysis of causality, or directionality of interaction, presented here, is explicitly based on the assumption that experimentalists deal with weakly interacting self-sustained oscillators. In this particular, but pretty often encountered case the direction of coupling can be efficiently quantified.

The main idea is to use the fact that weak coupling affects the phases of interacting oscillators, whereas the amplitudes remain practically unchanged. Hence, the dynamics can be reduced to those of two phases $\phi_{1,2}$:

$$\dot{\phi}_{1,2} = \omega_{1,2} + \varepsilon_{1,2} f_{1,2}(\phi_{2,1}, \phi_{1,2}) + \xi_{1,2}(t) \; . \tag{4.9}$$

Here, random terms $\xi_{1,2}$ describe noisy perturbations that are always present in real-world systems; small parameters $\varepsilon_{1,2} << \omega_{1,2}$ characterize the strength of the coupling. Equations (4.9) describe also the phase dynamics of coupled continuous-time chaotic systems; in this case $\xi_{1,2}$ are irregular terms that reflect the chaotic nature of amplitudes. The fact that the regular component of the phase dynamics is two-dimensional, essentially simplifies detection of the asymmetry in interaction. Functions $f_{1,2}$ are 2π-periodic in both arguments and combine the description of the phase dynamics of autonomous (uncoupled) systems and the coupling between them. If the coupling is bidirectional, f_1 and f_2 depend on both ϕ_1 and ϕ_2. In case of unidirectional driving, say from system number 1 to system number 2, $f_1 = f_1(\phi_1)$, whereas $f_2 = f_2(\phi_1, \phi_2)$ is the function of two arguments.

In the following discussion of the algorithms, we assume that the time series of phases are known. Practically, the phases $\phi_{1,2}(t_k)$, $t_k = k \cdot \Delta t$, $k = 1, 2, \ldots$, where Δt is the sampling interval, can be estimated from the experimental data as discussed above.

4.4.1 Evolution map approach

Here we briefly describe the technique introduced in [84], we call it the EMA. Let us consider increments of phases during some fixed time interval τ:

$$\Delta_{1,2}(k) = \phi_{1,2}(t_k + \tau) - \phi_{1,2}(t_k) \; ; \tag{4.10}$$

τ is the only parameter of the algorithm. Note that the phases are unwrapped, i.e. not reduced to the interval $[0, 2\pi)$; hence $\Delta_{1,2}$ can be larger than 2π. These increments can be considered as generated by some unknown two-dimensional noisy map

$$\Delta_{1,2}(k) = \omega_{1,2}\tau + \mathcal{F}_{1,2}\left(\phi_{2,1}(t_k), \phi_{1,2}(t_k)\right) + \eta_{1,2}(t_k) \; . \tag{4.11}$$

The deterministic parts $\mathcal{F}_{1,2}$ of the map can be estimated from the time series $\Delta_{1,2}(k)$ and $\phi_{1,2}(k)$. For this purpose, we fit (in the least mean square sense) the dependencies of Δ_1 and Δ_2 on ϕ_1, ϕ_2. As the phases are cyclic variables, the natural choice of the probe function is a finite Fourier series, $F_{1,2} = \sum_{m,l} A_{m,l} e^{im\phi_1 + il\phi_2}$. Note that fitting also filters out the noise. A similar procedure was used for noise reduction in discrete dynamical systems [75] and (with $\tau \to 0$) for extracting model equations from experimental noisy data [24].

From the smooth functions $F_{1,2}$ obtained via approximation one can compute the measures $c_{1,2}$ of the cross-dependencies of phase dynamics of two systems:

$$c_{1,2}^2 = \int\int_0^{2\pi} \left(\frac{\partial F_{1,2}}{\partial \phi_{2,1}} \right)^2 d\phi_1 \, d\phi_2 \; . \tag{4.12}$$

Finally, the *directionality index* is introduced as

$$d^{(1,2)} = \frac{c_2 - c_1}{c_1 + c_2} \; . \tag{4.13}$$

Normalized in this way, the index varies from 1 in the case of unidirectional coupling ($1 \to 2$) to -1 in the opposite case ($2 \to 1$) with intermediate values $-1 < d^{(1,2)} < 1$ corresponding to bidirectional coupling. Note that the index is an integrated measure of how strong each system is driven and of how sensitive it is to the drive.

To understand exactly how the asymmetry in coupling is characterized by the index d, i.e., how d is related to the parameters of the model equation (4.9), we estimate the deterministic components $\Delta_{1,2}$ of the phase increase within the interval τ. As follows from (4.9), in the absence of noise, we obtain for small $\varepsilon_{1,2}$

$$\Delta\phi_{1,2} \approx \omega_{1,2}\tau + \varepsilon_{1,2} \int_0^\tau f_{1,2}(\phi_{2,1}, \phi_{1,2}) dt = \omega_{1,2}\tau + \mathcal{F}_{1,2}(\phi_{2,1}, \phi_{1,2}) \; . \tag{4.14}$$

So, for a particular (but rather common) case of antisymmetric coupling function $f_1(\phi_2, \phi_1) = -f_2(\phi_1, \phi_2)$, we obtain from (4.12) $c_{1,2} = a\varepsilon_{1,2}$, where the constant a is determined by the integral in (4.14). In general case the coefficients $c_{1,2} = a_{1,2}\varepsilon_{1,2}$, where $a_1 \neq a_2$, reflect also the difference in coupling functions $f_{1,2}$. Thus, the directionality index d characterizes the asymmetry in coupling but does not incorporate the difference in the frequencies of autonomous systems.

4.4.2 Instantaneous period approach

Let us now compute the time needed for the phase $\phi_{1,2}(t_k)$ to increase by 2π; in other words we compute the instantaneous periods, or Poincaré return times, for all k.[5] Obviously, for uncoupled noisy and/or chaotic systems the return times fluctuate around a constant (mean period), $T_{1,2}(k) = T_{1,2}^0 + \eta_{1,2}(t_k)$, while for coupled systems $T_{1,2}(k) = T_{1,2}^0 + \Theta_{1,2}(\phi_{2,1}(t_k), \phi_{1,2}(t_k)) + \eta_{1,2}(t_k)$.

[5] Practically, for discrete data, this can be done in the following way. For any t_k we find t_j such that $\phi(t_j) \leq \phi(t_k) + 2\pi$ and $\phi(t_{j+1}) > \phi(t_k) + 2\pi$. Then t' correspondent to $\phi = \phi(t_k) + 2\pi$ is obtained via interpolation between t_j and t_{j+1}. If the sampling rate is high, simple linear interpolation suffices, otherwise spline interpolation (using several points around t_j) is recommended; this procedure also reduces the effect of noise.

The deterministic component $\Theta_{1,2}$ of this dependence can be again found by fitting a Fourier series, and the cross-dependencies of T_1 on ϕ_2 and of T_2 on ϕ_1 can be characterized in the same way as above, by computing coefficients $c_{1,2}$ from partial derivatives of $\Theta_{1,2}$ with respect to $\phi_{2,1}$, similarly to Eq. (4.12). Then, the new directionality index $r^{(1,2)} = (c_2 - c_1)/(c_2 + c_1)$ is computed (cf. Eq. (4.13)). An important advantage of the proposed algorithm is the absence of parameters.

Now we show that this algorithm provides different characterization of asymmetry than EMA. Indeed, for weak coupling, $\varepsilon_{1,2} << \omega_{1,2}$, the deterministic component of the instantaneous period T_1 can be estimated from (4.9) as

$$\begin{aligned} T_1(\phi_1,\phi_2) &= \int_{\phi_1}^{\phi_1+2\pi} \frac{d\phi'}{\omega_1 + \varepsilon_1 f_1(\phi_2,\phi')} \\ &= \frac{1}{\omega_1}\int_{\phi_1}^{\phi_1+2\pi} \frac{d\phi'}{1+\frac{\varepsilon_1}{\omega_1} f(\phi_2,\phi')} \\ &= \frac{2\pi}{\omega_1} - \frac{\varepsilon_1}{\omega_1^2}\int_{\phi_1}^{\phi_1+2\pi} f(\phi_2,\phi')d\phi' \\ &= T_1^0 + \Theta_1(\phi_2,\phi_1)\ , \end{aligned} \tag{4.15}$$

and similarly for T_2. Clearly, for coupling functions satisfying $f_1(\phi_2,\phi_1) = -f_2(\phi_1,\phi_2)$, this algorithm provides $c_{1,2} = a\varepsilon_{1,2}/\omega_{1,2}^2$. Hence, directionality index r reflects not only asymmetry in coupling coefficients $\varepsilon_{1,2}$ and asymmetry in coupling functions $f_{1,2}$, but also in natural frequencies $\omega_{1,2}$.

4.4.3 Mutual prediction approach

As already mentioned, mutual prediction is used for estimation of causal relations in the methods based on the concept of generalized synchronization. These methods imply existence of a functional relationship between the (phase) states of two systems; such a relation arises due to a comparatively strong coupling. We exploit here a different understanding of mutual prediction, and this allows us to assess a weaker interaction. Namely, we look whether the predictability of, say, first time series can be improved by the knowledge of the second signal. A similar concept, initially introduced by C. Granger, was very recently used by several groups [117].[6] The main distinction of our approach is that we work with phases, not raw signals.

Thus, we take one series, say, $\phi_1(t_k)$, and use some scheme to predict a future of its points. For the kth point we compute the *univariate prediction error* $E_1(t_k) = |\phi_1'(t_k) - \phi_1(t_k+\tau)|$, where $\phi_1'(t_k)$ is the τ-step ahead prediction of the point $\phi_1(t_k)$; remember that phases are unwrapped. Next, we repeat the prediction for $\phi_1(t_k)$, but this time we use both signals ϕ_1, ϕ_2 for construction of the predictor. In this way we obtain the *bivariate prediction error* $E_{12}(t_k)$. If system 2 influences the dynamics of system 1 then we expect $E_{12}(t_k) < E_1(t_k)$, otherwise (for sufficient statistics) $E_{12}(t_k) = E_1(t_k)$. The root mean squared

[6] Also: U. Feldmann and J. Bhattacharya, presentation at the 6th Experimental Chaos Conference; B. Schack and M. Arnold, private communication.

$E_1(t_k) - E_{12}(t_k)$, computed over all possible k and denoted by I_{12}, quantifies the *predictability improvement* for the first signal. This measure characterizes the degree of influence of the second system on the first one. Computing in the same way I_{21}, we end with the directionality index

$$p^{(1,2)} = \frac{I_{21} - I_{12}}{I_{12} + I_{21}} \ . \tag{4.16}$$

Particularly, we use simple prediction scheme, due to the low dimension of the phase dynamics [88, Appendix 7]. We emphasize that the MPA does not directly use the assumption of weakly coupled oscillators; generally, it can be applied to arbitrary signals. If the assumption of weak coupling is correct, then the choice of phases is crucial as these variables are mostly sensitive to the coupling.

To summarize this Section, we emphasize two points. First, it is clear that all methods fail if oscillators synchronize. Indeed, in this case $\phi_{1,2}$ are functionally related, and no information on the coupling direction can be obtained.[7] Practically it means that the points on the (ϕ_1, ϕ_2) torus collapse to a line, and the approximation procedure fails. Thus the direction of interaction can be revealed if the coupling is too weak in order to induce mode locking (i.e., in the quasiperiodic state) or the noise in the system is strong enough to cause large deviations from the synchronous state. If the noisy systems are close to a synchronous state, the points on the torus form a band with some (rare) excursions from it. In this case the described global approximation procedures, i.e., EMA and IPA, are not efficient and a scheme based on local approximation is required. Next, we emphasize that there is no unique way to quantify the directionality in case of bidirectional coupling; different methods can therefore give non-coinciding characteristics (e.g., d and r indices do not coincide). The choice of a quantification measure is to large extent a matter of taste.

[7] Indeed, for the simplest case of sine coupling function, $f_{1,2} = \sin(\phi_{2,1} - \phi_{1,2})$, in the synchronous regime the constant phase difference is $\phi_2 - \phi_1 = \arcsin \dfrac{\omega_2 - \omega_1}{\varepsilon_2 + \varepsilon_1}$, and we cannot extract information on $\varepsilon_{1,2}$ separately.

Chapter 5

Conclusions

1. It is demonstrated that synchronization phenomena in periodic, noisy and chaotic oscillators can be understood within a unified framework. This is achieved by extending the notion of phase to the case of continuous-time autonomous chaotic systems. Phase is introduced as a variable corresponding to the zero Lyapunov exponent.

   (a) If the system admits construction of a Poincaré map, then, for each piece of a trajectory between two cross-sections with the Poincaré surface of section, the phase is defined as linear function of time, so that it gains 2π with each return to the surface of section. The method can be adopted to phase estimation from scalar experimental signals.

   (b) The phase can be efficiently estimated from such a projection of the strange attractor, where all the trajectories rotate around the origin, as the polar angle in this projection. The phase can also be estimated from an oscillatory observable by means of the Hilbert Transform.

2. A chaotic oscillator can be $n : m$ entrained by a weak external force; two nonidentical oscillators can synchronize due to a weak coupling. These effects can be described in terms of phases and corresponding mean frequencies. Synchronization properties of chaotic systems are qualitatively similar to those of noisy oscillators. Depending on the distribution of the Poincaré return times chaotic system can synchronize like a limit cycle oscillator with bounded or unbounded noise (respective examples are the Rössler and the Lorenz systems). In the former case there is a range of parameter mismatch where frequencies are perfectly locked and the phase difference between the oscillators fluctuates around a constant; outside synchronization region the phase dynamics are intermittent.

3. Transition to phase synchronization is reflected in the spectrum of Lyapunov exponents: one of the zero Lyapunov exponents of the combined system becomes negative what corresponds to the stability of the phase difference. Two positive Lyapunov exponents remain positive, reflecting the irregularity of chaotic amplitudes; the latter are practically uncorrelated in the state of phase synchronization. Thus, phase synchronization transition is a transition within hyperchaos.

4. Ensembles of nonidentical chaotic oscillators exhibit Kuramoto self-synchronization transition. This is observed even for systems with ill-defined phase. Synchronization is also possible in chains of nonidentical nearest-neighbor coupled oscillators. Depending on the parameter mismatch, synchronization transition in chains occurs either smoothly or via formation of clusters.

5. Coupled nonidentical chaotic oscillators (e.g., Rössler systems) can exhibit effect of lag synchronization. If the coupling is increased beyond the threshold of phase synchronization, the amplitudes become dependent as well, and lag synchronization appears as a nearly perfect coincidence of shifted in time states of two systems, $\mathbf{x}_1(t+\tau_0) \approx \mathbf{x}_2(t)$.

6. Synchronization of systems for which there exist no well-defined phase can be however characterized indirectly. Onset of synchronization by external force can be traced by resonance-like increase of the average field in an ensemble of identical systems having different initial conditions. Next, synchronization can be revealed with the help of ensembles of auxiliary limit cycles oscillators. These ensembles can be considered as a device for locking-based frequency measurements. This method is easily implementable in experiments and can be exploited in analysis of many coupled oscillators.

7. Ideas of the synchronization theory can be used to reveal weak interaction from experimental data. As noisy and chaotic systems have qualitatively similar phase dynamics, synchronization approach to data analysis can be exploited for analysis of any irregular oscillators (noisy, chaotic, or noisy chaotic).

8. Algorithms for detection and quantification of weak interaction from noisy multivariate data have been developed and used in several experiments.

   (a) It was found that cardiovascular and respiratory systems in humans (in young athlets and in healthy newborns) can exhibit $n:m$ locking. Intensity of cardiorespiratory interaction in healthy newborns increases with the age within first 6 month of life.

   (b) Synchronization analysis allowed us to localize the sources of pathological brain activity in Parkinsonian patients from multichannel magnetoencephalography data, as well as reveal interaction between different brain areas involved in generation of Parkinsonian tremor.

9. Algorithms for detection of coupling direction from data have been developed. They are effective for analysis of signals generated by two weakly coupled noisy oscillators. With the help of these techniques it was found that the direction of cardiorespiratory interaction in healthy newborns is age-dependent.

Bibliography

[1] E. Allaria, F. T. Arecchi, A. Di Garbo, and R. Meucci. Synchronization of homoclinic chaos. *Phys. Rev. Lett.*, 86(5):791–794, 2001.

[2] A. A. Andronov, A. A. Vitt, and S. E. Khaykin. *Theory of Oscillators*. Gostekhizdat, Moscow, 1937. (In Russian); English Translation: Pergamon Press, Oxford - NY - Toronto, 1966.

[3] V. Anishchenko, A. Neiman, V. Astakhov, T. Vadiavasova, and L. Schimansky-Geier. *Chaotic and Stochastic Processes in Dynamic Systems*. Springer Verlag, Berlin, 20021.

[4] V. S. Anishchenko, A. G. Balanov, N. B. Janson, N. B. Igosheva, and G. V. Bordyugov. Entrainment between heart rate and weak noninvasive forcing. *Int. J. Bifurc. and Chaos*, 10(10):2339–2348, 2000.

[5] J. Aschoff, S. Daan, and G. A. Groos. *Vertebrate Circadian Systems. Structure and Physiology*. Springer, Berlin, 1982.

[6] R. E. Best. *Phase-Locked Loops*. McGraw-Hill, New York, 1984.

[7] L. Bezaeva, L. Kaptsov, and P. S. Landa. Synchronization threshold as the criterium of stochasticity in the generator with inertial nonlinearity. *Zhurnal Tekhnicheskoi Fiziki*, 32:467–650, 1987. (In Russian).

[8] I. I. Blekhman. *Synchronization of Dynamical Systems*. Nauka, Moscow, 1971. (In Russian).

[9] I. I. Blekhman. *Synchronization in Science and Technology*. Nauka, Moscow, 1981. (In Russian); English translation: 1988, ASME Press, New York.

[10] D. M. Bramble and D. R. Carrier. Running and breathing in mammals. *Science*, 219:251–256, 1983.

[11] M. Bračič and A. Stefanovska. Synchronization and modulation in the human cardiorespiratory system. *Physica A*, 283:451–461, 2000.

[12] L. Brunnet, H. Chaté, and P. Manneville. Long–range order with local chaos in lattices of diffusively coupled ODEs. *Physica D*, 78:141–154, 1994.

[13] J. Cernacek. Stabilography in neurology. *Agressologie*, 21D:25–29, 1980.

[14] J. J. Collins and I. N. Stewart. Coupled nonlinear oscillators and the symmetries of animal gaits. *J. Nonlinear Sci.*, 3:349–392, 1993.

[15] I. P. Cornfeld, S. V. Fomin, and Ya. G. Sinai. *Ergodic Theory*. Springer, New York, 1982.

[16] H. Daido. Discrete-time population dynamics of interacting self-oscillators. *Prog. Theor. Phys.*, 75(6):1460–1463, 1986.

[17] H. Daido. Intrinsic fluctuations and a phase transition in a class of large population of interacting oscillators. *J. Stat. Phys.*, 60(5/6):753–800, 1990.

[18] G. I. Dykman, P. S. Landa, and Yu. I. Neymark. Synchronizing the chaotic oscillations by external force. *Chaos, Solitons & Fractals*, 1(4):339–353, 1991.

[19] R. J. Elble and W. C. Koller. *Tremor*. John Hopkins University, Baltimore, 1990.

[20] J. Engel and T.A. Pedley. *Epilepsy: A Comprehensive Textbook*. Lippincott-Raven, Philadelphia, 1975.

[21] P. Engel, G. Hildebrandt, and H.-G. Scholz. Die Messung der Phasenkopplung zwischen Herzschlag und Atmung beim Menschen mit einem neuen Koinzidenzmeßgerät. *Pflügers Arch.*, 298:258–270, 1968.

[22] J. D. Farmer. Spectral broadening of period-doubling bifurcation sequences. *Phys. Rev. Lett*, 47(3):179–182, 1981.

[23] H.-J. Freund. Motor unit and muscle activity in voluntary motor control. *Physiological Reviews*, 63(2):387–436, 1983.

[24] R. Friedrich, S. Siegert, J. Peinke, St. Lück, M. Siefert, M. Lindemann, J. Raethjen, G. Deuschl, and G. Pfister. Extracting model equations from experimental data. *Phys. Lett. A*, 271:217–222, 2000.

[25] H. Fujisaka and T. Yamada. Stability theory of synchronized motion in coupled-oscillator systems. *Prog. Theor. Phys.*, 69(1):32–47, 1983.

[26] J. M. Furman. Posturography: Uses and limitations. In *Bailliére's Clinical Neurology*, volume 3, pages 501–513. Bailliére Tindall, 1994.

[27] D. Gabor. Theory of communication. *J. IEE London*, 93(3):429–457, 1946.

[28] L. Glass. Synchronization and rhythmic processes in physiology. *Nature*, 410:277–284, 2001.

[29] L. Glass and M. C. Mackey. *From Clocks to Chaos: The Rhythms of Life*. Princeton Univ. Press, Princeton, NJ, 1988.

[30] A. Goryachev and R. Kapral. Spiral waves in chaotic systems. *Phys. Rev. Lett.*, 76(10):1619–1622, 1996.

[31] V. S. Gurfinkel, Ya. M. Kots, and M. L. Shik. *Regulation of Posture in Humans*. Nauka, Moscow, 1965. (in Russian).

[32] H. Haken. *Advanced Synergetics: Instability Hierarchies of Self-Organizing Systems*. Springer, Berlin, 1993.

[33] H. Haken. *Principles of Brain Functioning: A Synergetic Approach to Brain Activity, Behavior, and Cognition*. Springer, Berlin, 1996.

[34] H. Haken. *Brain Dynamics. Pulse-Coupled Neural Nets with Delays and Noise*. Springer, Berlin, 2002.

[35] C. Hayashi. *Nonlinear Oscillations in Physical Systems*. McGraw-Hill, New York, 1964.

[36] C. Hugenii (Huygens). *Horologium Oscillatorium*. Apud F. Muguet, Parisiis, France, 1673. English translation: Iowa State University Press, Ames, 1986.

[37] T. Kenner, H. Pessenhofer, and G. Schwaberger. Method for the analysis of the entrainment between heart rate and ventilation rate. *Pflügers Arch.*, 363:263–265, 1976.

[38] I.Z. Kiss and J.L. Hudson. Phase synchronization and suppression of chaos through intermittency in forcing of an electrochemical oscillator. *Phys. Rev. E*, 64:046215, 2001.

[39] I.Z. Kiss, Y. Zhai, and J.L. Hudson. Collective dynamics of chaotic chemical oscillators and the law of large numbers. *Phys. Rev. Lett.*, 88(23):238301, 2002.

[40] I.Z. Kiss, Y. Zhai, and J.L. Hudson. Emerging coherence in a population of chemical oscillators. *Science*, 296:1676–1678, 2002.

[41] L. Kocarev and U. Parlitz. General approach for chaotic synchronization with applications to communication. *Phys. Rev. Lett.*, 74(25):5028–5031, 1995.

[42] L. Kocarev, A. Shang, and L. O. Chua. Transitions in dynamical regimes by driving: a unified method of control and synchronization of chaos. *International Journal of Bifurcation and Chaos*, 3(2):479–483, 1993.

[43] H. P. Koepchen. Physiology of rhythms and control systems: An integrative approach. In H. Haken and H. P. Koepchen, editors, *Rhythms in Physiological Systems*, volume 55 of *Springer Series in Synergetics*, pages 3–20, Berlin Heidelberg, 1991. Springer.

[44] Y. Kuramoto. Self-entrainment of a population of coupled nonlinear oscillators. In H. Araki, editor, *International Symposium on Mathematical Problems in Theoretical Physics*, page 420, New York, 1975. Springer Lecture Notes Phys., v. 39.

[45] Y. Kuramoto. *Chemical Oscillations, Waves and Turbulence*. Springer, Berlin, 1984.

[46] Yu. Kuznetsov, P. S. Landa, A. Ol'khovoi, and S. Perminov. Relationship between the amplitude threshold of synchronization and the entropy in stochastic self–excited systems. *Sov. Phys. Dokl.*, 30(3):221–222, 1985.

[47] P. S. Landa. *Self–Oscillations in Systems with Finite Number of Degrees of Freedom*. Nauka, Moscow, 1980. (In Russian).

[48] P. S. Landa and A. A. Zaikin. Noise-induced phase transitions in a pendulum with a randomly vibrating suspension axis. *Phys. Rev. E*, 54:3535–3544, 1996.

[49] M. Lipp and N. S. Longridge. Computerized dynamic posturography: Its place in the evolution of patients with dizziness and imbalance. *J. of Otolaryngology*, 23(3):177–183, 1994.

[50] W.A. MacKay. Synchronized neuronal oscillations and their role in motor processes. *Trends in Cognitive Sciences*, 1:176–183, 1997.

[51] F. Moss, D. Pierson, and D. O'Gorman. Stochastic resonance: Tutorial and update. *Int. J. of Bifurcation and Chaos*, 4(6):1383–1397, 1994.

[52] R. Mrowka, A. Patzak, and M. G. Rosenblum. Qantitative analysis of cardiorespiratory synchronization in infants. *Int. J. of Bifurcation and Chaos*, 10(11):2479–2488, 2000.

[53] A. Neiman, X. Pei, D. F. Russell, W. Wojtenek, L. Wilkens, F. Moss, H.A. Braun, M.T. Huber, and K. Voigt. Synchronization of the noisy electrosensitive cells in the paddlefish. *Phys. Rev. Lett.*, 82(3):660–663, 1999.

[54] A. Neiman, L. Schimansky-Geier, F. Moss, B. Shulgin, and J. J. Collins. Synchronization of noisy systems by stochastic signals. *Phys. Rev. E*, 60(1):284–292, 1999.

[55] P. Nunez. *Neocortical Dynamics and Human EEG.* Oxford University Press, NY, 1995.

[56] G. Osipov, A. Pikovsky, M. Rosenblum, and J. Kurths. Phase synchronization effects in a lattice of nonidentical Rössler oscillators. *Phys. Rev. E*, 55(3):2353–2361, 1997.

[57] R. K. Otnes and L. Enochson. *Digital Time Series Analysis.* John Wiley & Sons, New York, 1972.

[58] E. Ott. *Chaos in Dynamical Systems.* Cambridge Univ. Press, Cambridge, 1992.

[59] M. Palus. Detecting phase synchronization in noisy systems. *Phys. Lett. A*, 227:301–308, 1997.

[60] P. Panter. *Modulation, Noise, and Spectral Analysis.* McGraw–Hill, New York, 1965.

[61] E. H. Park, M. A. Zaks, and J. Kurths. Phase synchronization in the forced Lorenz system. *Phys. Rev. E*, 60(6):6627–6638, 1999.

[62] U. Parlitz, L. Junge, W. Lauterborn, and L. Kocarev. Experimental observation of phase synchronization. *Phys. Rev. E.*, 54(2):2115–2118, 1996.

[63] U. Parlitz and L. Kocarev. Synchronization of chaotic systems. In H. Schuster, editor, *Handbook of Chaos Control*, pages 271–303. Wiley-VCH, Weinheim, Germany, 1999.

[64] L. M. Pecora and T. L. Carroll. Synchronization in chaotic systems. *Phys. Rev. Lett.*, 64:821–824, 1990.

[65] L. M. Pecora, T. L. Carroll, and J. F. Heagy. Statistics for continuity and differentiability: An application to attractor reconstruction from time series. In C. D. Cutler and D. T. Kaplan, editors, *Nonlinear Dynamics and Time Series*, volume 11 of *Fields Inst. Communications*, pages 49–62. American Math. Soc., Providence, Rhode Island, 1997.

[66] H. Pessenhofer and T. Kenner. Zur Methodik der kontinuierlichen Bestimmung der Phasenbeziehung zwischen Herzschlag und Atmung. *Pflügers Archiv*, 355:77–83, 1975.

[67] G. A. Petrillo and L. Glass. A theory for phase locking of respiration in cats to a mechanical ventilator. *Am. J. Physiol.*, 246:311–320, 1984.

[68] A. Pikovsky, G. Osipov, M. Rosenblum, M. Zaks, and J. Kurths. Attractor-repeller collision and eyelet intermittency at the transition to phase synchronization. *Phys. Rev. Lett.*, 79:47–50, 1997.

[69] A. Pikovsky, M. Rosenblum, and J. Kurths. Synchronization in a population of globally coupled chaotic oscillators. *Europhys. Lett.*, 34(3):165–170, 1996.

[70] A. Pikovsky, M. Rosenblum, and J. Kurths. *Synchronization. A Universal Concept in Nonlinear Sciences.* Cambridge University Press, Cambridge, 2001.

[71] A. Pikovsky, M. Rosenblum, G. Osipov, and J. Kurths. Phase synchronization of chaotic oscillators by external driving. *Physica D*, 104:219–238, 1997.

[72] A. Pikovsky, M. Zaks, M. Rosenblum, G. Osipov, and J. Kurths. Phase synchronization of chaotic oscillations in terms of periodic orbits. *CHAOS*, 7(4):680–687, 1997.

[73] A. S. Pikovsky. On the interaction of strange attractors. *Z. Physik B*, 55(2):149–154, 1984.

[74] A. S. Pikovsky. Phase synchronization of chaotic oscillations by a periodic external field. *Sov. J. Commun. Technol. Electron.*, 30:85, 1985.

[75] A. S. Pikovsky. Discrete-time dynamic noise filtering. *Sov. J. Commun. Technol. Electron.*, 31:81, 1986.

[76] A. S. Pikovsky, M. G. Rosenblum, M. A. Zaks, and J. Kurths. Phase synchronization of regular and chaotic oscillators. In H. G. Schuster, editor, *Handbook of Chaos Control*, pages 305–328. Wiley-VCH, Weinheim, Germany, 1999.

[77] B. Pompe. Measuring statistical dependencies in a time series. *J. Stat. Phys.*, 73:587–610, 1993.

[78] L. R. Rabiner and B. Gold. *Theory and Application of Digital Signal Processing.* Prentice–Hall, Englewood Cliffs, NJ, 1975.

[79] F. Raschke. Coordination in the circulatory and respiratory systems. In L. Rensing, U. an der Heiden, and M.C. Mackey, editors, *Temporal Disorder in Human Oscillatory Systems*, volume 36 of *Springer Series in Synergetics*, pages 152–158, Berlin Heidelberg, 1987. Springer-Verlag.

[80] F. Raschke. The respiratory system - features of modulation and coordination. In H. Haken and H. P. Koepchen, editors, *Rhythms in Physiological Systems*, volume 55 of *Springer Series in Synergetics*, pages 155 – 164, Berlin Heidelberg, 1991. Springer-Verlag.

[81] A. Rényi. *Probability Theory*. Akadémiai Kiadó, Budapest, 1970.

[82] H. Z. Risken. *The Fokker–Planck Equation*. Springer, Berlin, 1989.

[83] E. Rosa Jr., E. Ott, and M. H. Hess. Transition to phase synchronization of chaos. *Phys. Rev. Lett.*, 80(8):1642–1645, 1998.

[84] M. Rosenblum and A. Pikovsky. Detecting direction of coupling in interacting oscillators. *Phys. Rev. E*, 64(4):045202(R), 2001.

[85] M. Rosenblum, A. Pikovsky, and J. Kurths. Phase synchronization of chaotic oscillators. *Phys. Rev. Lett.*, 76:1804, 1996.

[86] M. Rosenblum, A. Pikovsky, and J. Kurths. Effect of phase synchronization in driven and coupled chaotic oscillators. *IEEE Trans. CAS-I*, 44(10):874–881, 1997.

[87] M. Rosenblum, A. Pikovsky, and J. Kurths. From phase to lag synchronization in coupled chaotic oscillators. *Phys. Rev. Lett.*, 78:4193–4196, 1997.

[88] M. G. Rosenblum, L. Cimponeriu, A. Bezerianos, A. Patzak, and R. Mrowka. Identification of coupling direction: Application to cardiorespiratory interaction. *Phys. Rev. E*, 65(4):041909, 2002.

[89] M. G. Rosenblum, G. I. Firsov, R. A. Kuuz, and B. Pompe. Human postural control: Force plate experiments and modelling. In H. Kantz, J. Kurths, and G. Mayer-Kress, editors, *Nonlinear Analysis of Physiological Data*, pages 283–306. Springer, Berlin, 1998.

[90] M. G. Rosenblum and J. Kurths. Analysing synchronization phenomena from bivariate data by means of the Hilbert transform. In H. Kantz, J. Kurths, and G. Mayer-Kress, editors, *Nonlinear Analysis of Physiological Data*, pages 91–99. Springer, Berlin, 1998.

[91] M. G. Rosenblum, A. S. Pikovsky, J. Kurths, C. Schäfer, and P. A. Tass. Phase synchronization: From theory to data analysis. In F. Moss and S. Gielen, editors, *Neuro-informatics*, volume 4 of *Handbook of Biological Physics*, pages 279–321. Elsevier, 2001.

[92] O. E. Rössler. An equation for continuous chaos. *Phys. Lett. A*, 57(5):397, 1976.

[93] N. F. Rulkov, M. M. Sushchik, L. S. Tsimring, and H. D. I. Abarbanel. Generalized synchronization of chaos in directionally coupled chaotic systems. *Phys. Rev. E*, 51(2):980–994, 1995.

[94] H. Sakaguchi, S. Shinomoto, and Y. Kuramoto. Local and global self-entrainments in oscillator lattices. *Prog. Theor. Phys.*, 77(5):1005–1010, 1987.

[95] C. Schäfer, M. G. Rosenblum, J. Kurths, and H.-H. Abel. Heartbeat synchronized with ventilation. *Nature*, 392(6673):239–240, March 1998.

[96] C. Schäfer, M.G. Rosenblum, H.-H. Abel, and J. Kurths. Synchronization in the human cardiorespiratory system. *Physical Review E*, 60:857–870, 1999.

[97] M. Schiek, F. R. Drepper, R. Engbert, H.-H. Abel, and K. Suder. Cardiorespiratory synchronization. In H. Kantz, J. Kurths, and G. Mayer-Kress, editors, *Nonlinear Analysis of Physiological Data*, pages 191–209. Springer, Berlin, 1998.

[98] S. J. Schiff, P. So, T. Chang, R. E. Burke, and T. Sauer. Detecting dynamical interdependence and generalized synchrony through mutual prediction in a neural ensemble. *Phys. Rev. E*, 54(6):6708–6724, 1996.

[99] L. Schimansky-Geier, V. S. Anishchenko, and A. B. Neiman. Phase synchronization: From periodic to chaotic and noisy. In F. Moss and S. Gielen, editors, *Neuro-informatics*, volume 4 of *Handbook of Biological Physics*, pages 23–82. Elsevier, 2001.

[100] T. Schreiber. Measuring information transfer. *Phys. Rev. Lett.*, 85(2):461–464, 2000.

[101] T. Schreiber and A. Schmitz. Improved surrogate data for nonlinearity tests. *Phys. Rev. Lett.*, 77:635–638, 1997.

[102] H. Seidel and H.-P. Herzel. Analyzing entrainment of heartbeat and respiration with surrogates. *IEEE Engineering in Medicine and Biology*, 17(6):54–57, 1998.

[103] W. Singer and C.M. Gray. Visual feature integration and the temporal correlation hypothesis. *Annu. Rev. Neurosci.*, 18:555–586, 1995.

[104] A. Stefanovska, H. Haken, P. V. E. McClintock, M. Hozic, F. Bajrovic, and S. Ribaric. Reversible transitions between synchronization states of the cardiorespiratory system. *Phys. Rev. Lett.*, 85(22):4831–4834, 2000.

[105] E. F. Stone. Frequency entrainment of a phase coherent attractor. *Phys. Lett. A*, 163:367–374, 1992.

[106] R. L. Stratonovich. *Topics in the Theory of Random Noise*. Gordon and Breach, New York, 1963.

[107] J. Sturis, C. Knudsen, N. M. O'Meara, J. S. Thomsen, E. Mosekilde, E. Van Cauter, and K. S. Polonsky. Phase-locking regions in a forced model of slow insulin and glucose oscillations. *CHAOS*, 5(1):193–199, 1995.

[108] K. H. Stutte and G. Hildebrandt. Untersuchungen über die Koordination von Herzschlag und Atmung. *Pflügers Arch.*, 289:R47, 1966.

[109] D. Y. Tang, R. Dykstra, M. W. Hamilton, and N. R. Heckenberg. Experimental evidence of frequency entrainment between coupled chaotic oscillations. *Phys. Rev. E*, 57(3):3649–3651, 1998.

[110] P. Tass, J. Kurths, M. G. Rosenblum, J. Weule, A. S. Pikovsky, J. Volkmann, A. Schnitzler, and H.-J. Freund. Complex phase synchronization in neurophysiological data. In C. Uhl, editor, *Analysis of Neurophysiological Brain Functioning*, Springer Series in Synergetics, pages 252–273. Springer-Verlag, Berlin, 1999.

[111] P. Tass, M. G. Rosenblum, J. Weule, J. Kurths, A. S. Pikovsky, J. Volkmann, A. Schnitzler, and H.-J. Freund. Detection of $n : m$ phase locking from noisy data: Application to magnetoencephalography. *Phys. Rev. Lett.*, 81(15):3291–3294, 1998.

[112] J. Theiler, S. Eubank, A. Longtin, B. Galdrikian, and J.D. Farmer. Testing for nonlinearity in time series: The method of surrogate data. *Physica D*, 58:77–94, 1992.

[113] C. M. Ticos, E. Rosa Jr., W. B. Pardo, J. A. Walkenstein, and M. Monti. Experimental real-time phase synchronization of a paced chaotic plasma discharge. *Phys. Rev. Lett.*, 85(14):2929–2932, 2000.

[114] B. van der Pol and J. van der Mark. The heartbeat considered as a relaxation oscillation, and an electrical model of the heart. *Phil. Mag.*, 6:763–775, 1928.

[115] H. Voss and J. Kurths. Reconstruction of nonlinear time delay models from data by the use of optimal transformations. *Phys. Lett. A*, 234:336–344, 1997.

[116] W. Wang, I. Z. Kiss, and J. L. Hudson. Clustering of arrays of chaotic chemical oscillators by feedback and forcing. *Phys. Rev. Lett.*, 86(21):4954–4957, 2001.

[117] M. Wiesenfeldt, U. Parlitz, and W. Lauterborn. Mixed state analysis of multivariate time series. *Int. J. Bif. and Chaos*, 11:2217–2226, 2001.

[118] M. A. Zaks, E. H. Park, M. G. Rosenblum, and J. Kurths. Alternating locking ratios in imperfect phase synchronization. *Phys. Rev. Lett.*, 82(21):4228–4231, 1999.

Appendices

Paper 1 M. Rosenblum, A. Pikovsky, and J. Kurths. Phase synchronization of chaotic oscillators. *Phys. Rev. Lett.*, 76:1804, 1996.

Paper 2 A. Pikovsky, M. Rosenblum, and J. Kurths. Synchronization in a population of globally coupled chaotic oscillators. *Europhys. Lett.*, 34(3):165–170, 1996.

Paper 3 M. Rosenblum, A. Pikovsky, and J. Kurths. From phase to lag synchronization in coupled chaotic oscillators. *Phys. Rev. Lett.*, 78:4193–4196, 1997.

Paper 4 C. Schäfer, M. G. Rosenblum, J. Kurths, and H.-H. Abel. Heartbeat synchronized with ventilation. *Nature*, 392(6673):239–240, March 1998.

Paper 5 P. Tass, M. G. Rosenblum, J. Weule, J. Kurths, A. S. Pikovsky, J. Volkmann, A. Schnitzler, and H.-J. Freund. Detection of $n : m$ phase locking from noisy data: Application to magnetoencephalography. *Phys. Rev. Lett.*, 81(15):3291–3294, 1998.

Paper 6 R. Mrowka, A. Patzak, and M. G. Rosenblum. Qantitative analysis of cardiorespiratory synchronization in infants. *Int. J. of Bifurcation and Chaos*, 10(11):2479–2488, 2000.

Paper 7 M. G. Rosenblum, L. Cimponeriu, A. Bezerianos, A. Patzak, and R. Mrowka. Identification of coupling direction: Application to cardiorespiratory interaction. *Phys. Rev. E*, 65(4):041909, 2002.

Phase Synchronization of Chaotic Oscillators

Michael G. Rosenblum,* Arkady S. Pikovsky, and Jürgen Kurths
Max-Plank-Arbeitsgruppe "Nichtlineare Dynamik" an der Universität Potsdam, Am Neuen Palais 19, PF 601553, D-14415, Potsdam, Germany
(Received 7 September 1995)

We present the new effect of phase synchronization of weakly coupled self-sustained chaotic oscillators. To characterize this phenomenon, we use the analytic signal approach based on the Hilbert transform and partial Poincaré maps. For coupled Rössler attractors, in the synchronous regime the phases are locked, while the amplitudes vary chaotically and are practically uncorrelated. Coupling a chaotic oscillator with a hyperchaotic one, we observe another new type of synchronization, where the frequencies are entrained, while the phase difference is unbounded. A relation between the phase synchronization and the properties of the Lyapunov spectrum is studied.

PACS numbers: 05.45.+b

Cooperative behavior of chaotic dynamical systems and, in particular, synchronization phenomena have received much attention recently. Nevertheless, the notion of synchronization itself lacks a unique interpretation. Mostly, the synchronization is considered as the complete coincidence of the states of individual systems (subsystems). Such a regime can result from an interaction between systems [1] or subsystems [2,3], as well as from the influence of external noisy [4] or regular [5] fields; in all these situations synchronization is a threshold phenomenon.

Generally, synchronization can be treated as an appearance of some relations between functionals of two processes due to interaction [6]. The choice of the functionals is to some extent arbitrary and depends on the problem under consideration. In the classical case of *periodic* self-sustained oscillators, described as early as in the 17th century by Hugenii [7], synchronization is usually defined as locking of the phases $\phi_{1,2}, n\phi_1 - m\phi_2 =$ const [8], while the amplitudes can be quite different. This effect is widely used in engineering for improvement of the linewidth of a high-power generator with the help of a low-power but more stable (having narrower line) one. Some other types of synchronization in systems with quasiperiodic and chaotic behavior have been discussed in Ref. [9].

In this Letter we investigate phase synchronization of *chaotic* oscillators. Using the methods of analytic signal and the Poincaré map, we show that the interaction of nonidentical autonomous chaotic oscillators can lead to a perfect locking of their phases, whereas their amplitudes remain chaotic and noncorrelated. A similar effect of phase locking of chaotic oscillations by a periodic external force has been described in Refs. [10,11]. We also describe a weaker type of synchronization, when the frequencies are locked while the phase difference exhibits a random-walk-type motion.

Firstly, we have to determine the amplitude and the phase of an arbitrary signal *s(t)*. A general approach has been introduced by Gabor [12] and is based on the analytic signal concept [13]. The analytic signal $\psi(t)$ is a complex function of time defined as

$$\psi(t) = s(t) + j\tilde{s}(t) = A(t)e^{j\phi(t)}, \tag{1}$$

where the function $\tilde{s}(t)$ is the Hilbert transform of $s(t)$

$$\tilde{s}(t) = \pi^{-1}\text{P.V.}\int_{-\infty}^{\infty} \frac{s(\tau)}{t-\tau}\, d\tau \tag{2}$$

(where P.V. means that the integral is taken in the sense of the Cauchy principal value). The instantaneous amplitude $A(t)$ and the instantaneous phase $\phi(t)$ of the signal $s(t)$ are thus uniquely defined from (1). From (2), the Hilbert transform $\tilde{s}(t)$ of $s(t)$ may be considered as the convolution of the functions $s(t)$ and $1/\pi t$. Hence the Fourier transform $\tilde{S}(j\omega)$ of $\tilde{s}(t)$ is the product of the Fourier transforms of $s(t)$ and $1/\pi t$. For physically relevant frequencies $\omega > 0$, $\tilde{S}(j\omega) = -jS(j\omega)$; i.e., ideally $\tilde{s}(t)$ may be obtained from $s(t)$ by a filter whose amplitude response is unity, and whose phase response is a constant $\pi/2$ lag at all frequencies [13,14].

For chaotic oscillators, we can calculate the phase from taking as $s(t)$ any observable, so there is no unique phase of chaotic oscillations. However, in some cases "natural" observables provide phases that agree with an intuitive definition. For example, for the Rössler attractor [15] taking the observables $s_1 = x$ and $s_2 = y$ [see below Eqs. (3)] gives phases shifted by $\approx\pi/2$ and rotating with the same averaged velocity, corresponding to the main peak in the power spectrum.

To study phase synchronization of coupled chaotic oscillators, we calculate the phases of the oscillators and then check whether the weak locking condition $|n\phi_1 - m\phi_2| <$ const is satisfied. In this Letter, we restrict ourselves to the case $m = n = 1$.

As the simplest example of phase synchronization, we consider two coupled Rössler systems [15]

$$\begin{aligned} \dot{x}_{1,2} &= -\omega_{1,2}y_{1,2} - z_{1,2} + C(x_{2,1} - x_{1,2}), \\ \dot{y}_{1,2} &= \omega_{1,2}x_{1,2} + 0.15y_{1,2}, \\ \dot{z}_{1,2} &= 0.2 + z_{1,2}(x_{1,2} - 10). \end{aligned} \tag{3}$$

 0031-9007/96/76(11)/1804(4)$10.00

Here we introduce the parameters $\omega_{1,2} = 1 \pm \Delta\omega$ and C, which govern the frequency mismatch [16] and the strength of coupling, respectively [17]. As the coupling is increased for a fixed mismatch $\Delta\omega$, we observe a transition from a regime, where the phases rotate with different velocities $\phi_1 - \phi_2 \sim \Delta\Omega\, t$, to a synchronous state, where the phase difference does not grow with time $|\phi_1 - \phi_2| < \text{const}$; $\Delta\Omega = 0$. This transition is illustrated in Fig. 1(a). We emphasize that in contrast to the other types of synchronization of chaotic systems [1,2], here the instant fields $x_{1,2}$, $y_{1,2}$, and $z_{1,2}$ do not coincide. Moreover, the correlations between the amplitudes of x_1 and x_2 are pretty small [Fig. 1(b)], although the phases are completely locked and in this respect the motions are highly coherent.

For the Rössler attractor, because of its simple form, the phase can be introduced in a more straightforward way, based on the Poincaré map construction. One can say that the motion from one crossing with a secant surface until the next one corresponds to the phase shift 2π. When we consider coupled chaotic systems, we still can construct partial Poincaré maps, e.g., taking successive maxima of the variables $x_{1,2}$ in the coupled Rössler systems. Partial frequencies are then simply defined as an average number of crossings of the secant surfaces per unit time. According to this approach, the synchronization in coupled Rössler systems simply means that the average numbers of oscillations (number of maxima) per unit time in both systems coincide. The region of synchronization in the plane of parameters "coupling-frequency mismatch," obtained using these partial Poincaré maps, is presented in Fig. 2. Note that it seems to have no threshold: If the frequency mismatch is small $\Delta\omega \to 0$, synchronization appears already for vanishing coupling. This is a particular feature of the Rössler system, where the motion is highly coherent (in the power spectrum a very sharp peak is observed [18]). From the other side, it is possible to synchronize systems with frequency mismatch of more than 20% (see Fig. 2).

The instantaneous phase ϕ, defined through the Hilbert transform (2) provides, of course, additional information on the dynamics of synchronization (see, e.g., the time evolution of $\phi_1 - \phi_2$ for $C = 0.027$ in Fig. 1). We also note that in the case of asymmetric coupling the averaged value of the phase difference can be nonzero. This, e.g., happens in the asymmetric coupling of Rössler systems, where the variable x_1 is driven by y_2 [the first equation in (3) has a form $\dot{x}_1 = -\omega_1 y_1 - z_1 + c y_2$]. Here in the synchronous state the phase difference (both phases are obtained using observables $x_{1,2}$) fluctuates near the mean value $\pi/2$. With the method of partial Poincaré map this particular property is not detectable.

It is remarkable how the phase synchronization manifests itself in the Lyapunov spectrum (Fig. 3). In the absence of coupling, each oscillator has one positive, one negative, and one vanishing Lyapunov exponent. As the coupling is increased, the positive and negative exponents remain, whereas one of the zero exponents becomes negative. This behavior can be explained as follows: Without coupling, the vanishing exponents correspond to the translation along the trajectory, i.e., to the shift of the phase of the oscillator. The coupling produces an "attraction" of the phases such that the phase difference $\phi_1 - \phi_2$ decreases.

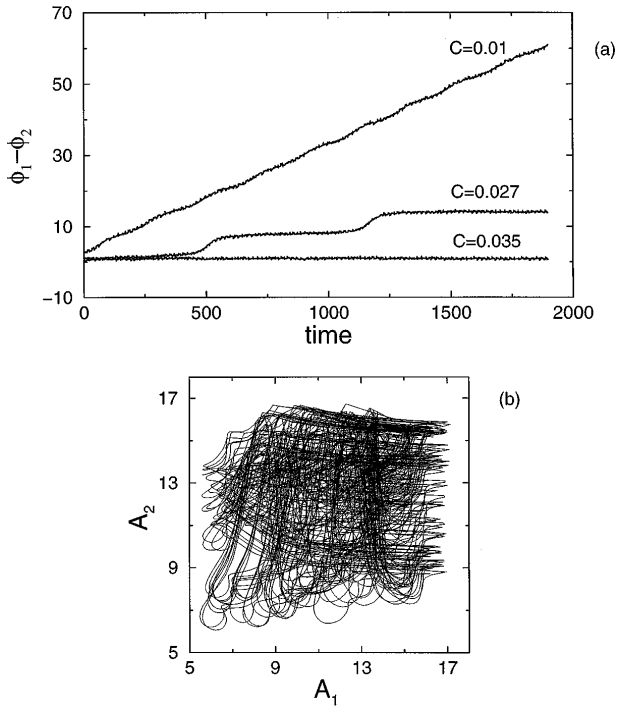

FIG. 1. Phase difference of two coupled Rössler systems [Eq. (3)] versus time for nonsynchronous ($C = 0.01$), nearly synchronous ($C = 0.027$), and synchronous ($C = 0.035$) states (a). In the last case the amplitudes $A_{1,2}$ remain chaotic (b), their cross correlation is less than 0.2. The frequency mismatch is $\Delta\omega = 0.015$.

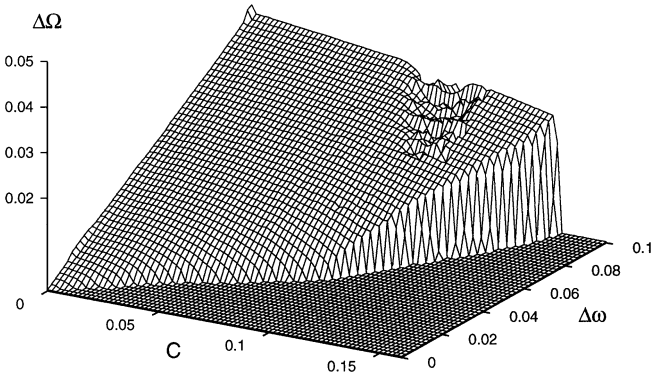

FIG. 2. The mean frequency difference $\Delta\Omega$ for the coupled Rössler systems (3), calculated with the method of partial Poincaré maps, as a function of the coupling C and the frequency mismatch $\Delta\omega$. For C large enough the frequency difference $\Delta\Omega$ is nearly zero; this region of synchronization is completely analogous to the phase-locking domain (the Arnold tongue) for coupled periodic oscillators. For small C there is no synchronization and the phase difference grows with the finite rate $\Delta\Omega$.

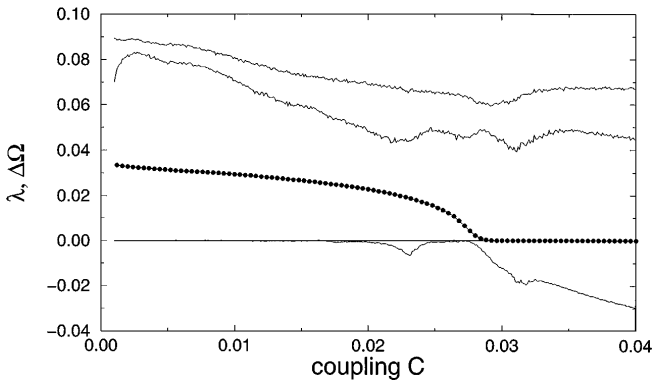

FIG. 3. The four largest Lyapunov exponents, one of which is always zero (lines) and $\Delta\Omega$ (circles) vs coupling C for system (3) with $\Delta\omega = 0.015$.

Thus one of the vanishing exponents becomes negative. For large coupling the attraction is so strong that the phases remain locked.

Qualitatively, the dynamics of the phase of an autonomous chaotic oscillator can be described with the equation (cf. [10,19])

$$\dot{\phi} = \omega + F(A). \tag{4}$$

Here ω is the mean frequency of the oscillations, and the term $F(A)$ accounts for the amplitude dependence of the frequency; the amplitude A is assumed to behave chaotically. For coupled oscillators a generalization of (4) reads

$$\dot{\phi}_{1,2} = \omega_{1,2} + F_{1,2}(A_{1,2}) + \varepsilon G(\phi_{2,1}, \phi_{1,2}). \tag{5}$$

Here G is 2π periodic in each argument function, describing coupling. In the simplest case we can assume that $G(\phi_1, \phi_2) = \sin(\phi_2 - \phi_1)$. Thus for the phase difference $\Delta\phi = \phi_1 - \phi_2$ we get from (5)

$$\frac{d\Delta\phi}{dt} = \omega_1 - \omega_2 - 2\varepsilon \sin(\Delta\phi) + F_1(A_1) - F_2(A_2). \tag{6}$$

This equation is similar to the equation describing phase locking of periodic oscillators in the presence of noise [20]. Here instead of external noisy force we have the term depending on the chaotic amplitudes. In the Rössler attractor the dependence of the frequency on the amplitude is very small, so the effective noise $F_1(A_1) - F_2(A_2)$ in Eq. (6) is negligible, and the dynamics of the phases is very similar to that in the coupled periodic oscillators. This explains the complete phase locking, as well as the absence of the threshold.

It is noteworthy that the phenomenon of phase synchronization is observed even when completely different systems, such as the Rössler oscillator and the Mackey-Glass differential-delay system [21], interact. Here we describe the interaction of the chaotic and the hyperchaotic Rössler oscillators [22]:

$$\begin{aligned}
\dot{x} &= -\omega y - z + C(u - x),\\
\dot{y} &= \omega x + 0.15y,\\
\dot{z} &= 0.2 + z(x - 10),\\
\dot{p} &= -u - v,\\
\dot{u} &= p + 0.25u + w + C(x - u),\\
\dot{v} &= 3 + pv,\\
\dot{w} &= -0.5v + 0.05w.
\end{aligned} \tag{7}$$

Clearly, for the interaction of such different systems there is no hope to observe synchronization in the usual sense [1,2]. However, the phase synchronization occurs in (7), as is demonstrated in Fig. 4. Here we plot the difference between averaged frequencies $\Delta\Omega = \langle\dot{\phi}_1 - \dot{\phi}_2\rangle$ vs ω (this parameter governs the frequency mismatch), for different coupling strengths C. For this system we have not found a regime with perfect phase locking: Even when $\Delta\Omega \approx 0$, the phase difference $\langle\phi_1 - \phi_2\rangle$ exhibits a random-type walk and is not constrained [23]. This *weak* phase synchronization can be qualitatively described with the model equation (6) with sufficiently large effective noise $F_1(A_1) - F_2(A_2)$.

In conclusion, we have demonstrated the possibility of phase synchronization of chaotic self-sustained oscillators. In this regime the phases are synchronized, while the amplitudes vary chaotically and are practically uncorrelated. We have described two types of phase synchronization: When interacting chaotic oscillators are highly coherent, the phases are perfectly locked; otherwise, the frequencies are entrained while the phase difference is unbounded. The effect of phase synchronization is also possible when the natural frequencies are in a rational relation (this is relevant for an important physiological problem of interaction of the cardiac and respiratory systems).

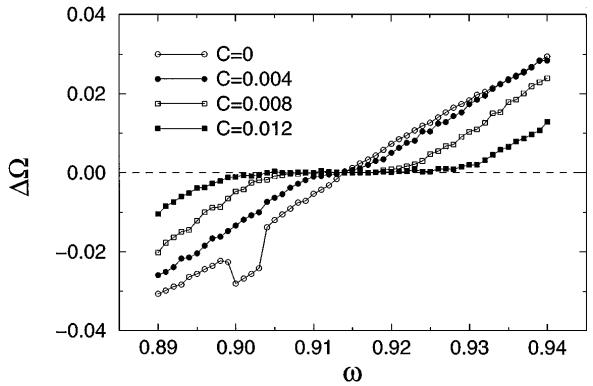

FIG. 4. The mean frequency difference $\Delta\Omega$ in system (7), calculated via Hilbert transform vs ω for several values of the coupling constant C.

We emphasize that the phase synchronization is observed already for extremely weak couplings, and in some cases can have no threshold, contrary to other types of synchronization. This phenomenon is a direct generalization of synchronization of periodic self-sustained oscillators. As the latter, it may find practical applications, in particular, when a coherent summation of outputs of slightly different generators operating in a chaotic regime is necessary. For this purpose, it is sufficient to synchronize phases, while amplitudes can remain uncorrelated. We expect this to be relevant for an important problem of output summation in arrays of semiconductor lasers [24]. For a description of such arrays, as well as of a number of other physical and biological phenomena, one often uses a model of globally coupled oscillators (see, e.g., [25]). Here mutual phase synchronization of individual chaotic states manifests itself as an appearance of a macroscopic mean field [26].

We also mention that the phenomenon of phase synchronization is a characteristic feature of autonomous continuous-time systems, and cannot be observed in discrete-time or periodically forced models. In the latter systems the phases are not free (in the sense of the existence of the zero Lyapunov exponent corresponding to the phase shift) and therefore cannot be adjusted by small coupling.

We thank M. Zaks for useful discussions. M. R. acknowledges support from the Alexander von Humboldt Foundation.

*Permanent address: Mech. Eng. Res. Inst., Russian Acad. Sci., Moscow, Russia.

[1] H. Fujisaka and T. Yamada, Prog. Theor. Phys. **69**, 32 (1983); A. S. Pikovsky, Z. Phys. B **55**, 149 (1984).
[2] L. Pecora and T. Carroll, Phys. Rev. Lett. **64**, 821 (1990); Phys. Rev. A **44**, 2374 (1991).
[3] M. de Sousa Vieira, A. Lichtenberg, and M. Lieberman, Phys. Rev. A **46**, R7359 (1992).
[4] A. S. Pikovsky, Radiophys. Quantum Electron. **27**, 576 (1984).
[5] Y. Kuznetsov, P. Landa, A. Ol'khovoi, and S. Perminov, Sov. Phys. Dokl. **30**, 221 (1985).
[6] I. Blekhman, *Synchronization in Science and Technology* (Nauka, Moscow, 1981) (in Russian) [Synchronization in Science and Technology (ASME Press, New York, 1988)].
[7] C. Hugenii, *Horoloquim Oscilatorium* (Parisiis, France, 1673).
[8] In the presence of noise, a weaker condition for phase locking $|n\phi_1 - m\phi_2| < \text{const}$ should be used instead.
[9] P. Landa and N. Tarankova, Radiotechnika i Electronica **21**, 260 (1976) (in Russian); V. S. Anischenko, T. E. Vadivasova, D. E. Postnov, and M. A. Safonova, Int. J. Bif. Chaos **2**, 633 (1992); P. Landa and M. Rosenblum, Appl. Mech. Rev. **46**, 414 (1993); I. Blekhman, P. Landa, and M. Rosenblum, *ibid.* **48**, 733 (1995); *Nonlinear Dynamics: New Theoretical and Applied Results* (Academic Verlag, Berlin, 1995), pp. 17–54.
[10] A. S. Pikovsky, Sov. J. Commun. Technol. Electron. **30**, 85 (1985).
[11] E. F. Stone, Phys. Lett. A **163**, 367 (1992).
[12] D. Gabor, J. IEE London **93**, 429 (1946).
[13] P. Panter, *Modulation, Noise, and Spectral Analysis* (McGraw-Hill, New York, 1965).
[14] For discrete signals given within the bounded time interval, the Hilbert transform can be approximately performed by means of a digital filter, see, e.g., M. J. Smith, *Introduction to Digital Signal Processing* (Wiley, New York, 1992).
[15] O. E. Rössler, Phys. Lett. A **57**, 397 (1976).
[16] Collective coherent behavior in a large array of coupled *identical* Rössler systems has been described in L. Brunnet, H. Chaté, and P. Manneville, Physica (Amsterdam) **78D**, 141 (1994).
[17] One can see that $\omega_{1,2}$ are indeed frequencies of the Rössler system if we rewrite it as $\ddot{y} - a\dot{y} + \omega^2 y = -\omega z$, $\dot{z} + fz = b + z(\dot{y} - ay)/\omega$.
[18] J. Crutchfield *et al.*, Phys. Lett. A **76**, 1 (1980).
[19] J. D. Farmer, Phys. Rev. Lett. **47**, 179 (1981).
[20] R. L. Stratonovich, *Topics in the Theory of Random Noise* (Gordon and Breach, New York, 1963).
[21] M. Mackey and L. Glass, Science **197**, 287 (1977).
[22] O. E. Rössler, Phys. Lett. A **71**, 155 (1979).
[23] A similar classification was used by H. Daido, Phys. Rev. Lett. **68**, 1073 (1992).
[24] H. G. Winful and L. Rahman, Phys. Rev. Lett. **65**, 1575 (1990); H. G. Winful *et al.*, in *Proceedings of the 1st Experimental Chaos Conference*, edited by S. Vohra, M. Spano, M. Shlesinger, L. Pecora, and W. Ditto (World Scientific, Singapore, 1992), p. 77.
[25] K. Wiesenfeld and P. Hadley, Phys. Rev. Lett. **62**, 1335 (1989); D. Hansel and H. Sompolinsky, Phys. Rev. Lett. **68**, 718 (1992); S. K. Han, C. Kurrer, and Y. Kuramoto, Phys. Rev. Lett. **75**, 3190 (1995).
[26] A. Pikovsky, M. Rosenblum, and J. Kurths (to be published).

EUROPHYSICS LETTERS 20 April 1996

Europhys. Lett., **34** (3), pp. 165-170 (1996)

Synchronization in a population of globally coupled chaotic oscillators

A. S. Pikovsky, M. G. Rosenblum(*) and J. Kurths

Max-Planck-Arbeitsgruppe "Nichtlineare Dynamik" an der Universität Potsdam Am Neuen Palais 19, PF 601553, D-14415 Potsdam, Germany (**)

(received 30 November 1995; accepted in final form 9 March 1996)

PACS. 05.45+b – Theory and models of chaotic systems.
PACS. 64.60Cn – Order-disorder and statistical mechanics of model systems.

Abstract. – We demonstrate synchronization transition in a large ensemble of non-identical chaotic oscillators, globally coupled via the mean field. We show that this coherent behaviour is due to synchronization of phases of these oscillators, while their amplitudes remain chaotic. Two types of transition, depending on the phase coherence properties of the individual systems, are described.

A number of physical, chemical and biological systems can be viewed as large ensembles of weakly interacting non-identical oscillators [1]. One of the most popular models here is an ensemble of globally coupled non-linear oscillators. Such systems appear in the studies of Josephson junction arrays [2], oscillatory neuronal systems [3], multimode lasers [4], charge-density waves [5], etc. Investigations of ensembles of non-linear continuous-time oscillators have revealed such interesting phenomena as clustering [6], existence of splay states [7], finite-size–induced transition [8], dephasing and bursting [9] and collective chaotic behaviour [6], [10]. A non-trivial transition to self-synchronization in a population of periodic oscillators with different natural frequencies coupled through a mean field has been described by Kuramoto [11]. In this system, as the coupling parameter increases, a sharp transition is observed for which the mean-field intensity serves as an order parameter. This transition owes to a mutual synchronization of the oscillators, so that their fields become coherent (*i.e.* their phases are locked), thus producing a macroscopic mean field. In its turn, this field acts on the individual oscillators, locking their phases, so that the synchronous state is self-sustained. Different aspects of this transition have been studied in [12], where also an analogy with a second-order phase transition has been exploited.

In this letter we describe self-synchronization transitions in a population of *chaotic* systems. We explain this by the recently found phenomenon of phase synchronization of chaotic oscillators [13].

As a basic model we consider a population of *non-identical* Rössler oscillators

$$\begin{cases} \dot{x}_i = -\omega_i y_i - z_i + \varepsilon X, \\ \dot{y}_i = \omega_i x_i + a y_i, \\ \dot{z}_i = 0.4 + z_i(x_i - 8.5), \end{cases} \tag{1}$$

(*) A. von Humboldt Fellow. Permanent address: Mech. Eng. Res. Institute, Russian Academy of Sciences, Moscow, Russia.

(**) Homepage: www.agnld.uni-potsdam.de.

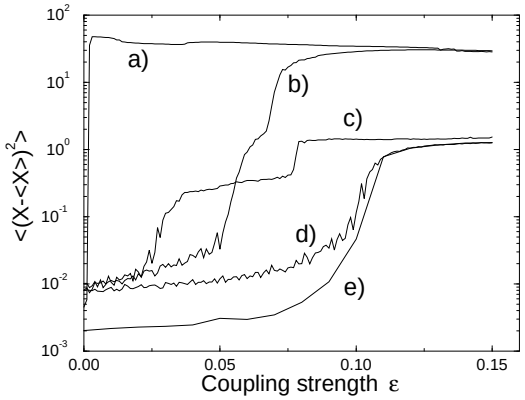

Fig. 1. – Variance of the mean field X *vs.* coupling parameter ε for different topologies of the Rössler system ($a = 0.15, \omega_0 = 1$ for curves *a*) and *b*); $a = 0.25, \omega_0 = 0.97$ for curves *c*) and *d*)) and different distributions of natural frequencies ($\Delta\omega = 0$ for curves *a*) and *c*); $\Delta\omega = 0.02$ for curves *b*) and *d*)). The number of oscillators is $N = 5000$ for curves *a*)-*d*). Curve *e*) differs from curve *d*) only in the size of the ensemble ($N = 20\,000$); it demonstrates the finite-size effect on the order parameter.

coupled via the mean field $X = N^{-1} \sum_1^N x_i$. Here N is the number of elements in the ensemble, ε is the coupling constant, a and ω_i are parameters of the Rössler oscillators [14]. The parameter ω_i governs the natural frequency of an individual system [13]. We take a set of frequencies ω_i Gaussian distributed around the mean value ω_0 with variance $(\Delta\omega)^2$. Because the Rössler system typically shows windows of periodic behaviour as the parameter ω is changed, we usually choose such a mean frequency ω_0 that avoids large periodic windows. The parameter a governs the topological type of the Rössler attractor; its significance is discussed below.

In our computer simulations we solve eqs. (1) numerically for rather large ensembles $N =$ 3000–5000. From our numerical calculations we have good indications that these ensembles are large enough to describe the dynamics correctly in the thermodynamic limit $N \to \infty$.

With an increase of the coupling strength ε, the appearance of a non-zero macroscopic mean field X is observed, as is shown in fig. 1. There the order parameter (the variance of the mean field) is depicted *vs.* the coupling ε for two values of the parameter a of the Rössler system

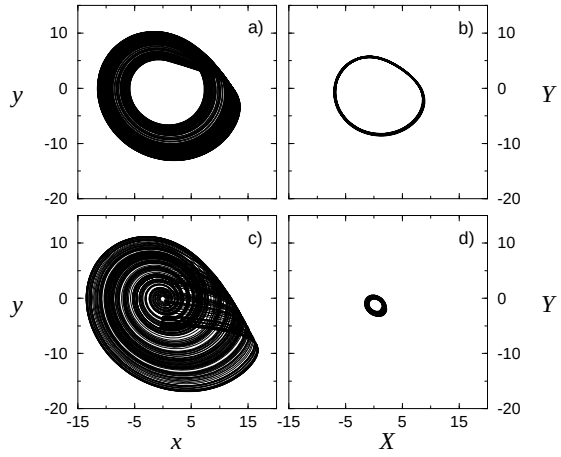

Fig. 2. – Projections of the phase portraits of the Rössler oscillators (left column) and of the mean fields $X = \langle x_i \rangle$, $Y = \langle y_i \rangle$ in an ensemble of $N = 5000$ oscillators. *a*) Phase-coherent Rössler attractor, $\omega_0 = 1$, $a = 0.15$. *b*) Mean field in the ensemble of oscillators *a*) with Gaussian distribution of frequencies $\Delta\omega = 0.02$ and coupling $\varepsilon = 0.1$. *c*) Funnel attractor $\omega_0 = 0.97$, $a = 0.25$. *d*) Mean field in the ensemble of oscillators *c*) with Gaussian distribution of frequencies $\Delta\omega = 0.02$ and coupling $\varepsilon = 0.15$.

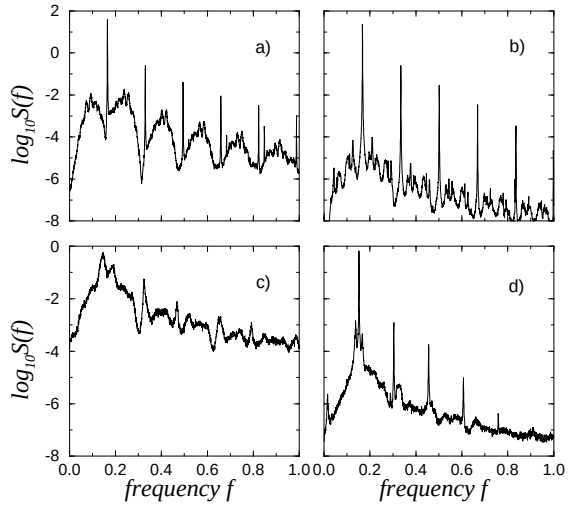

Fig. 3. – Power spectra of the processes $x(t)$ and $X(t)$ from fig. 2.

and for ensembles of identical ($\Delta\omega = 0$) and non-identical ($\Delta\omega > 0$) oscillators. The non-zero value of the order parameter (≈ 0.01) for small couplings is due to finite-size effects (finiteness of N, compare curves *d*) and *e*)).

We first focus on the non-identical case (curves *b*) and *d*)). One can see that although qualitatively a macroscopic mean field appears for both values of the parameter a, for $a = 0.15$ the field is much stronger than for $a = 0.25$. Also the threshold $\varepsilon_c \approx 0.05$ for $a = 0.15$ is significantly smaller than $\varepsilon_c \approx 0.1$ for $a = 0.25$. We attribute this to the quite different topologies of the corresponding strange attractors and hence the corresponding phase coherence properties to be described below.

The phase portrait of the Rössler attractor for $a = 0.15$ is shown in fig. 2 *a*). Here, the motion can be well represented as oscillations with a chaotic amplitude modulation, while the dynamics of the phase is relatively regular. In the power spectrum of the variable $x(t)$, this manifests itself as a sharp peak above a broad-band component (fig. 3 *a*)) [15], [16]. This type of attractor is called phase-coherent. In fact, we can introduce the phase of the Rössler attractor by making a projection of (1) on the plane (x, y) and taking the value of

$$\phi_i(t) = \arctan(x_i(t)/y_i(t)) \tag{2}$$

for the instantaneous phase. As has been argued in [17], [13], the dynamics of the phase is similar to that of a periodic oscillator and can be described by the following model equation:

$$\dot{\phi}_i = \omega_i + F(A_i). \tag{3}$$

Here ω_i is the mean frequency of oscillations and $F(A)$ is the amplitude-dependent non-linear term responsible for the non-uniform phase motion. Due to the chaotic nature of the attractor, $F(A)$ can be considered as a noisy term responsible for the phase diffusion.

Regarding the mean field $X(t)$ in eq. (1) as an external force having nearly constant amplitude (which is confirmed by numerics, see fig. 2 *b*)) and the phase ψ, we can write the dynamics of the phase ϕ_i under this force as

$$\dot{\phi}_i = \omega_i + F(A_i) + \varepsilon G(\phi_i, \psi)\,, \tag{4}$$

where G is a 2π-periodic in each argument function describing phase entrainment by the external force; in the first approximation one can take $G(\phi, \psi) \sim \sin(\phi - \psi)$. Comparing with the model of globally coupled periodic noise-driven oscillators having distribution of natural

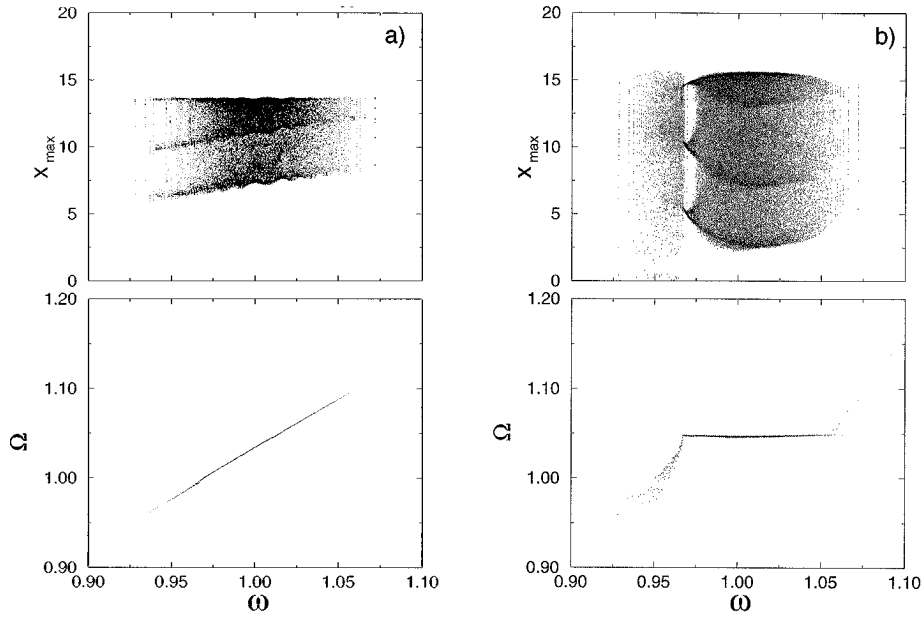

Fig. 4. – Successive maxima (upper panel) and observed frequencies, eq. (5) (bottom panel) *vs.* natural frequencies in the ensemble of coupled phase-coherent Rössler systems of fig. 2*a*). *a*) The coupling $\varepsilon = 0.05$ is slightly below the transition threshold, the observed frequencies Ω are proportional to the natural frequencies ω. *b*) Above threshold ($\varepsilon = 0.1$) most of the oscillators form a coherent cluster (plateau in the bottom panel), while the amplitudes remain chaotic (with the exception of the period-3 window for $\omega \approx 0.97$).

frequencies [18], we can see that the difference is in the term $F(A)$, which, instead of being Gaussian white noise, describes rather specific properties of phase dynamics in a particular chaotic system. Nevertheless, one can expect that qualitatively this term acts as an effective noise, thus allowing to consider the transition in the ensemble of chaotic *autonomous* oscillators as a phenomenon analogous to the synchronization transition in a network of coupled *noisy* limit-cycle oscillators.

In fact, for the Rössler attractor (fig. 2 *a*)) this term is rather small, so the phase can be easily locked by an external periodic force [17], [16] or due to the interaction of different oscillators [13]. Thus, the self-induced synchronization in the population of the Rössler systems can be explained as a Kuramoto-type transition in a network of oscillators without noise: the phases of some part of the ensemble become locked and the coherent summation of corresponding contributions leads to a non-zero mean field, while the amplitudes remain chaotic and uncorrelated. (A similar synchronization has been reported in [19] for a lattice of locally coupled identical Rössler systems.)

This is illustrated in fig. 4 where we plot the observed frequency Ω_i of the i-th oscillator, defined as the average derivative of the phase (2):

$$\Omega_i = \langle \dot{\phi}_i \rangle = \langle (x_i \dot{y}_i - \dot{x}_i y_i)(x_i^2 + y_i^2)^{-1} \rangle, \tag{5}$$

vs. the natural frequency ω_i.

In the absence of coupling ($\varepsilon = 0$) the observed frequency Ω_i is, as one could expect, proportional to ω_i. With the increase of coupling we observe the appearance of a plateau in the plot, *i.e.* these averaged frequencies of a large number of oscillators become equal. Respectively, these systems oscillate in-phase, and their contributions to the mean field produce a non-zero component. In the upper panel of fig. 4, we plot the values of the maxima

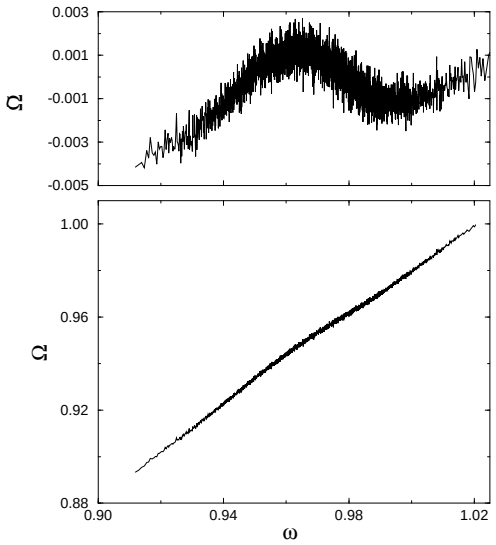

Fig. 5. – The observed frequency Ω in the ensemble of coupled funnel attractors with parameters of fig. 2 *d*). The upper panel shows the deviation $\tilde{\Omega}$ from the linear fit: the tendency to synchronization is clearly seen in this panel, although it is rather small.

of the field x_i for each oscillator. The distribution of these maxima gives an impression about the chaoticity of the amplitudes; we see that even in the case when almost all systems are synchronized, the amplitudes remain chaotic (with the exception of a small number of systems with periodic behaviour; it is worth noting that both chaotic and periodic systems are nevertheless synchronized). This agrees with recent findings [13], where the synchronization of two Rössler attractors has been considered and the chaoticity of the amplitudes has been verified by calculations of the Lyapunov exponents. Because the phases of different oscillators are locked, the mean field is fairly periodic, as demonstrated in a phase portrait (fig. 2 *b*)), where $Y = N^{-1} \sum_1^N y_i$ is plotted *vs.* X and in the power spectrum of the variable X (fig. 3 *b*)). Some modulation of the mean field visible there seems to be a finite-size effect.

We now discuss the situation when the Rössler oscillator has a rather weak phase coherence, *e.g.* for $a = 0.25$. The corresponding so-called funnel attractor [15], [16] is presented in fig. 2 *c*) and the power spectrum of $x(t)$ in fig. 3 *c*). The spectrum has no sharp peak because sometimes a trajectory makes a roundtrip around the origin in the (x, y)-plane, and sometimes it makes only a half of this roundtrip (fig. 2 *c*)). These irregular phase shifts can be interpreted as a large effective noise term $F(A)$ in eqs. (3), (4) which breaks the phase coherence. Nevertheless, for sufficiently large couplings a macroscopic highly coherent mean field appears (fig. 1, curve *d*); fig. 3 *d*)), although this field is much smaller than in the case of the phase-coherent attractor (fig. 2 *a*)). We interpret this transition as a synchronization transition, described for noisy coupled phase oscillators in [1], [18]. There it has been demonstrated that in an ensemble of globally coupled noisy phase oscillators a transition to a non-uniform distribution of the phases and to a macroscopic mean field occurs at a critical value of coupling. Similar transitions in coupled two-well noisy oscillators have been described in [20].

A qualitative difference between these two types of synchronization becomes clear if we consider the dependence of the observed frequency on the natural one. In the case of the phase-coherent attractor, the phases of the entrained oscillators are completely locked, and their observed frequencies coincide almost perfectly (fig. 4 *b*)). For funnel attractors there is no plateau in the distributions of frequencies; only a small "attraction" to the frequency of the mean field is seen (fig. 5). Exactly such an attraction occurs at the synchronization of

a noisy oscillator by a periodic force [21]. Nevertheless, this attraction produces the visible macroscopic effect.

Another difference is that the synchronization of the phase-coherent oscillators occurs already for very small couplings, if the distribution of natural frequencies is narrow; for noisy oscillators even for identical natural frequencies a finite threshold of synchronization exists, depending on the noise strength. This is illustrated in fig. 1, where the mean field is shown for the ensemble of identical systems ($\Delta\omega = 0$) with phase-coherent (curve a)) and funnel (curve c)) attractors.

In conclusion, we have demonstrated that in a population of globally coupled chaotic oscillators a transition to phase synchronization can be observed. The order parameter for this transition is the intensity of the mean field. The features of the transition depend crucially on the phase coherence properties of the individual systems. If the chaotic oscillators are phase-coherent, *i.e.* have a sharp peak in the spectrum, the dynamics of the phase is very similar to that in the population of periodic oscillators, the amplitudes of the oscillators remain, however, chaotic. Such a transition is also observed for the systems with coupled non–phase-coherent funnel attractors. In the latter case it is similar to the transition in a population of noisy phase oscillators. Statistical properties of the mean field and the finite-size effects remain a problem for future studies.

***

We thank M. Zaks for useful discussions. MGR acknowledges support from Alexander von Humboldt Foundation.

REFERENCES

[1] Kuramoto V., *Chemical Oscillations, Waves and Turbulence* (Springer, Berlin) 1984.
[2] Hadley P., Beasley M. R. and Wiesenfeld K., *Phys. Rev. B*, **38** (1988) 8712.
[3] Sompolinsky H., Golomb D. and Kleinfeld D., *Phys. Rev. A*, **43** (1991) 6990.
[4] Wiesenfeld K., Bracikowski C., James G. and Roy R., *Phys. Rev. Lett.*, **65** (1990) 1749.
[5] Strogatz S. H., Marcus C. M., Westervelt R. M. and Mirollo R. E., *Physica D*, **36** (1989) 23.
[6] Golomb D., Hansel D., Shraiman B. and Sompolinsky H., *Phys. Rev. A*, **45** (1992) 3516.
[7] Nichols S. and Wiesenfeld K., *Phys. Rev. A*, **45** (1992) 8430; Strogatz S. H. and Mirollo R. E., *Phys. Rev. E*, **47** (1993) 220.
[8] Pikovsky A. S., Rateitschak K. and Kurths J., *Z. Phys. B*, **95** (1994) 541.
[9] Han S. K., Kurrer C. and Kuramoto Y., *Phys. Rev. Lett.*, **75** (1995) 3190.
[10] Wiesenfeld K. and Hadley P., *Phys. Rev. Lett.*, **62** (1989) 1335; Hakim V. and Rappel W.-J., *Phys. Rev. A*, **46** (1992) R7347; Nakagawa N. and Kuramoto Y., *Prog. Theor. Phys.*, **89** (1993) 313.
[11] Kuramoto Y., *Prog. Theor. Phys. Suppl.*, **79** (1974) 223; in *International Symposium on Mathematical Problems in Theoretical Physics*, edited by H. Araki (Springer, New York, N.Y.) 1975.
[12] Sakaguchi H., Shinomoto S. and Kuramoto Y., *Prog. Theor. Phys.*, **77** (1987) 1005; Daido H., *Prog. Theor. Phys.*, **75** (1986) 1460; Daido H., *J. Stat. Phys.*, **60** (1990) 753.
[13] Rosenblum M., Pikovsky A. and Kurths J., *Phys. Rev. Lett.*, **76** (1996) 1804.
[14] Rössler O. E., *Phys. Lett. A*, **57** (1976) 397.
[15] Crutchfield J. *et al.*, *Phys. Lett. A*, **76** (1980) 1.
[16] Stone E. F., *Phys. Lett. A*, **163** (1992) 367.
[17] Pikovsky A. S., *Sov. J. Commun. Technol. Electron.*, **30** (1985) 1970.
[18] Sakaguchi H., *Prog. Theor. Phys.*, **79** (1988) 39; Bonilla L. L., Neu J. C. and Spigler R., *J. Stat. Phys.*, **67** (1992) 313.
[19] Brunnet L., Chaté H. and Manneville P., *Physica D*, **78** (1994) 141.
[20] Desai R. C. and Zwanzig R., *J. Stat. Phys.*, **19** (1978) 1.
[21] Stratonovich R. L., *Topics in the Theory of Random Noise* (Gordon and Breach, New York, N.Y.) 1963.

From Phase to Lag Synchronization in Coupled Chaotic Oscillators

Michael G. Rosenblum,* Arkady S. Pikovsky, and Jürgen Kurths
Department of Physics, Potsdam University, Am Neuen Palais 10, D-14415, Potsdam, Germany
(Received 15 October 1996)

We study synchronization transitions in a system of two coupled self-sustained chaotic oscillators. We demonstrate that with the increase of coupling strength the system first undergoes the transition to phase synchronization. With a further increase of coupling, a new synchronous regime is observed, where the states of two oscillators are nearly identical, but one system lags in time to the other. We describe this regime as a state with correlated amplitudes and a constant phase shift. These transitions are traced in the Lyapunov spectrum. [S0031-9007(97)03271-7]

PACS numbers: 05.45.+b

Synchronization phenomena in coupled chaotic systems have been extensively studied in the context of laser dynamics [1], electronic circuits [2,3], chemical and biological systems [4], and secure communication [5]. Complete, generalized, and phase synchronizations of chaotic oscillators have been described theoretically and observed experimentally. Complete (full) synchronization (CS) implies coincidence of states of interacting systems, $\mathbf{x}_1(t) = \mathbf{x}_2(t)$ [6–8]; it appears only if interacting systems are identical. Otherwise, if the parameters of coupled oscillators slightly mismatch, the states are close $|\mathbf{x}_1(t) - \mathbf{x}_2(t)| \approx 0$ but remain different [7,9]. A generalized synchronization (GS) [10], introduced for drive-response systems, is defined as the presence of some functional relation between the states of response and drive, i.e., $\mathbf{x}_2(t) = \mathcal{F}[\mathbf{x}_1(t)]$ [11]. The phase synchronization (PS) described in [12,13] and experimentally observed in [14] means entrainment of phases of chaotic oscillators, whereas their amplitudes remain chaotic and noncorrelated; the notion of phase is discussed in details in [15]. The relation between these different types of synchronization and the scenarios of transitions to or between them have not been addressed yet.

In this Letter we study synchronization of symmetrically coupled *nonidentical* oscillators. We demonstrate that, with the increase of coupling, first the transition from nonsynchronous state to PS occurs. For larger couplings a new regime which we call lag synchronization (LS) is observed. LS appears as a coincidence of *shifted in time* states of two systems, $\mathbf{x}_1(t + \tau_0) = \mathbf{x}_2(t)$. Finally, with a further increase of coupling, the time shift decreases and this regime tends to CS. We show that these transitions are related to the changes in the spectrum of Lyapunov exponents (LE).

Synchronization is a universal nonlinear phenomenon, and its main features are typically independent of particular properties of a model. As a first example, we study two coupled Rössler systems [16],

$$\begin{aligned} \dot{x}_{1,2} &= -\omega_{1,2} y_{1,2} - z_{1,2} + \varepsilon(x_{2,1} - x_{1,2}), \\ \dot{y}_{1,2} &= \omega_{1,2} x_{1,2} + a y_{1,2}, \\ \dot{z}_{1,2} &= f + z_{1,2}(x_{1,2} - c), \end{aligned} \tag{1}$$

where $a = 0.165$, $f = 0.2$, and $c = 10$. The parameters $\omega_{1,2} = \omega_0 \pm \Delta$ and ε determine the mismatch of natural frequencies and the coupling, respectively. These equations serve as a good model for real systems having a strange attractor that appears via period-doubling cascade, e.g., for electronic circuits [2,3] or chemical systems [17].

To describe the phase and the lag synchronization, we need to introduce corresponding quantities. For the Rössler attractor the phase and the amplitude can be conveniently introduced as [13,15,17]

$$\phi = \arctan \frac{y}{x}, \quad A = (x^2 + y^2)^{1/2}. \tag{2}$$

The phase can be easily calculated for each subsystem, thus allowing one to determine mean frequencies $\Omega_{1,2} = \langle \dot{\phi}_{1,2} \rangle$ and relations of locking between them. To characterize LS, we introduce a similarity function S as a time averaged difference between the variables x_1 and x_2 (with mean values being subtracted) taken with the time shift τ [18],

$$S^2(\tau) = \frac{\langle [x_2(t + \tau) - x_1(t)]^2 \rangle}{[\langle x_1^2(t) \rangle \langle x_2^2(t) \rangle]^{1/2}}, \tag{3}$$

and search for its minimum $\sigma = \min_\tau S(\tau)$. If the signals x_1 and x_2 are independent, the difference between them is of the same order as the signals themselves; respectively, $S(\tau) \sim 1$ for all τ. If $x_1(t) = x_2(t)$, as in the case of CS, $S(\tau)$ reaches its minimum $\sigma = 0$ for $\tau = 0$. Below, we demonstrate a nontrivial case, when the similarity function $S(\tau)$ has a minimum for nonzero time shift τ, meaning a time lag exists between the two processes.

First, we describe the transition to PS in the system (1) (see also [12]). The parameters $\omega_0 = 0.97$ and $\Delta = 0.02$ are chosen by trial in such a way that appearance of large windows of periodic behavior is avoided. The calculation of the average frequencies $\Omega_{1,2}$ allows us to follow the transition at $\varepsilon = \varepsilon_p \approx 0.036$ to the frequency entrainment $\Omega_1 = \Omega_2 = \Omega$ (see Fig. 1). Because of high coherence of the Rössler attractor, the phase difference in the synchronous regime is bounded and oscillates around some mean value $\delta\phi = \langle \phi_1(t) - \phi_2(t) \rangle \neq 0$.

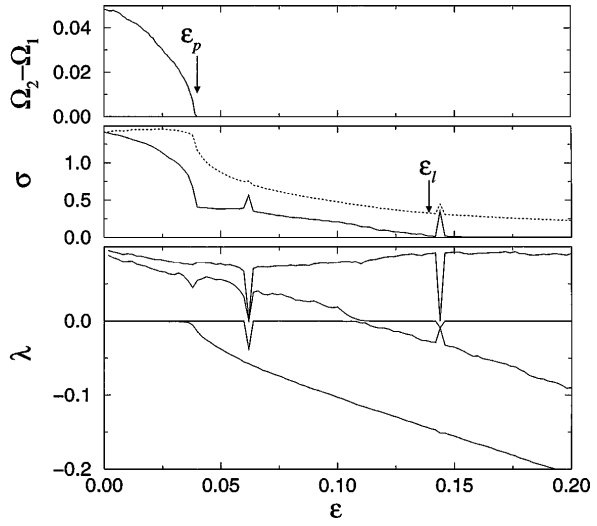

FIG. 1. The frequency difference $\Omega_1 - \Omega_2$, the minimum of the similarity function σ, and the four largest Lyapunov exponents λ of two coupled Rössler oscillators vs the coupling ε. Three different regions are clearly seen on the σ vs ε plot correspondent to a nonsynchronous state, phase, and lag synchronization, respectively. The transitions between these regimes are reflected in the spectrum of Lyapunov exponents: At the first transition, one of the zero LE becomes negative, while the second transition corresponds to the zero crossing of one of the positive LE. The dashed line shows the dependence of $S(0)$ on the coupling; from this plot one can see that comparison of states of interacting systems without time shift does not reveal the transition to LS. Two "outbursts" on the σ vs ε plot at $\varepsilon \approx 0.06$ and $\varepsilon \approx 0.145$ correspond to period 3 windows.

For stronger coupling $\varepsilon = \varepsilon_l \approx 0.14$ we observe a new transition to lag synchronization (see the σ vs ε curve in Fig. 1). In Fig. 2 we show numerically obtained similarity functions in system (1) for relatively weak, intermediate, and strong coupling. For weak coupling $\varepsilon < \varepsilon_p$ (curves 1 and 2), $S \sim 1$ and practically does not depend on τ, as can be expected for independent signals. For intermediate coupling strength $\varepsilon_p < \varepsilon < \varepsilon_l$, a minimum of $S(\tau)$ appears (curves 3 and 4) indicating the existence of some characteristic time shift τ_0 between x_1 and x_2. This shift is related to the phase difference as $\tau_0 = \delta\phi/\Omega$. Note that in this regime the amplitudes are uncorrelated, so the value of $S(\tau_0)$ is relatively large. Further increase of coupling makes, at $\varepsilon \approx \varepsilon_l$, this minimum very sharp (curves 5 and 6) and practically equal to zero. It means that the states of the systems become identical, but shifted in time with respect to each other. The regime of LS is clearly demonstrated in Fig. 3 by plotting $x_1(t + \tau_0)$ vs $x_2(t)$. It is important that calculations of $S(0)$, i.e., the comparison of x_1 and x_2 without time shift, reveal no transition at $\varepsilon = \varepsilon_l$. For larger couplings $\varepsilon > \varepsilon_l$, the time lag τ_0 continuously decreases, but no qualitative transitions are observed.

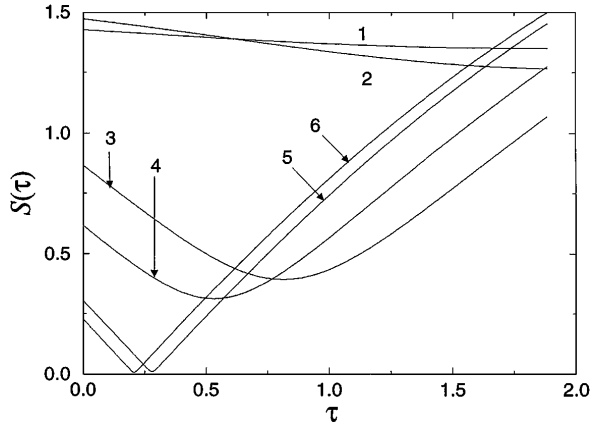

FIG. 2. Similarity function $S(\tau)$ for different values of coupling strength ε (1: $\varepsilon = 0.01$, 2: $\varepsilon = 0.015$, 3: $\varepsilon = 0.05$, 4: $\varepsilon = 0.075$, 5: $\varepsilon = 0.15$, 6: $\varepsilon = 0.2$). With the increase of coupling, a minimum appears, indicating the existence of a certain phase shift between interacting systems (curves 3 and 4). In the regime of lag synchronization (curves 5 and 6), the minimum is extremely small.

The transitions between different types of synchronization can be related to the changes in the Lyapunov spectrum (see Fig. 1). For small coupling $\varepsilon < \varepsilon_p$, there are two positive LE (corresponding to chaotic amplitudes) and two nearly zero LE (corresponding to independently rotating phases). At the phase locking transition at $\varepsilon \approx \varepsilon_p$, one of the zero LEs becomes negative, corresponding to a definite stable relation between phases (one zero LE, corresponding to a simultaneous phase shift of both Rössler oscillators, remains for all couplings, as it should in an autonomous system) [12]. The second transition to

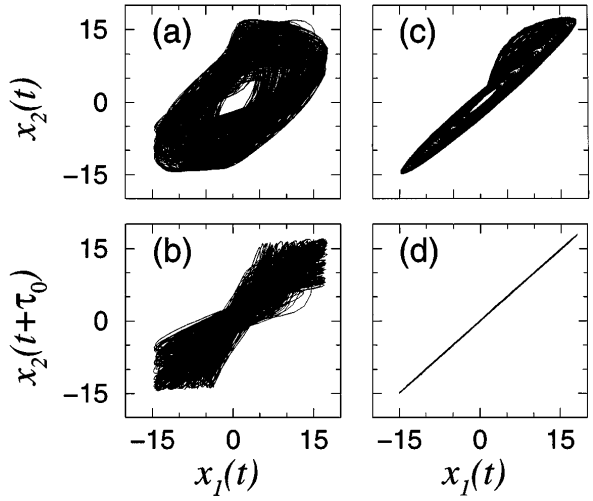

FIG. 3. Projections of the attractor of the coupled system on the plane $(x_1(t), x_2(t))$ and delayed-coordinate plots $x_2(t + \tau_0)$ vs $x_1(t)$ for different values of coupling. (a),(b) $\varepsilon = 0.05$, a regime with phase synchronization, (c),(d) $\varepsilon = 0.2$, a regime with lag synchronization. The qualitative difference between PS and LS is clearly seen from (b),(d), where time shifts, $\tau_0 = 0.87$ and $\tau_0 = 0.21$, respectively, correspond to the minima of the similarity function $S(\tau)$. The panel (d) demonstrates that the state of one of the oscillators is delayed in time with respect to the other; the same can be shown for the variables $y_{1,2}$ and $z_{1,2}$ as well.

LS corresponds to the change of the sign by the second positive LE, but does not exactly coincide with it due to the intermittency discussed below. This means that the relation appears not only between the phases but also between the amplitudes. The phase shift remains, and therefore a time lag between the signals x_1 and x_2 is observed.

To develop an approximate theory of the phase and lag synchronization in the model (1), let us rewrite it in the variables (2):

$$\begin{aligned}\dot{A}_{1,2} &= aA_{1,2}\sin^2\phi_{1,2} - z_{1,2}\cos\phi_{1,2} \\ &\quad + \varepsilon(A_{2,1}\cos\phi_{2,1}\cos\phi_{1,2} - A_{1,2}\cos^2\phi_{1,2}), \\ \dot{\phi}_{1,2} &= \omega_{1,2} + a\sin\phi_{1,2}\cos\phi_{1,2} + z_{1,2}/A_{1,2}\sin\phi_{1,2} \\ &\quad - \varepsilon(A_{2,1}/A_{1,2}\cos\phi_{2,1}\sin\phi_{1,2} - \cos\phi_{1,2}\sin\phi_{1,2}), \\ \dot{z}_{1,2} &= f - cz_{1,2} + A_{1,2}z_{1,2}\cos\phi_{1,2}.\end{aligned} \tag{4}$$

The main idea in analyzing this system is to use averaging over rotations of the phases $\phi_{1,2}$, assuming that the amplitudes vary slowly. Although there is no small parameter allowing one to perform this procedure mathematically correct, we will see that the results correspond rather well to the properties of the full system. Introducing the "slow" phases $\theta_{1,2}$ according to $\phi_{1,2} = \omega_0 t + \theta_{1,2}$, and averaging the equations for them, we get

$$\frac{d}{dt}(\theta_1 - \theta_2) = 2\Delta - \frac{\varepsilon}{2}\left(\frac{A_2}{A_1} + \frac{A_1}{A_2}\right)\sin(\theta_1 - \theta_2). \tag{5}$$

When we neglect the fluctuations of the amplitudes on the right-hand side, this equation has a stable fixed point

$$\theta_1 - \theta_2 = \arcsin\frac{4\Delta A_1 A_2}{\varepsilon(A_2^2 + A_1^2)} \tag{6}$$

which corresponds to the phase locking of the Rössler systems. The transition point to phase synchronization can thus be estimated as $\varepsilon_p \approx 4\Delta\langle A_1A_2/(A_2^2 + A_1^2)\rangle$. If we neglect the variations of the amplitudes we obtain $\varepsilon_p \approx 2\Delta = 0.04$ (for the parameters used), in rough agreement with the numerical result $\varepsilon_p \approx 0.036$.

Now we turn to the description of the next transition, and for this purpose we assume constant slow phases in the equations for A and z. Here we also perform the averaging, except for the terms containing both the fast phases $\phi_{1,2}$ and the variables $z_{1,2}$, because the latter, contrary to the amplitudes, cannot be considered as slow. As a result we obtain

$$\begin{aligned}\dot{A}_{1,2} &= \frac{a}{2}A_{1,2} - z_{1,2}\cos(\omega_0 t + \theta_{1,2}) \\ &\quad + \frac{\varepsilon}{2}[A_{2,1}\cos(\theta_1 - \theta_2) - A_{1,2}], \\ \dot{z}_{1,2} &= f - cz_{1,2} + A_{1,2}z_{1,2}\cos(\omega_0 t + \theta_{1,2}).\end{aligned} \tag{7}$$

This is a system of two coupled periodically driven oscillators. It is important that the driving in both systems is not identical, but comes with the phase shift (6). If we neglect for a moment this phase shift, the system (7) becomes a system of coupled *identical* chaotic oscillators, with a transition to *complete* synchronization to be observed [6,7]. In the system (7) this happens for $\varepsilon = 0.095$, to be compared with $\varepsilon_l = 0.14$ in the full system. With the phase shift, the transition to lag synchronization occurs. Indeed, if we introduce the lag variables for the second system $\tilde{A}_2 = A_2(t + \tau_0)$, $\tilde{z}_2 = z_2(t + \tau_0)$, where $\tau_0 = (\theta_1 - \theta_2)\omega_0^{-1}$, we can reduce (7) to the system of two identical oscillators, driven with the same force but where the coupling term contains one amplitude that is time shifted. Because the amplitudes in this model are slow, this time shift does not influence the full synchronization significantly, so we get $A_1 \approx \tilde{A}_2, z_1 \approx \tilde{z}_2$. In the initial variables this means the onset of lag synchronization:

$$x_2(t + \tau_0) \approx x_1(t), \quad y_2(t + \tau_0) \approx y_1(t), \quad z_2(t + \tau_0) \approx z_1(t).$$

This consideration also explains the discrepancy between the transition point to lag synchronization at $\varepsilon = \varepsilon_l \approx 0.14$ and the point where the second Lyapunov exponent becomes negative ($\varepsilon \approx 0.11$). Indeed, it is known that the transition to complete synchronization is extremely sensitive to small perturbations. Even when the second LE is negative, the local instability can lead to bursts of nonsynchronous behavior [19], see Fig. 4. Because of this intermittency, σ gradually decreases in the region $0.11 < \varepsilon < 0.14$ until these local instabilities disappear.

We now discuss the relation between the lag synchronization and the generalized one. The relation $\mathbf{x}_1(t) \approx \mathbf{x}_2(t + \tau_0)$ can be rewritten as $\mathbf{x}_1(t) \approx T^\tau\mathbf{x}_2(t)$, where T^t is the generating operator of the flow of the dynamical system. If the coupling ε and the time lag τ are small, we can approximate T with the generating operator of a partial (uncoupled) Rössler flow; it can be considered as a function in the three-dimensional phase space. Thus, the lag synchronization is similar to GS with the function being defined by the dynamics of the partial system.

To check the universal character of the LS, we investigate numerically two dynamical models of real physical systems. One is the electronic circuit experimentally studied in [3] in the context of CS; the other is the hybrid laser system experimentally studied in [20]. Both systems are

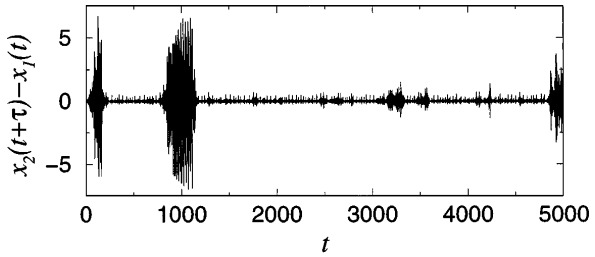

FIG. 4. The time series $x_2(t + \tau) - x_1(t)$ in the intermittent region $\varepsilon = 0.13$, $\tau = 0.32$. The bursts can be viewed as the excursions from the low-dimensional "synchronous" attractor.

described with low-dimensional models and allow one to implement coupling in a straightforward way. We have observed regimes of chaotic lag synchronization in both cases [21], with the similarity function having a rather sharp minimum. E.g., in coupled circuits [3] the similarity function $S(\tau)$ attains its minimum $\sigma = 0.01$ for $\tau = 0.21$ [to be compared with $S(0) = 0.07$]. For the coupled laser system the LS is even more pronounced: $\sigma = 0.005$ for $\tau = 0.3$, while $S(0) = 0.19$.

In summary, we have studied the synchronization properties of two mutually coupled self-sustained chaotic oscillators and have found a new synchronous state, which we refer to as the lag synchronization. We have shown that with the increase of the coupling strength the system can undergo several transitions. First, phase synchronization appears; by this transition, one of the zero LE becomes negative. Further increase of coupling leads to the occurrence of the relationship between the chaotic amplitudes. As a result, the states of two interacting systems coincide (if shifted in time); in the Lyapunov spectrum this transition corresponds to the zero crossing by one of the positive LEs. The motion in the originally six-dimensional phase space is now confined to a nearly three-dimensional manifold, thus corresponding to characterization of a synchronous regime via attractor dimensions [22]. Further increase of coupling decreases the time shift τ_0, and the systems tend to be completely synchronized. We emphasize that, in the LS state, full coherence of *nonidentical* systems is achieved due to interaction. This may be important, e.g., for coherent summation of radiation in laser arrays. As real systems can be hardly found fully identical, the LS can be more frequently encountered in experiments with coupled systems than CS. Finally, with the help of LS we can consider synchronization of periodic and chaotic oscillators within a common theoretical framework. Indeed, due to phase shift in the synchronous state, mutual entrainment of periodic oscillators having different frequencies can be viewed as a particular case of lag synchronization, but not of the complete one.

We thank C. Grebogi, U. Feudel, L. Kocarev, U. Parlitz, and M. Zaks for valuable discussions. M. R. and A. P. acknowledge support from the Max Planck Society.

*Permanent address: Mechanical Engineering Res. Inst., Russian Acad. Sci., Moscow, Russia.
Electronic address: www.agnld.uni-potsdam.de

[1] L. Fabiny, P. Colet, and R. Roy, Phys. Rev. A **47**, 4287 (1993); R. Roy and K. S. Thornburg, Jr., Phys. Rev. Lett. **72**, 2009 (1994).

[2] V. S. Anischenko, T. E. Vadivasova, D. E. Postnov, and M. A. Safonova, Int. J. Bifurcation Chaos Appl. Sci. Eng. **2**, 633 (1992).

[3] J. F. Heagy, T. L. Caroll, and L. M. Pecora, Phys. Rev. A **50**, 1874 (1994).

[4] I. Schreiber and M. Marek, Physica (Amsterdam) **5D**, 258 (1982); S. K. Han, C. Kurrer, and Y. Kuramoto, Phys. Rev. Lett. **75**, 3190 (1995).

[5] L. Kocarev and U. Parlitz, Phys. Rev. Lett. **74**, 5028 (1995).

[6] H. Fujisaka and T. Yamada, Prog. Theor. Phys. **69**, 32 (1983).

[7] A. S. Pikovsky, Z. Phys. B **55**, 149 (1984).

[8] L. M. Pecora and T. L. Carroll, Phys. Rev. Lett. **64**, 821 (1990); M. de Sousa Vieira, A. J. Lichtenberg, and M. A. Lieberman, Int. J. Bifurcation Chaos Appl. Sci. Eng. **1**, 691 (1991).

[9] V. Afraimovitch, N. Veritchev, and M. Rabinovitch, Izv. Vyssh. Uchebn. Zaved. Radiofiz. **29**, 1050 (1986) (in Russian).

[10] N. F. Rulkov, M. M. Suschik, L. S. Tsimring, and H. D. I. Abarbanel, Phys. Rev. E **51**, 980 (1995); H. D. I. Abarbanel, N. F. Rulkov, and M. M. Suschik, Phys. Rev. E **53**, 4528 (1996).

[11] Sometimes no restrictions on the function $\mathcal{F}$ are imposed [see L. Kocarev and U. Parlitz, Phys. Rev. Lett. **76**, 1816 (1996)]. However, only in the case of relatively smooth function $\mathcal{F}$ does this definition fit the intuitive idea of synchronization [cf. K. Pyragas, Phys. Rev. E **54**, R4508 (1996)].

[12] M. Rosenblum, A. Pikovsky, and J. Kurths, Phys. Rev. Lett. **76**, 1804 (1996); G. Osipov, A. Pikovsky, M. Rosenblum, and J. Kurths, Phys. Rev. E **55**, 2353 (1997).

[13] A. Pikovsky, M. Rosenblum, and J. Kurths, Europhys. Lett. **34**, 165 (1996).

[14] U. Parlitz, L. Junge, W. Lauterborn, and L. Kocarev, Phys. Rev. E **54**, 2115 (1996).

[15] A. Pikovsky, M. Rosenblum, G. Osipov, and J. Kurths, Physica D (Amsterdam) (to be published).

[16] O. E. Rössler, Phys. Lett. **57A**, 397 (1976).

[17] A. Goryachev and R. Kapral, Phys. Rev. Lett. **76**, 1619 (1996).

[18] To characterize more complex relations between x_1 and x_2, one could use a nonlinear similarity statistic based on entropy or a conditional predictor.

[19] A. Pikovsky and P. Grassberger, J. Phys. A **24**, 4587 (1991).

[20] F. Mitschke and N. Flüggen, Appl. Phys. B **35**, 59 (1984).

[21] The equations of the electronic circuit are taken from [3]; the coupling is implemented by adding the term $\varepsilon(x_{2,1} - x_{1,2})$ in the equation for $\dot{x}$; the parameters are (see [3]): $\Gamma_{1,2} = 0.05$, $\gamma_{1,2} = 0.1$, $\mu = 15$, $\beta_1 = 0.45$, $\beta_2 = 0.6$, and $\varepsilon = 0.7$. The dimensionless equations of the coupled hybrid lasers are [20] $\dot{x}_{1,2} = \omega_{1,2} y_{1,2} + \varepsilon(x_{2,1} - x_{1,2})$, $\dot{y}_{1,2} = \omega_{1,2}(z_{1,2} - x_{1,2} - 0.5y) + \varepsilon(y_{2,1} - y_{1,2})$, and $\dot{z}_{1,2} = -0.5 z_{1,2} - y_{1,2} + 8(x_{1,2} - 1)^2$, with $\omega_1 = 0.94$, $\omega_2 = 1$, and $\varepsilon = 0.105$.

[22] P. S. Landa and M. G. Rosenblum, Sov. Phys. Dokl. **37**, 237 (1992); P. S. Landa and M. G. Rosenblum, Appl. Mech. Rev. **46**, 414 (1993).

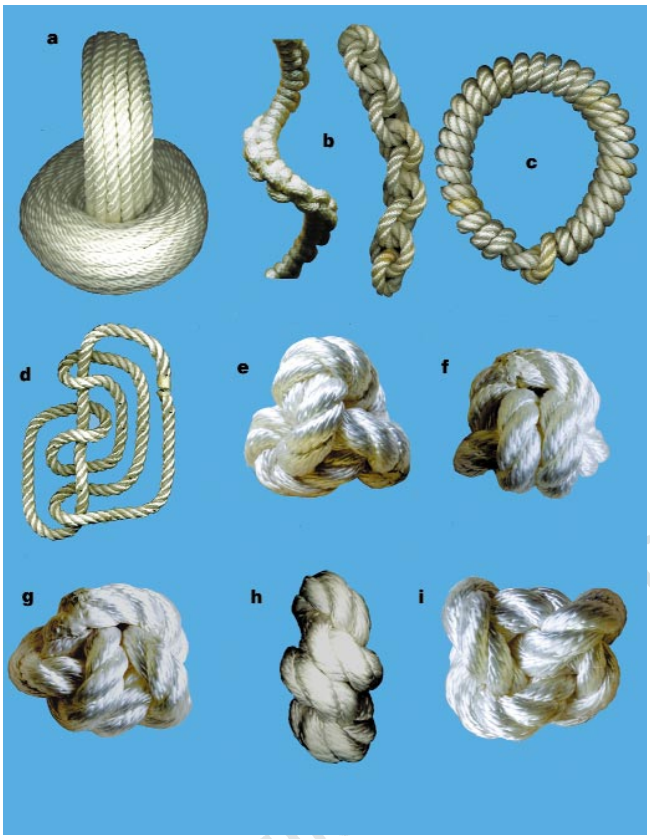

Figure 1 Knot conformations. **a**, Packed Hopf tori. **b**, Linear' conformations. Left, a product of trefoils; right, a thick chain with a linear relationship between crossing number and rope length. The chain also seems to be a continuous family of minima for rope length, in which case minima are not isolated in the link class. **c**, 'Linear' conformation of a twist knot – apparent minimum. **d**, An *N*-crossing knot fits in a square of side order *N*. **e**,**f**, Minima for figure-eight and square knot respectively. No particular accuracy is claimed – these knots were tied before the calculation of the computer data[7], and both the conformation and the values for rope length match almost exactly, as did several other knots. **g**, Minimum for the 'granny' knot, differing in shape from the minimum found by computer[11], and having a different symmetry. **h**, Another view. We estimate this to be the true global minimum. **i**, Some support for the accuracy of the rope calculations is given by this conformation of the five-crossing torus knot, which by rope seemed to be a lower minimum than the conformation reported in ref. 7. Further computation confirmed this.

shape, scaled so that $R(K)=1$, with total length L. The inverse-square 'energy' ($S(K)$, A, writhe, and so on) can be estimated by assuming the 'mass' of the knot is concentrated at points p on the integer lattice. Concentric shells of unit thickness about each p each contribute the same amount, so the contribution for p is that constant multiplied by the number of shells, which is of the order of $L^{1/3}$. Multiplying by the number of points, L, gives $L^{4/3}$. The proof that $S(K)$ linearly bounds A is simple vector geometry.

The 4/3 exponent is sharp. Consider the Hopf link of two tori in its natural geometrical position. Fill each torus with N loops parallel to the centre curve, each loop a strand of radius 1 (Fig. 1a). Then with any tight packing of the loops, the minor radii of the tori is of the order of $\sqrt{N}$. The conformation fits inside a sphere of radius $4\sqrt{N}$, so the total rope length is about $N^{3/2}$. Each loop is linked with N loops in the perpendicular torus, so the crossing number is about N^2. Therefore the rope length is of the order of $C(K)^{3/4}$. Because $11L(K)^{4/3} \geq 4\pi A(K) \geq C(K)$, this example has A in the order of $L(K)^{4/3}$.

The minimum rope length for a knot is bounded by $3C(K)^2$. This can be seen by arranging the knot so that the crossings are evenly spaced along a line (Fig. 1d). For the simpler knot types, $L(K)$, $S(K)$ and A in minimized conformations all 'appear' to be linearly related[7]. An explanation is that the simpler conformations are 'planar': from most perspectives a unit arc of the knot crosses only a few other unit arcs.

As complexity increases, there are many families of knots and links with three-dimensional growth, exhibiting the 4/3 power law. Families with single-dimensional growth (Fig. 1b,c) have a linear relationship among the measures. With planar growth, we expect A to be linear with $C(K)$ and $S(K)$ to be of the order of $L(K)\log L(K)$.

We propose that the rope length required (Fig. 1e–i) to tie an N-crossing knot or link varies only between $k_1N^{3/4}$ and k_2N. Other investigators have also recently observed the 4/3 law in knots on the cubic lattice[9] and in vector fields[10].

A good knot energy has only a finite number of knot types realized below any given energy level. Our theorem gives us this property for $L(K)$ and $S(K)$, proving that there is a finite number of knots that can be tied with a finite length of mathematical rope.

Gregory Buck
Department of Mathematics, Saint Anselm College, Manchester New Hampshire 03102, USA
email: gbuck@anselm.edu

1. Simon, J. in *Mathematical Approach to Biomolecular Structure and Dynamics* (Proc. of 1994 IMA Summer Program on Molecular Biology; eds Mesirov, J. P., Schulten, K. & Sumners, D.W.) 39–58 (IMA 82, Springer, New York, 1996).
2. Stasiak, A., Katritch, V., Bednar, J., Michoud, D. & Dubochet, J. *Nature* **384,** 122 (1996).
3. Buck, G. & Simon, J. *Topol. Appl.* (in the press).
4. O'Hara, J. *Topology* **30,** 241–247 (1991).
5. Moffatt, H. K. *Nature* **347,** 367–369 (1990).
6. Buck, G. & Orloff, J. *Topol. Appl.* **61,** 205–214 (1995).
7. Katritch *et al. Nature* **384,** 142–145 (1996).
8. Buck, G. (Preprint no. 2, Math. Dept, St Anselm College, 1993).
9. Diao, Y. & Ernst, K. *Topol. Appl.* (in the press).
10. Cantarella, J., DeTurck, D. & Gluck, H. (Preprint, Math. Dept., Univ. Pennsylvania, 1997).
11. Katritch, V., Olson, W. K., Pieranski, P., Dubochet, J. & Stasiak, A. *Nature* **388,** 148–151 (1997).

Heartbeat synchronized with ventilation

It is widely accepted that cardiac and respiratory rhythms in humans are unsynchronised[1]. However, a newly developed data analysis technique allows any interaction that does occur in even weakly coupled complex systems to be observed. Using this technique, we found long periods of hidden cardiorespiratory synchronization, lasting up to 20 minutes, during spontaneous breathing at rest.

Synchronization is a universal phenomenon that occurs when two or more nonlinear oscillators are coupled. It is observed in many fields of science and is widely applied in engineering. The case of synchronisation in periodic, or even noisy, oscillators is well understood[2–4]. The notion of synchronization has often been used to analyse the interaction between physiological (sub)systems[1], but these studies have been restricted to almost periodic rhythms. No approach has been suggested to probe the weak interactions between such irregular and non-stationary oscillators as the human heart and respiratory system.

These two physiological systems are known to be coupled by several mechanisms, but apart from respiratory modulation of heart rate, first observed in 1847 and known as 'respiratory sinus arrhythmia' (RSA)[5–7], no other effects have been reported. Moreover, in spite of some early communications[8], it has been concluded that "there is comparatively weak coupling between respiration and the cardiac rhythm, and the resulting rhythms are generally not phase locked"[1].

We used the concept of phase synchronization of chaotic oscillators[9,10] to develop a technique to analyse irregular non-stationary bivariate data. We analysed data obtained in non-invasive examinations of eight healthy volunteers (14–17-year-old, high-performance swimmers; four of them male and four female). While subjects lay at rest, electrocardiograms (ECGs) were recorded while respiratory

Table 1 **Subjects, ordered by the amplitude of respiratory sinus arrhythmia (RSA) determined as the averaged difference between the longest and shortest R–R interval within every respiratory cycle***

Code	Sex	Age	R-R (ms)		Resp. cycle (ms)		RSA (ms)		Synchronization
			Median	ΔQuart.	Median	ΔQuart.	Median	ΔQuart.	
A	m	16.1	1,104	28	3,110	390	15	40	3:1 (1,000 s), 5:2 (300 s), 8:3 (20 s)
B	m	14.6	1,018	95	3,210	610	31	38	3:1 (several spells of 40 s)
C	m	13.9	975	110	3,230	850	46	57	3:1 (20 s), 7:2 (20 s), 4:1 (20 s)
D	f	15.2	1,157	157	2,930	780	56	57	5:2 and 3:1 (several spells of 30 s)
E	m	16.9	1,026	89	3,650	620	67	47	7:2 (60 s), 3:1 and 4:1 (20s)
F	f	15.0	1,024	143	2,960	700	74	75	11:4 (20 s)
G	f	15.9	733	70	5,615	1,550	83	70	No synchronization detectable
H	f	16.3	1,256	197	4,260	2,100	264	296	No synchronization detectable

*If an R-R interval spans two adjacent cycles, it is considered to belong to that one which contains more than 50% of the interval. For R-R intervals, respiratory cycles and the RSA, the medians of respective distributions and differences between the first and third quartile (ΔQuart.) are given. We observe that cardiorespiratory synchronization tends to become weak with increasing RSA.

flow was simultaneously measured with a thermistor at the nose. Both signals were digitized with a 1,000-hertz sampling rate and 12-bit resolution. Each record lasted 30 minutes.

The resulting time series were irregular, strongly non-stationary and noisy. These characteristics made it inappropriate, in analysing the mutual dependencies involved, to use even sliding versions of traditional spectral and correlations techniques, or direct computation of instantaneous phase differences[9,10]. So instead of these techniques, we used a new kind of data presentation which we call a cardiorespiratory synchrogram (CRS), to detect different synchronous states and transitions between them.

We first used the Hilbert transform[9] to calculate the instantaneous phase $\phi_r(t)$ of the respiratory signal. $\phi_r(t)$ is defined on the real line (not restricted to the $[0,2\pi]$ interval). Next, we regarded the respiratory phase stroboscopically at times t_k, where the R-peak in the kth heartbeat occurs and hence the phase of the heart rhythm increases by 2π. In the simplest case of n:1 synchronization, there are n heartbeats in each respiratory cycle; these beats appear at n certain values of respiratory phases, which are constant over all cycles.

Plotting these relative phases ψ as a function of time shows n horizontal stripes. In the general case of n:m synchronization, such a structure appears if we relate the phases of the heart beats to the beginning of m adjacent respiratory cycles, $\psi(t_k)=(\phi_r(t_k) \mod 2\pi m)/2\pi$; we have n horizontal stripes within m respiratory cycles.

This technique allows us to distinguish between different periods of synchronization, even for noisy and non-stationary data. For example, we observe 5:2 locking between the respiratory frequency ω_r and the heart rate ω_h ($5\omega_r \approx 2\omega_h$) during a period of about 300 seconds, then after a transition period, a regime of 3:1 phase locking is found for about 20 minutes (Fig. 1). These two kinds of locking can be recognized using histograms (Fig. 1c) and the autocorrelation function of phases (Fig. 1d).

Our analysis showed cardiorespiratory synchronization of several locking ratios occurring in six out of eight subjects (Table 1). Subjects with the strongest synchronization had no remarkable RSA, whereas both subjects with the highest RSA exhibited no synchronization.

We conclude that phase locking of respiratory and the cardiac rhythms, and respiratory modulation of heart rate, are two competing aspects of cardiorespiratory interaction. From a physical viewpoint, synchronization and modulation are different phenomena and are related to different coupling. RSA generation is associated mainly with the baroreflex feedback loop and its respiratory phase-dependent information processing[7].

Perhaps cardiorespiratory synchronization is an expression of another kind of cardiorespiratory interaction, such as a central coupling between cardiovascular and respiratory neuronal activities.

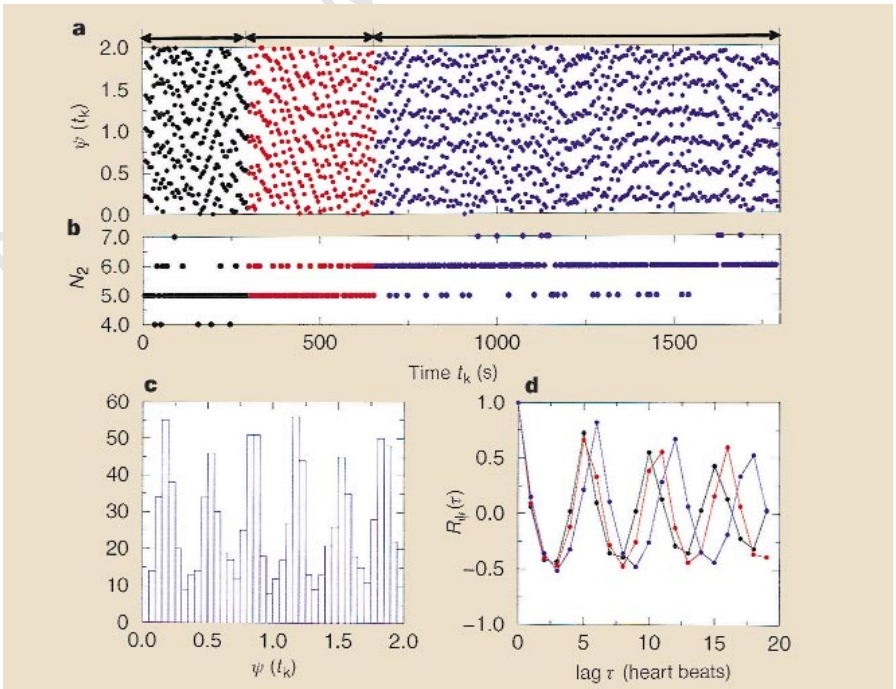

Figure 1 Analysis of cardiorespiratory cycles. **a,** Cardiorespiratory synchrogram, showing the transition (red) from 5:2 frequency locking (black) to 3:1 phase locking (blue). Each point shows the normalized relative phase of a heartbeat within two adjacent respiratory cycles $\psi(t_k)=(\phi_r(t_k) \mod 4\pi)/2\pi$. **b,** Number of heartbeats within two adjacent respiratory cycles. **c,** Histogram of phases. The six horizontal stripes in the blue region of the CRS result in six well-pronounced peaks in the distribution of phases. **d,** Autocorrelation function of phases $R_\psi(\tau)=\Sigma_k(\psi(t_k)-\langle\psi\rangle)(\psi(t_{k+\tau})-\langle\psi\rangle)/\Sigma_k(\psi(t_k)-\langle\psi\rangle)^2$. The coloured curves correspond to respective regions.

Carsten Schäfer, Michael G. Rosenblum, Jürgen Kurths
Department of Physics, University of Potsdam, Am Neuen Palais 10, PF 601553, 14415 Potsdam, Germany
e-mail: carsten@agnld.uni-potsdam.de
Hans-Henning Abel
Department of Cardioanaesthesiology, Städt Klinikum Braunschweig, Salzdahlumer Strasse 90, 38126 Braunschweig, Germany

1. Mackey, M. C. & Glass, L. *From Clocks to Chaos: The Rhythms of Life* Ch. 7 (Univ. Press, Princeton, 1988).
2. Stratonovich, R. L. *Topics in the Theory of Random Noise* (Gordon and Breach, New York, 1963).
3. Blekhman, I. I. *Synchronization in Science and Technology* (ASME, New York, 1988).
4. Strogatz, S. H. & Steward, I. *Sci. Am.* **269,** 102–109 (1993).
5. Ludwig, C. *Arch. Anat. Physiol.* **13,** 242–302 (1847).
6. Anrep, G. V., Pascual, W., Rössler, R. *Proc. R. Soc. Lond. B* **119,** 191–230 (1936).
7. Eckberg, D. L., Kifle, Y. T., Roberts, V. L. *J. Physiol., Lond,* **304,** 489–502 (1980).
8. Pessenhofer, H. & Kenner, T. *Pflügers Arch.* **355,** 77–83 (1975).
9. Rosenblum, M. G., Pikovsky, A. S., Kurths, J. *Phys. Rev. Lett.* **76,** 1804–1807 (1996).
10. Pikovsky, A. S., Rosenblum, M. G., Osipov, G. V., Kurths, J. *Physica D* **104,** 219–238 (1997).

Detection of n:m Phase Locking from Noisy Data: Application to Magnetoencephalography

P. Tass,[1] M. G. Rosenblum,[2] J. Weule,[1] J. Kurths,[2] A. Pikovsky,[2] J. Volkmann,[1] A. Schnitzler,[1] and H.-J. Freund[1]
[1]*Department of Neurology, Heinrich-Heine-University, Moorenstrasse 5, D-40225 Düsseldorf, Germany*
[2]*Department of Physics, University of Potsdam, Am Neuen Palais 19, PF 601553, D-14415, Potsdam, Germany*
(Received 5 June 1998)

We use the concept of phase synchronization for the analysis of noisy nonstationary bivariate data. Phase synchronization is understood in a statistical sense as an existence of preferred values of the phase difference, and two techniques are proposed for a reliable detection of synchronous epochs. These methods are applied to magnetoencephalograms and records of muscle activity of a Parkinsonian patient. We reveal that the temporal evolution of the peripheral tremor rhythms directly reflects the time course of the synchronization of abnormal activity between cortical motor areas. [S0031-9007(98)07333-5]

PACS numbers: 87.22.Jb, 05.45.+b, 87.22.As

Irregular, nonstationary, and noisy bivariate data abound in many fields of research. Usually, two simultaneously registered time series are characterized by means of traditional cross-correlation (cross-spectrum) techniques or nonlinear statistical measures like mutual information or maximal correlation [1]. Only very recently a tool of nonlinear dynamics, mutual nonlinear prediction, was used for characterization of dynamical interdependence among systems [2]. In this Letter we use a synchronization approach to the analysis of such bivariate time series and introduce a new method to detect alternating epochs of phase locking from nonstationary data. By doing so we extract information on the interdependence of weakly interacting systems that cannot be obtained by traditional methods.

Our technique, based on theoretical studies of phase synchronization of chaotic oscillators [3], can be fruitfully applied, e.g., in neuroscience, where synchronization processes are of crucial importance, e.g., for visual pattern recognition [4] and motor control [5]. Recent animal experiments have led to the conclusion that the control of coordinated movements is based on a synchronization of the firing activity of groups of neurons in the primary and in secondary motor areas [5]. Synchronization is also assumed to be involved in the generation of pathological movements, e.g., resting tremor in Parkinson's disease (PD) [6]. Although experimental studies indicate which parts of the nervous system are engaged in generating tremor activity, the dynamics of this process is not yet understood [7].

Here we study synchronization between the activity of remote brain areas in humans by means of noninvasive measurements. This is possible because a group of synchronously firing neurons within a single area generates a magnetic field which can be registered outside the head by means of multichannel magnetoencephalography (MEG) [8]. Accordingly, synchronization of neuronal activity between remote areas is reflected as phase locking between MEG channels. Our analysis reveals phase synchronization (a) between the activity of certain brain areas and (b) between the activity of these areas and the muscle activity detected by electromyography (EMG).

In particular, we find that the phase locking between the activity of primary and secondary motor areas is related to the coordination of antagonistic muscles.

Our approach is based on the notion of phase synchronization. Classically synchronization of two periodic nonidentical oscillators is understood as adjustment of their rhythms, or appearance of *phase locking*, due to interaction. The locking condition reads

$$|\varphi_{n,m}(t)| < \text{const}, \quad \text{where } \varphi_{n,m}(t) = n\phi_1(t) - m\phi_2(t), \tag{1}$$

n and m are some integers, $\phi_{1,2}$ are phases of two oscillators, and $\varphi_{n,m}$ is the generalized phase difference, or relative phase; all phases are divided by 2π for normalization, and $\varphi_{n,m}$, as well as $\phi_{1,2}$, are defined not on the circle $[0, 1]$ but on the whole real line. In this simplest case condition (1) is equivalent to the notion of *frequency locking* $n\Omega_1 = m\Omega_2$, where $\Omega_{1,2} = \langle\dot{\phi}_{1,2}\rangle$ and brackets mean time averaging. Note that for the determination of synchronous states it is irrelevant whether the amplitudes of both oscillators are different or not.

The definition of synchronization in *noisy and/or chaotic systems* is not so trivial. Recently it has been shown [3] that the notion of phase can generally be introduced for chaotic systems as well, and phase locking in the sense of (1) can be observed. The amplitudes of synchronized systems remain chaotic and effect the phase dynamics qualitatively in the same way as external noise [3]. Therefore in the following we consider noisy and chaotic cases within a common framework, i.e., by the term "noise" we denote both random and purely deterministic perturbations to phases. If this noise is weak (and bounded) then in the synchronous state the relative phase fluctuates around some constant value, and the condition of frequency locking is fulfilled. Strong noise can cause *phase slips*, i.e., rapid unit jumps of the relative phase. In this case the question "synchronous or not synchronous" cannot be answered unambigously, but can be treated only in a statistical sense. Following the basic work of Stratonovich [9] we understand synchronization of noisy systems as appearance of peaks in the *distribution of the*

cyclic relative phase $\Psi_{n,m} = \varphi_{n,m} \bmod 1$, that enables us to detect preferred values of the phase difference irrespective of the noise-induced phase jumps. The probability of these upward and downward jumps may either be equal or different, i.e., the relative phase performs either unbiased or biased random walks. In the first case the averaged frequencies $\Omega_{1,2} = \langle \dot{\phi}_{1,2} \rangle$ coincide, whereas in the second case they are different. However, in a statistical sense synchronization is characterized by the existence of one or a few preferred values of $\Psi_{n,m}$, no matter whether the oscillators' averaged frequencies are equal or different.

For illustration we consider two coupled nonidentical Rössler systems subject to noisy perturbations:

$$\begin{aligned} \dot{x}_{1,2} &= -\omega_{1,2} y_{1,2} - z_{1,2} + \xi_{1,2} + \varepsilon(x_{2,1} - x_{1,2}), \\ \dot{y}_{1,2} &= \omega_{1,2} x_{1,2} + 0.15 y_{1,2}, \\ \dot{z}_{1,2} &= 0.2 + z_{1,2}(x_{1,2} - 10). \end{aligned} \tag{2}$$

Here we introduce the parameters $\omega_{1,2} = 1 \pm 0.015$ and ε which govern the frequency mismatch and the strength of coupling, respectively; $\xi_{1,2}$ are two Gaussian delta-correlated noise terms, $\langle \xi_i(t) \xi_j(t') \rangle = 2D\delta(t - t')\delta_{i,j}$. The system is simulated by Euler's technique with the time step $\Delta t = 2\pi/1000$. If the noisy perturbations are rather weak, $D = 0.2$, the phase difference oscillates around some constant level, and its distribution obviously has a sharp peak. Therefore we can speak of frequency and phase locking here (Fig. 1a, curve 1). If the noise is stronger, $D = 1$, the relative phase performs a biased random walk, so there is obviously no frequency locking (Fig. 1a, curve 2). Nevertheless, the distribution of the phase definitely indicates locking in the statistical sense (Fig. 1b), in contrast to the nonsynchronous case (Fig. 1a, curve 3 and Fig. 1c).

It is very important to emphasize that synchronization is not equivalent to correlation. Hence, our analysis reveals different characteristics of the systems' interdependence. To illustrate this, we consider signals $u = (1 - \mu)x_1 + \mu x_2$ and $w = \mu x_1 + (1 - \mu)x_2$. By doing so we imitate the real situation: each MEG sensor measures signals originating from more than one area of neuronal activity. Nevertheless, this mixture of signals does not lead to a spurious detection of synchronization, although u and w are correlated (Fig. 1).

Now we use our approach to extract information about the underlying dynamics of the system from bivariate data at its output. With this aim in view we compute the instantaneous phase ϕ_j of each observed signal by means of the Hilbert transform (see [3], and references therein). A straightforward approach to search for n:m locking is to pick n and m by trial and error, plot the relative phase $\varphi_{n,m}$ vs time, and look for horizontal plateaus in this presentation [10]. Because of phase fluctuations and slips this can be misleading for noisy data (cf. Fig. 1). Thus, the above described statistical approach is needed.

To characterize the strength of synchronization, we have to quantify the deviation of the actual distribution of the relative phase from a uniform one. For this purpose, we propose two measures, or *n:m synchronization indices*. (i) *Index based on the Shannon entropy* is defined as $\tilde{\rho}_{nm} = (S_{\max} - S)/S_{\max}$, where $S = -\sum_{k=1}^{N} p_k \ln p_k$ is the entropy of the distribution of $\Psi_{n,m}$ and $S_{\max} = \ln N$, where N is the number of bins. Normalized in this way, $0 \le \tilde{\rho}_{nm} \le 1$, where $\tilde{\rho}_{nm} = 0$ corresponds to a uniform distribution (no synchronization) and $\tilde{\rho}_{nm} = 1$ corresponds to a Dirac-like distribution (perfect synchronization). (ii) *Index based on conditional probability:* Suppose we have two phases $\phi_1(t_j)$ and $\phi_2(t_j)$ defined on the interval $[0, n]$ and $[0, m]$, respectively; index j corresponds to time. We divide each interval into N bins. Then, for each bin l, $1 \le l \le N$, we calculate $r_l(t_j) = M_l^{-1} \sum e^{i\phi_2(t_j)}$ for all j, such that $\phi_1(t_j)$ belongs to this bin l, and M_l is the number of points in this bin. If there is a complete dependence between two phases, then $|r_l(t_j)| = 1$, whereas it is zero if there is no dependence at all. Finally, we calculate the average over all bins, $\tilde{\lambda}_{nm}(t_j) = 1/N \sum_{l=1}^{N} |r_l(t_j)|$. Thus, $\tilde{\lambda}_{nm}$ measures the conditional probability for ϕ_2 to have a certain value provided ϕ_1 is in a certain bin [11]. To find n and m we try different values and pick up those that give larger indices.

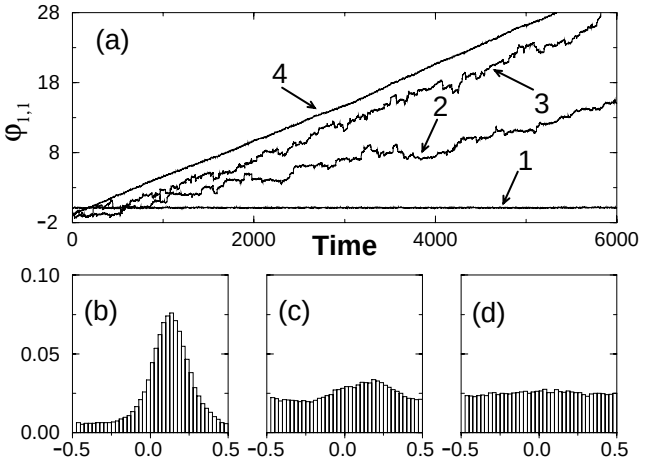

FIG. 1. The relative phases $\varphi_{1,1}$ (a) and distribution of $\Psi_{1,1} = \varphi_{1,1} \bmod 1$[(b),(c)] for system (2). If the noise is weak, $D = 0.2$, the phase difference of two synchronized oscillators ($\varepsilon = 0.04$) fluctuates around some constant value (curve 1), and its distribution is obviously sharp (not shown). In the presence of strong noise, $D = 1$, the phase difference performs a biased random walk (curve 2, $\varepsilon = 0.04$), as well as in the nonsynchronous case (curve 3, $\varepsilon = 0.01$). The distributions of $\Psi_{1,1}$ [(b),(c)] clearly distinguish these states. The phase difference [(a), curve 4] computed from u and w that are linear combination (see text) of outputs from uncoupled oscillators and its distribution (d) do not lead to a spurious detection of synchronization, although cross-spectrum analysis by means of Welch technique with the Bartlett window reveals significant coherence $\gamma^2 = 0.43$ between u and w; parameters are $D = 0.2$, $\mu = 0.02$.

Here we analyze MEG and EMG data from a PD patient who had a tremor of the right hand and forearm with a principal frequency component between 5 and 7 Hz (Fig. 2). We registered EMG from two antagonistic

muscles, namely, the right flexor digitorum superficialis muscle and the right extensor indicis muscle; standard preprocessing (cf. [7]) was used so that the resulting signal represents the time course of the muscular contraction. Next, MEG and EMG were filtered with a bandpass corresponding to the principal EMG frequency component (5–7 Hz). MEG signals were additionally filtered with a bandpass corresponding to the tremor's first harmonics (10–14 Hz). As the data are nonstationary, we perform a sliding window analysis and compute for every time point t the distribution of $\Psi_{n,m}$ within the window $[t - T/2, t + T/2]$ and synchronization indices [12].

To avoid spurious detection of locking due to noise and bandpass filtering, we derive significance levels $\rho^{\mathrm{S}}_{n,m}$ and $\lambda^{\mathrm{S}}_{n,m}$ for each n:m synchronization index $\tilde{\rho}_{n,m}$ and $\tilde{\lambda}_{n,m}$ by applying our analysis to surrogate data (white noise filtered exactly as the original signals). The 95th percentile of the distribution of the n:m synchronization indices ($\tilde{\rho}_{n,m}$ or $\tilde{\lambda}_{n,m}$) of the surrogates serves as significance level ($\rho^{\mathrm{S}}_{n,m}$ or $\lambda^{\mathrm{S}}_{n,m}$). Only relevant values of the n:m synchronization indices are taken into account by introducing the significant n:m synchronization indices $\rho_{n,m} = \max\{\tilde{\rho}_{n,m} - \rho^{\mathrm{S}}_{n,m}, 0\}$ and $\lambda_{n,m} = \max\{\tilde{\lambda}_{n,m} - \tilde{\lambda}^{\mathrm{s}}_{n,m}, 0\}$. For our data, computation of both indices gives consistent results.

Let us summarize our results. Pronounced tremor activity starts after ~50 s (Fig. 3a). During this epoch, besides the expected *peripheral coordination*, i.e., 1:1 antiphase locking of EMG's of flexor and extensor muscles, (Fig. 3b), we also find *corticomuscular* (CMS) as well as *cortico-cortical synchronization* (CCS). Namely, the activity of both sensorimotor cortex and premotor areas are 1:2 phase locked with the EMG activity of both flexor and extensor muscles (Figs. 3c and 4), whereas the activities of these two brain areas are 1:1 locked (Fig. 3d). It is important that when the strength of peripheral coordination decreases during the last ~50 s, the strength of CMS and CCS is also reduced. We find that MEG activity in the range of 10–14 Hz is responsible for both CMS and CCS.

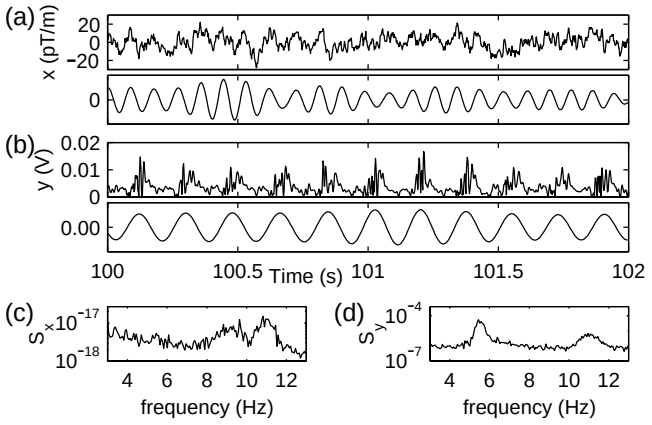

FIG. 2. An original and filtered MEG signal (from a channel over the left sensorimotor cortex) (a) and its power spectrum (c). The EMG signal of the right flexor digitorum muscle (b) and its power spectrum (d).

Our analysis reveals the brain areas with MEG activity phase locked to tremor activity (Fig. 4), while the traditional cross-spectrum technique fails here. Contralateral sensorimotor MEG signals are coherent with EMG, in accordance with the concept of Volkmann *et al.* [13] which is based on their MEG study, animal experiments, and recordings during neurosurgery in PD patients. Nevertheless, we also found tremor coherent MEG activity extended over the right hemisphere in contradiction to this concept [7]. Inefficiency of the coherence technique can additionally be seen from the fact that MEG channels overlying sensorimotor and premotor areas are coherent with practically all other MEG channels.

To conclude, we proposed a method to detect n:m phase locking and quantify the strength of synchronization from noisy bivariate data. A very important feature of our approach is that we can avoid the hardly solvable dilemma "noise vs chaos": irrespective of the origin of the observed signals the approach and techniques of the analysis are unique. In this way we addressed a fundamental problem in neuroscience whether cortico-cortical synchronization is necessary for establishing coordinated muscle activity.

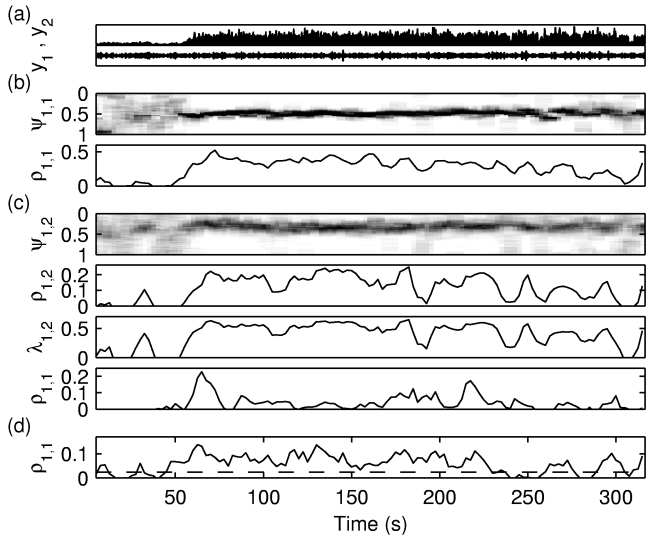

FIG. 3. (a) EMG of the right flexor muscle (RFM, upper trace) and an MEG over the left sensorimotor cortex (LSC) (lower trace). (b) 1:1 synchronization between right flexor and extensor muscles: the distribution of the cyclic phase difference $\Psi_{1,1}$ computed in the running window $[t - 5, t + 5]$ is shown as a gray-scale plot, where white and black correspond to minimal and maximal values, respectively (upper plot); the lower plot shows the corresponding significant synchronization index $\rho_{1,1}$. (c) 1:2 corticomuscular synchronization: time course of the distribution of the cyclic phase difference $\Psi_{1,2}$ between MEG signal from the LSC and EMG of the RFM (uppermost plot) and of the corresponding indices $\rho_{1,2}$ and $\lambda_{1,2}$; for comparison, 1:1 synchronization index $\rho_{1,1}$ between LSC and RFM is shown below. (d) 1:1 cortico-cortical synchronization between LSC and a premotor MEG channel. The dashed line indicates the value of $\rho_{1,1}$ corresponding to 99.9th percentile of the surrogates. Significance levels are $\rho^{\mathrm{S}}_{1,2} = 0.03$, $\lambda^{\mathrm{S}}_{1,2} = 0.26$, $\rho^{\mathrm{S}}_{1,1} = 0.07$ [(b) and (c)], and $\rho^{\mathrm{S}}_{1,1} = 0.03$ (d).

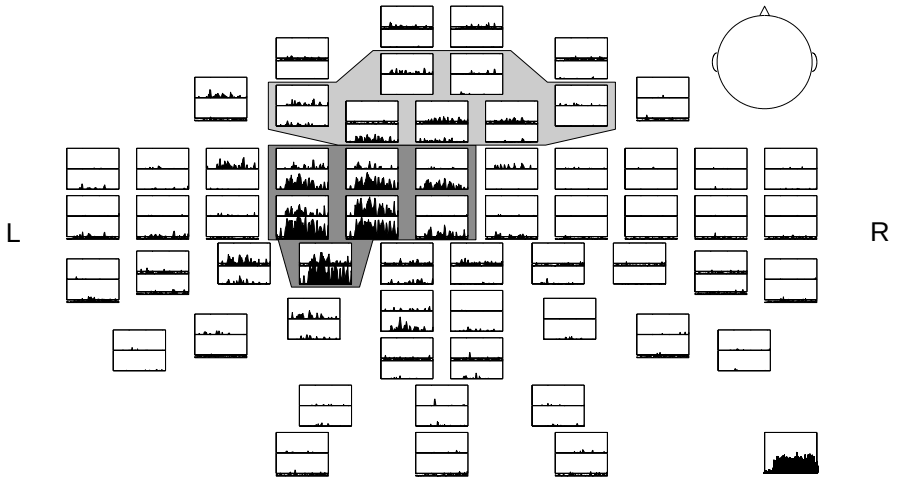

FIG. 4. Time dependence of the significant synchronization index $\rho_{1,2}$ characterizing 1:2 locking between the EMG of the right flexor muscle (reference channel, plotted in the lower right corner) and all MEG channels. Each rectangle corresponds to an MEG sensor, time axis spans 310 s and y axis scales from 0 to 0.25. The head is viewed from above, "L" and "R" mean left and right (see the "head" in the upper right corner). The upper and lower gray regions correspond to premotor and contralateral sensorimotor areas, respectively. The results are similar for the extensor muscle. Significance level $\rho^{S}_{1,2} = 0.03$ and window length $T = 10$ s.

By means of our technique we showed for the first time that the temporal evolution of the coordinated peripheral tremor activity directly reflects the time course of the strength of the synchronization of abnormal rhythmic activity within a neural network involving cortical motor areas. Additionally, we localized areas with tremor related brain activity from noninvasive measurements.

This study was supported by grants from the Deutsche Forschungsgemeinschaft (SFB 194, A5, Z2) and from the Volkswagenstiftung.

[1] L. R. Rabiner and B. Gold, *Theory and Application of Digital Signal Processing* (Prentice-Hall, Englewood Cliffs, NJ, 1975); A. Rényi, *Probability Theory* (Akadémiai Kiadó, Budapest, 1970); B. Pompe, J. Stat. Phys. **73**, 587–610 (1993); H. Voss and J. Kurths, Phys. Lett. A **234**, 336–344 (1997).

[2] S. Schiff, P. So, T. Chang, R. E. Burke, and T. Sauer, Phys. Rev. E **54**, 6708 (1996).

[3] M. G. Rosenblum, A. S. Pikovsky, and J. Kurths, Phys. Rev. Lett. **76**, 1804 (1996); A. S. Pikovsky, M. G. Rosenblum, and J. Kurths, Europhys. Lett. **34**, 165 (1996); M. G. Rosenblum, A. S. Pikovsky, and J. Kurths, Phys. Rev. Lett. **78**, 4193 (1997); A. S. Pikovsky, M. G. Rosenblum, G. V. Osipov, and J. Kurths, Physica (Amsterdam) **104D**, 219 (1997).

[4] W. Singer, Concepts Neurosci. **1**, 1 (1989).

[5] P. R. Roelfsema, A. K. Engel, P. König, and W. Singer, Nature (London) **385**, 157 (1997); for a review, see W. A. MacKay, Trends Cognitive Sci. **1**, 176 (1997).

[6] Tremor is an involuntary shaking with a frequency around 3 to 8 Hz which predominantly affects the distal portion of the upper limb; H.-J. Freund, Physiol. Rev. **63**, 387 (1983).

[7] J. Volkmann *et al.*, Neurology **46**, 1359 (1996).

[8] In our study brain signals were recorded with a whole-head system (Neuromag-122) consisting of 122 SQUID's arranged in a helmet-shaped array; M. Hämäläinen *et al.*, Rev. Mod. Phys. **65**, 413 (1993).

[9] R. L. Stratonovich, *Topics in the Theory of Random Noise* (Gordon and Breach, New York, 1963).

[10] M. G. Rosenblum, A. S. Pikovsky, and J. Kurths, IEEE Trans. Circuits Syst. I **44**, 874 (1997).

[11] We note that calculation of the indices in both directions, i.e., taking first or second signal as the reference one, gives coinciding results, so the information on the directionality of driving cannot be obtained in this way.

[12] We use bandpass FIRCLS filters [I. W. Selesnick, M. Lang, and C. S. Burrus, IEEE Trans. Signal Processing, **44**, 1897 (1996)]. We tested the filters between 3.5–7 and 5–6.5 Hz for the lower band and between 7–14 and 10–13 Hz for the higher band. The window length T was varied between 2 and 20 s. Our results are robust with respect to variations of T and the band edges of all filters used. Below we present the results obtained for the following parameters: bandpass of EMG signals: 5–7 Hz, bandpass of MEG signals: 5–7 and 10–14 Hz (for quantification of 1:1 and 1:2 locking, respectively). Our findings were additionally confirmed by analyzing the data filtered with two-band filters (e.g., 5–7 Hz plus 10–14 Hz).

[13] Volkmann *et al.* [7] suggested that rhythmic thalamic activity drives premotor areas (premotor cortex and supplementary motor area) which drive the primary motor cortex. The latter drives the spinal motoneuron pool which gives rise to rhythmic bursts of the muscles' action potentials detected by means of EMG. The peripheral feedback reaches the motor cortex via the thalamus.

Papers

International Journal of Bifurcation and Chaos, Vol. 10, No. 11 (2000) 2479–2488

QUANTITATIVE ANALYSIS OF CARDIORESPIRATORY SYNCHRONIZATION IN INFANTS

RALF MROWKA and ANDREAS PATZAK
Charité, Johannes-Müller Institute for Physiology,
Humboldt University, Tucholsky Str. 2, D-10117 Berlin, Germany

MICHAEL ROSENBLUM*
Department of Physics, University of Potsdam,
Am Neuen Palais 10, D-14415 Potsdam, Germany

Received November 18, 1999; Revised January 1, 2000

We investigate the phase synchronization of heartbeat and respiration in a group of healthy infants. Having presented and compared two quantitative measures of synchronization, we conclude that one of these measures — the conditional probability index — allows reliable detection of synchronous epochs of different order $n:m$ and, thus, makes possible an automatic processing of large data sets. In our analysis of experimental time series, we have found numerous epochs of phase synchronization. It turned out that the average degree of synchronization varies with the age of the newborns.

1. Introduction

Generation of rhythms is an inherent property of many physiological systems, of which breathing and heartbeat are the obvious examples. Patterns of autonomic neural regulation of human respiratory and cardiovascular systems are imprinted on these rhythms, therefore their analysis may give insight into the functioning and interaction of these systems.

Both respiratory and cardiac rhythms have been extensively examined with regard to their ability to detect pathological conditions. Different tools of linear and nonlinear univariate time series analysis have been used in numerous attempts to quantify the state of either cardiovascular or respiratory systems and to reveal malfunction [Akselrod *et al.*, 1981; Kluge *et al.*, 1988; Schechtman *et al.*, 1989, 1990; Goldberger & Rigney, 1991; Kurths *et al.*, 1995; Patzak *et al.*, 1996, 1997; Persson, 1997].

Nevertheless, the separate analysis of both rhythms does not seem to be sufficient. Indeed, it is well known that cardiovascular and respiratory systems are not independent. Normally, their interaction is rather weak, its most pronounced manifestation being called respiratory sinus arrhythmia (RSA) [Ludwig, 1847; Saul *et al.*, 1989]. In physical terms, RSA can be regarded as the modulation of heart rate by a respiratory related signal; it has been characterized and analyzed in many studies [Kim & Khoo, 1997; Loula *et al.*, 1997; Koh *et al.*, 1998]. On the other hand, in certain conditions there is apparently a very tight coupling between the circulatory and the respiratory systems. An example is Cheyne–Stokes respiration [Guyton *et al.*, 1956] that is a definite sign of a severe pathology.[1] Appearance of this phenomenon is supposed to be

*URL: www.agnld.uni-potsdam.de

[1]This effect can be viewed as a complex modulation of the respiratory activity, so that there are epochs where there is no breathing at all. The Cheyne–Stokes respiration occurs in such situations as intoxication, chronic hypoxemia (low blood oxygen level), and diffuse brain damage.

related to the change of certain parameters of the circulatory system [Guyton *et al.*, 1956; Glass & Mackey, 1988]. Thus, the interdependence of oscillatory activity of respiratory and cardiovascular systems may be physiologically relevant. Therefore, the joint analysis of the two rhythms may provide additional physiological information and may be useful for early detection of malfunctioning.

Coordinated activity of respiratory and cardiovascular systems has been addressed in early work by Hildebrandt, Kenner, Pessenhofer, Raschke, and others [Hinderling, 1967; Engel *et al.*, 1968; Pessenhofer & Kenner, 1975; Kenner *et al.*, 1976; Raschke, 1981, 1987, 1991; Raschke & Hildebrandt, 1987]. In these papers, different *ad hoc* methods have been used and an indication of the $n:1$ synchronization between heartbeat and respiration has been found. For example, Raschke and Hildebrandt [1987] have computed the histograms of ratios of the periods of respiratory and cardiac cycles and found peaks around integers three and four. Synchronization between these systems has been also accessed by analysis of other signals, such as blood pressure and respiration. Koepchen and Thurau [1958] discussed a central neural mechanism for fixed ratio synchronization between blood pressure and respiration. Synchronization between the 0.1 Hz component of blood pressure oscillation and respiration was described by Golenhofen and Hildebrandt [1958].

Recently, several groups addressed different aspects of cardiorespiratory interaction [Hoyer *et al.*, 1997; Schiek *et al.*, 1998; Seidel & Herzel, 1998]. In particular, the concept of phase synchronization was used for this goal [Schäfer *et al.*, 1998, 1999; Toledo *et al.*, 1998]. As a result, different $n:m$ synchronous regimes have been revealed by means of a graphic tool called "cardiorespiratory synchrogram" (CRS), and an attempt was made to assess the cardiorespiratory synchronization quantitatively [Toledo *et al.*, 1998; Rosenblum *et al.*, 2000a, 2000b]. Nevertheless, until now, only a small group of adults (young athletes, normal healthy and heart transplant subjects) have been examined, and it is not clear yet whether synchronization is a typical feature of cardiorespiratory interaction. For example, there are no studies of synchronization phenomena in infants.

Here we discuss the methods that allow to quantify the strength of synchronization from bivariate data. We present the results of a quantitative analysis of cardiorespiratory interaction in a group of 25 healthy newborn babies and address the age dependence of cardiorespiratory synchronization.

2. Quantification of Phase Synchronization

The notion of phase synchronization implies the appearance of some interrelation between suitably introduced phases of two (or many) self-sustained oscillators whereas the amplitudes can be generally uncorrelated; for the introduction to the concept and the references see the tutorial paper in this issue [Pikovsky *et al.*, 2000]. Here we briefly summarize the facts needed in the following for quantification of the synchronization from noisy data.

For two weakly interacting periodic oscillators one can obtain in the first approximation the equations for the phase dynamics:

$$\frac{d\phi_1}{dt} = \omega_1 + \varepsilon g_1(\phi_1, \phi_2)\,, \quad \frac{d\phi_2}{dt} = \omega_2 + \varepsilon g_2(\phi_2, \phi_1)\,, \tag{1}$$

where the phases $\phi_{1,2}$ are defined not on the $[0, 2\pi]$ circle but on the whole real line, the coupling terms $g_{1,2}$ are 2π-periodic in both arguments, and ε is the coupling coefficient. For a general case of $n:m$ locking one can introduce the *generalized phase difference*, or relative phase

$$\varphi_{n,m}(t) = n\phi_1(t) - m\phi_2(t) \tag{2}$$

and obtain for it the equation

$$\frac{d\varphi_{n,m}}{dt} = n\omega_1 - m\omega_2 + \varepsilon G(\phi_1, \phi_2)\,, \tag{3}$$

where $G(\cdot,\cdot)$ is 2π-periodic in both arguments. As it is well known, Eq. (3) admits solutions of two kinds: the relative phase is either unbounded or bounded. The first case corresponds to the quasiperiodic motion with two incommensurate frequencies, whereas a solution of the second type corresponds to phase locking

$$|n\phi_1(t) - m\phi_2(t) - \delta| < \text{const}\,, \tag{4}$$

where δ is some (average) phase shift. We emphasize, that in the synchronous state the relative phase generally oscillates around a constant value; these oscillations vanish only if the coupling depends on the relative phase: $G(\phi_1, \phi_2) = G(n\phi_1 - m\phi_2)$ [Pikovsky *et al.*, 2000].

Noise is inevitable in live systems, and we must take its influence on the phase locking into account. As known [Stratonovich, 1963], noise causes the fluctuations of the relative phase and (sometimes) rapid 2π jumps of $\varphi_{n,m}$ (phase slips). Chaotic systems exhibit qualitatively similar phase dynamics [Rosenblum *et al.*, 1996], so that in the following we do not discuss whether the system we analyze is noisy or chaotic and noisy.

To introduce the quantitative measures of synchronization we consider first the simple case: let the oscillation of the relative phase in the locked state vanish and no noise be present. Then the relative phase is constant, $\varphi_{n,m}(t) = \delta$, if synchronization occurs, and $\varphi_{n,m}(t) \sim (n\omega_1 - m\omega_2)t$, if the motion is quasiperiodic. Respectively, the distribution of the cyclic relative phase $\varphi_{n,m}(t) \bmod 2\pi$ is either a δ-function, or broad. Now we can consider the influence of a weak noise: the distribution becomes smeared, but remains, nevertheless, unimodal [Stratonovich, 1963]. To characterize this distribution, we compute the intensity of its first Fourier mode

$$\gamma_{n,m}^2 = \langle \cos\, \varphi_{n,m}(t) \rangle^2 + \langle \sin\, \varphi_{n,m}(t) \rangle^2 \,, \quad (5)$$

where the brackets denote the average over time [Rosenblum *et al.*, 2000a, 2000b]. The synchronization index γ varies from 0 (no synchronization) to 1 (synchronization in the noise-free case). Due to the noise, γ does not attain unity any more, nevertheless it remains almost 1 in the middle of the synchronization region and continuously decreases with the loss of synchronization.

The situations gets more complicated if in the synchronous regime the relative phase oscillates, so that the general condition (4) must be taken into account. If this oscillation is not negligible then the distribution of $\varphi_{n,m}(t) \bmod 2\pi$ is not unimodal and narrow any more, even in the absence of noise, and the noise makes it practically uniform. This is especially essential if the interaction is not very weak, or if synchronization occurs via modulating (parametric) action of one oscillator on the second one [Schäfer *et al.*, 1999; Rosenblum *et al.*, 2000a, 2000b]. Therefore, the synchronization index γ can be rather small even if the synchronization does occur, and we need another measure of locking. Such a measure can be obtained by means of the stroboscopic approach.

Consider again Eq. (3). For convenience we treat now the cyclic phases $\tilde{\phi}_{1,2} = \phi_{1,2} \bmod 2\pi$. Let us fix the value of the phase of, say, first oscillator at some constant value θ, and observe the phase of the second oscillator for each time t_i when $\tilde{\phi}_1 = \theta$:

$$\eta_i = \tilde{\phi}_2(t)|_{\tilde{\phi}_1(t)=\theta} \,. \quad (6)$$

This is nothing else than the construction of the Poincaré secant surface that reduces Eq. (3) to the well-known circle map. In case of 1:1 phase locking it has a fixed point, so that $\eta_i = \text{const}$; due to the presence of a weak noise the values of η_i are scattered around this constant value. The distribution of η_i can be characterized in a similar way as above by computing the intensity of its first Fourier mode. To improve the statistics, we average over different values of θ. Numerically, it can be done if we introduce a binning for the phase of the first oscillator, compute the estimate of the index for the lth bin as

$$\Lambda_l^2 = M_l^{-2} \left(\sum_{i=1}^{M_l} \cos\, \eta_i \right)^2 + M_l^{-2} \left(\sum_{i=1}^{M_l} \sin\, \eta_i \right)^2 , \quad (7)$$

where $l = 1, \ldots, N$, and M_l is the number of points in the corresponding Poincaré section, and average Λ_l over all N bins in order to get a synchronization index

$$\lambda = N^{-1} \sum_{l=1}^{N} \Lambda_l \,. \quad (8)$$

The last step is to generalize the index λ for the case of $n:m$ locking. When the integers n and m are *a priori* known, we expect to observe nm points in the Poincaré section. To focus on any of them alone, we rescale the phases, $\phi_1 \to \phi_1/m$, $\phi_2 \to \phi_1/n$, and use the above described approach in order to obtain the $n:m$ locking index; this rescaling is equivalent to "making" the frequencies of two oscillators equal and thus reducing the problem to the 1:1 case.

According to its definition, $\lambda_{n,m}$ measures the conditional probability for $\tilde{\phi}_2$ to have a certain value provided $\tilde{\phi}_1$ is in a certain bin [Tass *et al.*, 1998], see Fig. 1. One can see, that if the oscillation of the relative phase vanishes, then the indices $\lambda_{n,m}$ and $\gamma_{n,m}$ coincide. In practice, the integers n and m are chosen by trial and error.

We emphasize that appearance of a certain interdependence between phases indicates, strictly speaking, only the presence of coupling between systems, but does not necessarily imply that they are synchronized. Indeed, if the coupling is not sufficient in order to induce synchronization, but

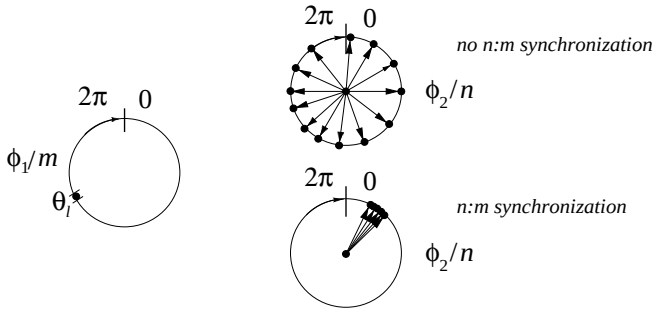

Fig. 1. Synchronization index based on the conditional probability. Phase of the second oscillator ϕ_2 rescaled by n and wrapped onto the circle [0, 2π] is observed stroboscopically, i.e. when phase of the first oscillator ϕ_1/m mod 2π is found in the certain bin θ_l of the interval [0, 2π]. If there is no $n:m$ synchronization then the stroboscopically observed ϕ_2 is scattered over the circle, otherwise it groups around some value. The sum of the vectors pointing to the position of the phase on the circle provides a quantitative measure of synchronization.

close to this threshold value, the distribution of the relative phase is also unimodal.

3. Experimental Data and Preprocessing

We measured the electrocardiograms (ECG) using a bipolar limb lead (Biomonitor 501, Meßgerätewerk Zwönitz, Germany) and obtained thoracic respiration with the inductive plethysmographic method (Respitrace, Studley Data Systems, Oxford, UK) in 25 newborn infants. Measurements were performed on each of the first five days of life, then every week and later monthly up to the sixth month of life.

Data acquisition began 30–60 min after feeding, in the evening hours between 8 p.m. to 11 p.m., and took approximately 1 h. Data were stored on a DAT multichannel recorder (DAT, DTR-1800, biologic, France) for further analysis. The data were offline digitized with a computer based monitoring system (XmAD, ftp://sunsite.unc.edu/pub/Linux/science/lab/) with a sampling rate of 1000 Hz.

An artifact free, 10 min long segment of each measurement was chosen for further analysis. R-waves were detected with the precision of 1 ms by means of a convolution technique applied to a high pass filtered ECG (20 ms moving average) and a typical QRS-template. Instantaneous phase of the ECG was estimated as

$$\phi_h(t) = 2\pi k + 2\pi \frac{t - t_k}{t_{k+1} - t_k}, \qquad (9)$$

where t_k are the times of appearance of a kth R-peak.

The respiratory signal was filtered with a high-pass (3 sec length moving average) and a low-pass (50 ms length moving average) filter prior to a resampling at 100 Hz. Instantaneous phases of the respiratory signal were computed by means of the analytic signal approach [Gabor, 1946; Panter, 1965] based on the Hilbert transform; technical implementation of that technique is discussed, e.g. in [Rosenblum & Kurths, 1998; Schäfer *et al.*, 1999]. The instantaneous phases of the respiratory signal were smoothed with the help of a second order Savitzky–Golay filter [Press *et al.*, 1992] of length 1000. Synchronization indices γ and λ were calculated in a sliding window of length 2000 points; the window was moved step by step.

4. Results

We have analyzed 221 records. A typical data set along with the computed synchronization indices is shown in Fig. 2. For visualization of entrainment between heartbeat and respiration we used the phase stroboscope, or synchrogram technique [Schäfer *et al.*, 1999]. Briefly, it can be explained in the following way. The phase of the respiration ϕ_r is observed stroboscopically at the instants t_k of occurrence of the kth R-peak in the ECG. Afterwards, $\phi_r(t_k)$ is plotted versus t_k. In the noise-free case of $n:1$ synchronization (n heartbeats within each respiratory cycle), we would observe n distinct values within one respiratory cycle so that such a plot would exhibit n horizontal lines. In our plots n colors are used in a cyclical order, so that the lines are clearly seen. Noise smears these lines, and some bands are expected to be observed instead. To look for $n:m$ locking one has to use the wrapping of the respiratory phase into [0, $2\pi m$] interval, i.e. consider m adjacent oscillations as one cycle, and plot

$$\psi_m(t_k) = \frac{1}{2\pi}(\phi_r(t_k) \bmod 2\pi m) \qquad (10)$$

versus t_k.

We have found a considerable number of epochs, where synchronization of different order $n:m$ occurs; these results are summarized in Table 1. To analyze the efficiency of two indices $\gamma_{n,m}$ and $\lambda_{n,m}$, we compared their values for the epochs where synchronization can be detected by visual inspection of cardiorespiratory synchrograms and by

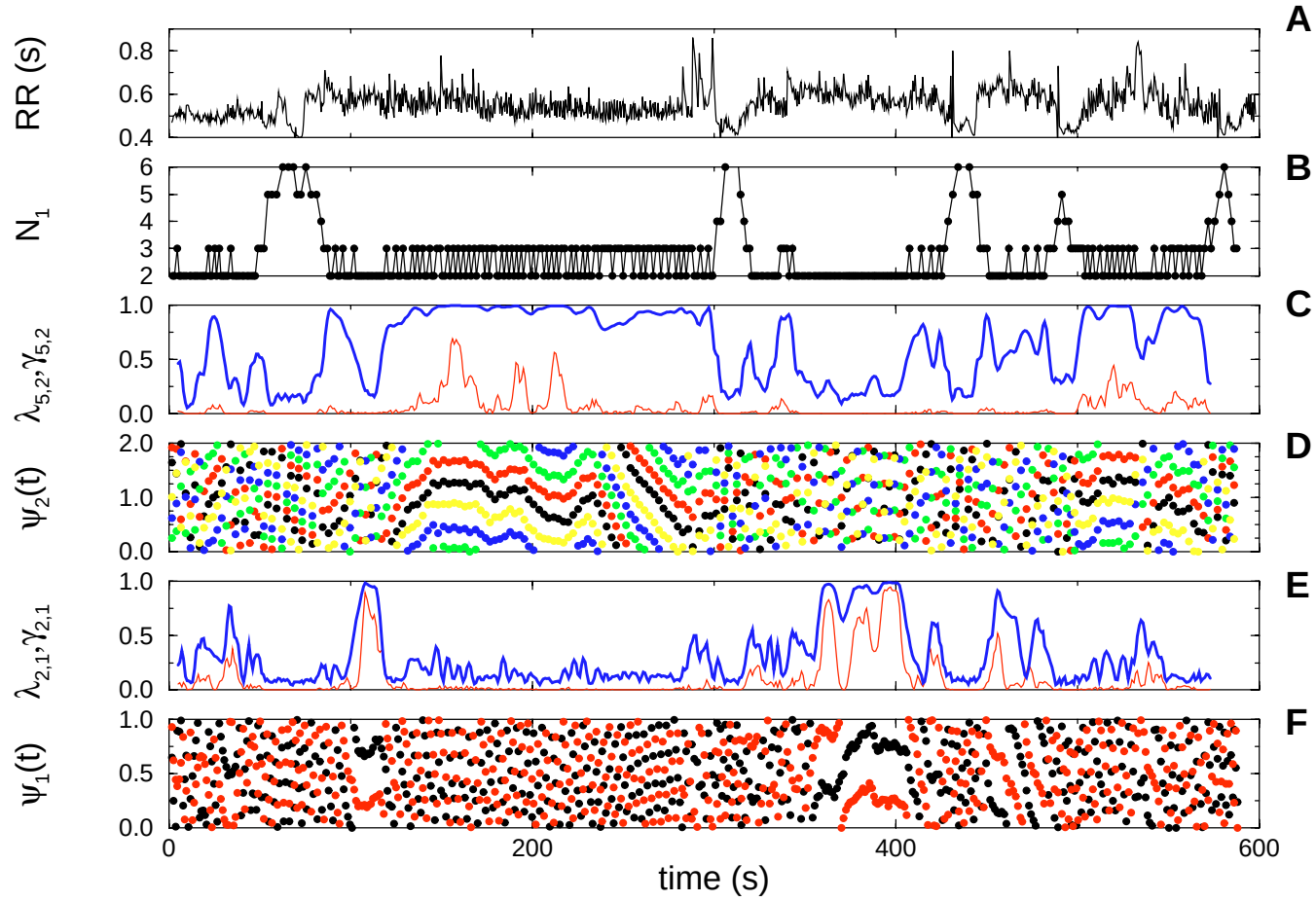

Fig. 2. An example of occurrence of 2:1 and 5:2 synchronization. A: R–R (interbeat) intervals. B: Number of heartbeats per respiratory cycle. C and E: Quantitative measures of $n:m$ synchronization: conditional probability index $\lambda_{n,m}$ (blue) and index $\gamma_{n,m}$ based on computation of the Fourier mode of the distribution of relative phase (red). D and F: Cardiorespiratory synchrograms demonstrating alternating epochs of 2:1 and 5:2 synchronization.

Table 1. The number of epochs of $n:m$ synchronization found in 221 data sets. The rows correspond to the number n of cardiac cycles, whereas the columns correspond to the number m of cycles of respiration. Only the epochs that lasted longer than 20 seconds are counted; synchronization is identified if the conditional probability index $\lambda_{n,m} \geq 0.95$.

	resp. cycle (m)		
R–R cycle (n)	1	2	3
2	3		
3	25	7	
4	39		6
5	15	52	19
7		85	85
8			94
9		82	

counting the number of heartbeats N_1 within each respiratory cycle. We find that the index $\gamma_{n,m}$ is less sensitive than the conditional probability index $\lambda_{n,m}$; this becomes especially essential with the increase of the order of synchronization. So, comparing Figs. 2C and 2D we see that the index $\gamma_{n,m}$ indicates synchronization of order 2:1 but fails to detect the epochs of 5:2 synchronization. Inspection of another data set (Fig. 3), where 4:1 synchronization appears for almost all 10 minutes, shows that the index $\gamma_{n,m}$ drops strongly if a phase slip occurs (the slips can be easily seen in Fig. 3B). Summarizing the comparison of two quantitative measures of synchronization in Table 2, we conclude that reliable detection of synchronous epochs can be achieved by means of the conditional probability index $\lambda_{n,m}$.

Next, we investigate how the occurrence of synchronization depends on the postnatal age. We

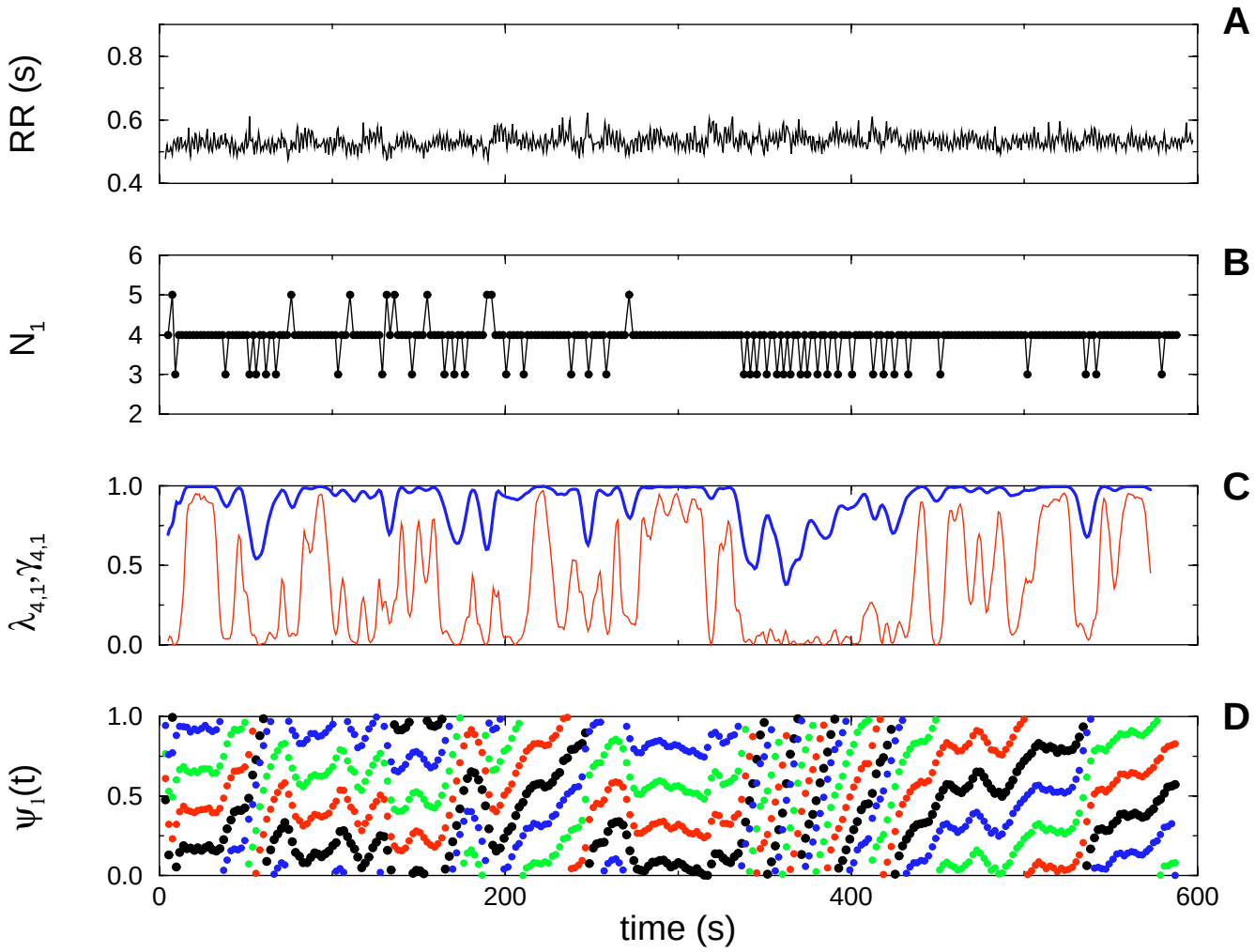

Fig. 3. An example of 4:1 synchronization. A: R–R intervals. B: Number of heartbeats per respiratory cycle. C: Conditional probability index $\lambda_{n,m}$ (blue) and index $\gamma_{n,m}$ (red). D: Cardiorespiratory synchrogram demonstrating long synchronous epochs interrupted by phase slips.

Table 2. Probability of the synchronization index $\gamma_{n,m}$ to be larger than 0.707 provided that $\lambda_{n,m} > 0.95$. The rows correspond to the number n of cardiac cycles, whereas the columns correspond to the number m of cycles of respiration. The results suggest that the index $\gamma_{n,m}$ may not be used for reliable automatic detection of synchronization.

	resp. cycle (m)		
R–R cycle (n)	1	2	3
3	0.744	0	
4	0.391		0
5	0.0317	0	0
7		0.0008	0
8			0
9		0.0081	

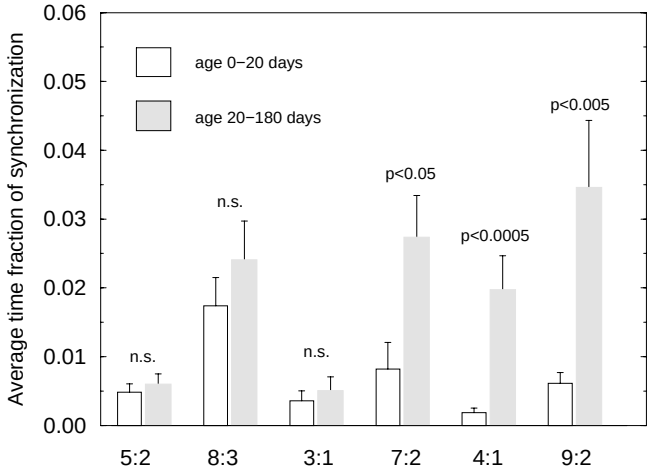

Fig. 4. Average time fraction of $n:m$ synchronization identified by $\lambda_{n,m} > 0.95$ within first 20 days of life and for the age 20–180 days. The error bars indicate the standard error of mean.

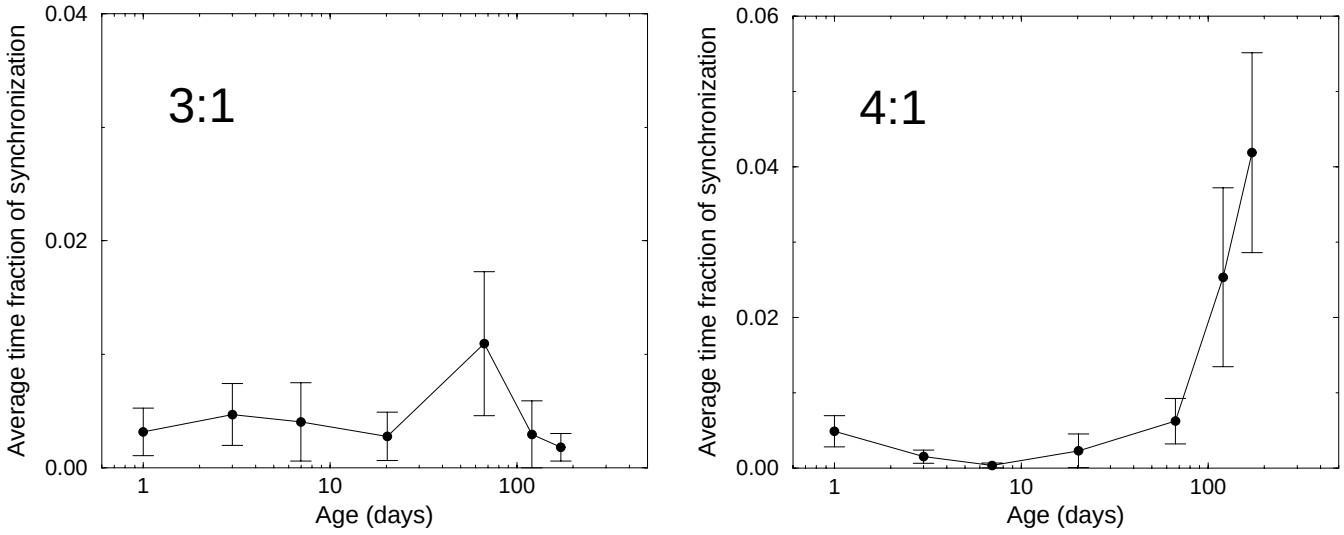

Fig. 5. Average time fraction of 3:1 and 4:1 synchronization as a function of the postnatal age. The error bars indicate the standard error of mean.

have found that the average time fraction of the 7:2, 4:1, and 9:2 synchronization is significantly smaller in the first three weeks of life compared to the fractions at the age from three weeks up to six months. In contrast, the average time fraction of a 5:2, 8:3, and 3:1 synchronization did not show any statistically significant age dependency. These results are summarized in Fig. 4. The detailed age development of the average time fraction for 3:1 and 4:1 synchronization is shown in Fig. 5.

Furthermore, from Fig. 4 it becomes clear that the time fraction where synchronization occurs is small compared to the fraction of nonsynchronized periods. However, in some cases long epochs of synchronization were observed (cf. Fig 3).

5. Discussion and Outlook

The exact physiological mechanisms responsible for cardiorespiratory synchronization are so far poorly understood. There are several levels where the interaction occurs.

First, the frequency of the primary pacemaker of the heart (sino-atrial node) is modulated by the autonomic neural and hormonal control. It is known that the efferent neural activity incorporates the respiratory related rhythms [Jewett, 1964]. Furthermore, there is a mechanical coupling between the systems. In the examinations of the heart transplant patients, in which the neural autonomic control is abolished, it was found that respiratory modulation effects [Slovut *et al.*, 1998] are still present and synchronization is possible [Toledo *et al.*, 1998]. This interaction is thought to originate from the mechanical stretch of the sinus node caused by variation of the intra-thoracic pressure, which in its turn causes the variation of the atrial filling pressure. This breathing dependent stretch alters the electrical properties of the sino-atrial node membrane, and therefore influences the frequency of the heart excitation.

Secondly, the respiratory rhythm is generated in the cardiorespiratory center of the brain stem [Koshiya & Smith, 1999]. The nerves coming from the arterial baroreceptors provide the brain stem with information regarding blood pressure, and, hence, on heart rhythm. Furthermore, it has been found that the baroreceptor reflex depends on the phase of respiration [Seidel *et al.*, 1997]. These are examples of physiological cross-connection between the "generators" of cardiac and respiratory rhythms which may yield synchronization.

Synchronization of heartbeat and respiration in infants occurs in different ratios $n:m$. The typical change in mean heart rate and respiration frequency [Mrowka *et al.*, 1996] after birth may predispose for certain synchronization ratios. The frequency ratio of heartbeat and respiration, recomputed using the data of Mrowka *et al.* [1996], is shown in Fig. 6. This dependence explains the age development of the average time fraction of 3:1 and 4:1 synchronization illustrated in Fig. 5. Indeed, the average frequency ratio is ≈ 2.5 for the age up to 20 days, ≈ 3 for the age from 40 to 80 days, and ≈ 4 for the

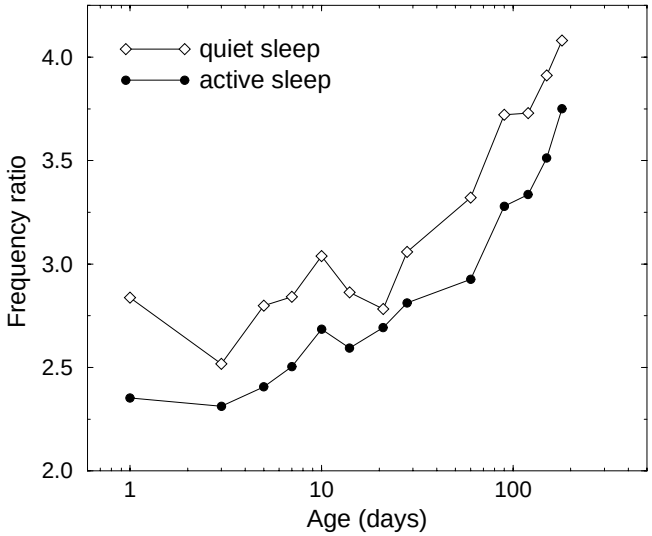

Fig. 6. Average ratio of respiratory frequency and heartrate in dependence on postnatal age shown for different sleep stages. (Recalculated after [Mrowka *et al.*, 1996].)

age after 100 days. Thus, synchronization of order 5:2 is more likely to occur within the first three weeks of life, whereas synchronization of order 4:1 (and with close ratios 7:2 and 9:2) is more probable at the age 20–180 days. On the other hand, analyzing the average occurrence of synchronous epochs shown in Fig. 4, we see that the probability to observe 4:1, 7:2 and 9:2 synchronization is large than the probability to encounter the 5:2 synchronization. Moreover, for any ratio, the probability of synchronization increases with age. Therefore, we conclude that the strength of coupling between respiratory and cardiovascular systems increases with the age of infants.

The duration of epochs of synchronization compared to the nonsynchronous ones is usually rather small,[2] nevertheless in some cases synchronization is a long-lasting effect (see Fig. 3). It is not clear yet whether synchronization is essential for efficient cardiovascular and respiratory control. However, one might speculate that the lack of synchronization might indicate blunted feedback mechanisms or interconnections in pathological conditions, or in individuals at risk. The examination of data originating from different diseased stages may provide understanding of synchronization and its relevance.

Acknowledgments

This work was partly supported by the BMBF project "Perinatale Lunge" (grant 01 ZZ 9511). We are grateful to A. Pikovsky, Ch. Zemlin, and M. Zaks for useful discussions and comments.

References

Akselrod, S., Gordon, D., Ubel, F. A., Shannon, D. C., Berger, A. C. & Cohen, R. J. [1981] "Power spectrum analysis of heart rate fluctuation: A quantitative probe of beat-to-beat cardiovascular control," *Science* **213**(4504), 220–222.

Engel, P., Hildebrandt, G. & Scholz, H.-G. [1968] "Die Messung der Phasenkopplung zwischen Herzschlag und Atmung beim Menschen mit einem neuen Koinzidenzmeßgerät," *Pflügers Arch.* **298**, 258–270.

Gabor, D. [1946] "Theory of communication," *J. IEE London* **93**(3), 429–457.

Glass, L. & Mackey, M. C. [1988] *From Clocks to Chaos: The Rhythms of Life* (Princeton Univ. Press, Princeton, NJ).

Goldberger, A. L. & Rigney, D. R. [1991] "Nonlinear dynamics at the bedside," *Theory of Heart*, eds. Glass, L., Hunter, P. & McCulloch, A. (Springer-Verlag, NY), pp. 583–605.

Golenhofen, K. & Hildebrandt, G. [1958] "Die Beziehung des Blutdruckrhythmus zu Atmung und peripherer Durchblutung," *Pflügers Arch.* **267**, 27–45.

Guyton, A. C., Crowell, J. W. & Moore, J. W. [1956] "Basic oscillating mechanism of Cheyne–Stokes breathing," *Am. J. Physiol.* **187**, 395–398.

Hinderling, P. [1967] "Weitere Charakterisierung von Synchronismen zwischen Kreislauf und Atmung," *Helv. Physiol. Pharmacol. Acta* **25**, 24–31.

Hoyer, D., Hader, O. & Zwiener, U. [1997] "Relative and intermittent cardiorespiratory coordination," *IEEE Engin. Med. Biol.* **16**(6), 97–104.

Jewett, D. L. [1964] "Activity of single efferent fibres in the cervical vagus nerve of the dog, with special reference to possible cardio-inhibitory fibres," *J. Physiol.* **175**, 321–357.

Kenner, T., Pessenhofer, H. & Schwaberger, G. [1976] "Method for the analysis of the entrainment between heart rate and ventilation rate," *Pflügers Arch.* **363**, 263–265.

Kim, T. S. & Khoo, M. C. [1997] "Estimation of cardiorespiratory transfer under spontaneous breathing conditions: A theoretical study," *Am. J. Physiol.* **273**, H1012–H1023.

[2]Obviously, the time fraction of synchronization depends on the threshold value of the index that is chosen for the identification of synchronization; the results we present were obtained with a rather high value, $\lambda_{n,m} \geq 0.95$. Additional computations show that this choice is not essential for the analysis of the age dependence of the synchronization occurrence.

Kluge, K. A., Harper, R. M., Schechtman, V. L., Wilson, A. J., Hoffman, H. J. & Southall, D. P. [1988] "Spectral analysis assessment of respiratory sinus arrhythmia in normal infants and infants who subsequently died of sudden infant death syndrome," *Pediatr Res.* **24**(6), 677–682.

Koepchen, H. P. & Thurau, K. [1958] "Untersuchungen über Zusammenhänge zwischen Blutdruckwellen und Ateminnervation," *Pflügers Arch.* **267**, 10–26.

Koh, J., Brown, T. E., Beightol, L. A. & Eckberg, D. L. [1998] "Contributions of tidal lung inflation to human R–R interval and arterial pressure fluctuations," *J. Auton. Nerv. Syst.* **68**(1&2), 89–95.

Koshiya, N. & Smith, J. C. [1999] "Neuronal pacemaker for breathing visualized in vitro," *Nature* **400**(6742), 360–363.

Kurths, J., Voss, A., Witt, A., Saparin, P., Kleiner, H. J. & Wessel, N. [1995] "Quantitative analysis of heart rate variability," *Chaos* **5**(1), 88–94.

Loula, P., Jantti, V. & Yli-Hankala, A. [1997] "Respiratory sinus arrhythmia during anaesthesia: Assessment of respiration related beat-to-beat heart rate variability analysis methods," *Int. J. Clin. Monit. Comput.* **14**(4), 241–249.

Ludwig, C. [1847] "Beiträge zur kenntniss des einflusses der respirationsbewegungen auf den blutlauf im aortensysteme," *Arch Anat Physiol Leipzig* **13**, 242–302.

Mrowka, R., Patzak, A., Schubert, E. & Persson, P. B. [1996] "Linear and non-linear properties of heart rate in postnatal maturation," *Cardiovasc. Res.* **31**(3), 447–454.

Panter, P. [1965] *Modulation, Noise, and Spectral Analysis* (McGraw-Hill, NY).

Patzak, A., Orlow, W., Mrowka, R., Schlüter, B., Trowitzsch, E., Gerhardt, D., Barschdorff, D. & Schubert, E. [1996] "Heart rate control in infants at risk," *J. Electrocardiol.* **29**, p. 214.

Patzak, A., Schlüter, B., Orlow, W., Mrowka, R., Gerhardt, D., Schubert, E., Persson, P. B., Barschdorff, D. & Trowitzsch, E. [1997] "Linear and nonlinear properties of heart rate control in infants at risk," *Am. J. Physiol.* **273**, R540–R547.

Persson, P. B. [1997] "Spectrum analysis of cardiovascular time series," *Am. J. Physiol.* **273**, R1201–R1210.

Pessenhofer, H. & Kenner, T. [1975] "Zur methodik der kontinuierlichen bestimmung der phasenbeziehung zwischen herzschlag und atmung," *Pflügers Archiv.* **355**, 77–83.

Pikovsky, A. S., Rosenblum, M. G. & Kurths, J. [2000] "Phase synchronization in regular and chaotic systems," *Int. J. Bifurcation and Chaos* **10**(10), 2291–2305.

Press, W. H., Teukolsky, S. T., Vetterling, W. T. & Flannery, B. P. [1992] *Numerical Recipes in C: the Art of Scientific Computing*, 2nd edition (Cambridge Univ. Press, Cambridge, England).

Raschke, F. [1981] "Die Kopplung zwischen Herzschlag und Atmung beim Menschen," PhD thesis, Phillips-Universität Marburg.

Raschke, F. [1987] "Coordination in the circulatory and respiratory systems," *Temporal Disorder in Human Oscillatory Systems, Springer Series in Synergetics*, eds. Rensing, L., an der Heiden, U. & Mackey, M. C., Vol. 36 (Springer-Verlag, Berlin Heidelberg), pp. 152–158.

Raschke, F. & Hildebrandt, G. [1987] "Coordination and synchronization in the cardiovascular respiratory system," *Chronobiology and Chronomedicine: Basic Research and Application*, eds. Hildebrandt, G., Moog, R. & Raschke, F. (Peter Lang, Frankfurt a.M., Bern, NY, Paris), pp. 164–171.

Raschke, F. [1991] "The respiratory system — features of modulation and coordination," *Rhythms in Physiological Systems, Springer Series in Synergetics*, eds. Haken, H. & Koepchen, H. P., Vol. 55 (Springer-Verlag, Berlin Heidelberg), pp. 155–164.

Rosenblum, M. G., Pikovsky, A. S. & Kurths, J. [1996] "Phase synchronization of chaotic oscillators," *Phys. Rev. Lett.* **76**(11), 1804–1807.

Rosenblum, M. G. & Kurths, J. [1998] "Analysing synchronization phenomena from bivariate data by means of the Hilbert transform," *Nonlinear Analysis of Physiological Data*, eds. Kantz, H., Kurths, J. & Mayer-Kress, G. (Springer, Berlin), pp. 91–99.

Rosenblum, M. G., Pikovsky, A. S., Schäfer, C., Tass, P. A. & Kurths, J. [2000a] "Detection of phase synchronization from the data: Application to physiology," *Stochaos: Stochastic and Chaotic Dynamics in the Lakes*, eds. Broomhead, D. S., Luchinskaya, E. A., McClintock, P. V. E. & Mullin, T. (American Institute of Physics, Woodbury, NY), pp. 154–161.

Rosenblum, M. G., Pikovsky, A. S., Schäfer, C., Tass, P. A. & Kurths, J. [2000b] "Phase synchronization: From theory to data analysis," *Handbook of Biological Physics*, ed. Moss, F. (Elsevier), in press.

Saul, J. P., Berger, R. D., Chen, M. H. & Cohen, R. J. [1989] "Transfer function analysis of autonomic regulation. II. Respiratory sinus arrhythmia," *Am. J. Physiol.* **256**, H153–H161.

Schäfer, C., Rosenblum, M. G., Kurths, J. & Abel, H.-H. [1998] "Heartbeat synchronized with ventilation," *Nature* **392**(6673), 239–240.

Schäfer, C., Rosenblum, M. G., Abel, H.-H. & Kurths, J. [1999] "Synchronization in the human cardiorespiratory system," *Phys. Rev.* **E60**(1), 857–870.

Schechtman, V. L., Harper, R. M., Kluge, K. A., Wilson, A. J., Hoffman, H. J. & Southall, D. P. [1989] "Heart rate variation in normal infants and victims of the sudden infant death syndrome," *Early Hum. Dev.* **19**(3), 167–181.

Schechtman, V. L., Harper, R. M., Kluge, K. A., Wilson, A. J. & Southall, D. P. [1990] "Correlations between cardiorespiratory measures in normal infants and victims of sudden infant death syndrome," *Sleep* **13**(4), 304–317.

Schiek, M., Drepper, F. R., Engbert, R., Abel, H.-H. & Suder, K. [1998] "Cardiorespiratory synchronization," *Nonlinear Analysis of Physiological Data*, eds. Kantz, H., Kurths, J. & Mayer-Kress, G. (Springer, Berlin), pp. 191–209.

Seidel, H., Herzel, H. & Eckberg, D. L. [1997] "Phase dependencies of the human baroreceptor reflex," *Am. J. Physiol.* **272**, H2040–H2053.

Seidel, H. & Herzel, H. P. [1998] "Analyzing entrainment of heartbeat and respiration with surrogates," *IEEE Engin. Med. Biol.* **17**(6), 54–57.

Slovut, D. P., Wenstrom, J. C., Moeckel, R. B., Wilson, R. F., Osborn, J. W. & Abrams, J. H. [1998] "Respiratory sinus dysrhythmia persists in transplanted human hearts following autonomic blockade," *Clin. Exp. Pharmacol. Physiol.* **25**(5), 322–330.

Stratonovich, R. L. [1963] *Topics in the Theory of Random Noise* (Gordon and Breach, NY).

Tass, P., Rosenblum, M. G., Weule, J., Kurths, J., Pikovsky, A. S., Volkmann, J., Schnitzler, A. & Freund, H.-J. [1998] "Detection of $n:m$ phase locking from noisy data: Application to magnetoencephalography," *Phys. Rev. Lett.* **81**(15), 3291–3294.

Toledo, E., Rosenblum, M. G., Schäfer, C., Kurths, J. & Akselrod, S. [1998] "Qantification of cardiorespiratory synchronization in normal and heart transplant subjects," *Proc. Int. Symp. Nonlinear Theory and its Applications*, Vol. 1 (Presses Polytechniques et Universitaires Romandes, Lausanne), pp. 171–174.

Identification of coupling direction: Application to cardiorespiratory interaction

Michael G. Rosenblum*
Department of Physics, University of Potsdam, Am Neuen Palais, PF 601553, D-14415 Potsdam, Germany

Laura Cimponeriu and Anastasios Bezerianos
Department of Medical Physics, University of Patras, 26 500 Rion Patras, Greece

Andreas Patzak and Ralf Mrowka
Charité, Johannes-Müller Institute for Physiology, Humboldt University, Tucholsky Strasse 2, D-10117 Berlin, Germany
(Received 4 December 2001; published 28 March 2002)

We consider the problem of experimental detection of directionality of weak coupling between two self-sustained oscillators from bivariate data. We further develop the method introduced by Rosenblum and Pikovsky [Phys. Rev. E **64**, 045202 (2001)], suggesting an alternative approach. Next, we consider another framework for identification of directionality, based on the idea of mutual predictability. Our algorithms provide directionality index that shows whether the coupling between the oscillators is unidirectional or bidirectional, and quantifies the asymmetry of bidirectional coupling. We demonstrate the efficiency of three different algorithms in determination of directionality index from short and noisy data. These techniques are then applied to analysis of cardiorespiratory interaction in healthy infants. The results reveal that the direction of coupling between cardiovascular and respiratory systems varies with the age within the first 6 months of life. We find a tendency to change from nearly symmetric bidirectional interaction to nearly unidirectional one (from respiration to the cardiovascular system).

DOI: 10.1103/PhysRevE.65.041909 PACS number(s): 87.90.+y, 05.45.Tp, 05.45.Xt, 05.40.Ca

I. INTRODUCTION

Theoretical insights in nonlinear dynamics have been widely used in time series analysis [1]. In particular, the concepts of generalized [2] and phase [3–5] synchronization have been exploited for the identification of interdependences between coupled sub(systems) from multivariate data and have found a number of applications in the studies of biological time series [5–11]. One can formulate two main problems in such an analysis. The first problem is to reveal whether the systems under investigation are coupled and to quantify the intensity of interaction, while the second one is to characterize the driver-response (causal) relationships, or directionality of coupling.

Many natural phenomena can be modeled by coupled irregular self-sustained oscillators. The description of a weak interaction between such systems can be reduced to the phase dynamics [5,12]. Hence, if one considers an inverse problem—characterization of weak coupling from data—it is sufficient to analyze interrelation between the phases ϕ of oscillators; the phases can be beforehand estimated from the scalar signals. In this way, the intensity of interaction can be assessed quantitatively [5,9,11]. Moreover, a recent approach [13] demonstrated that the asymmetry in interaction of two oscillators could be also detected. The idea of this approach is as follows: if, say, system 1 is driven by system 2, then the evolution of ϕ_1 depends also on ϕ_2; in other words, prediction of ϕ_1 from its previous values can be improved by taking into account the prehistory of ϕ_2 only if system 2 drives system 1.

In the present paper we further develop the technique for detection of the directionality in coupling. We propose two algorithms and compare them with that of Ref. [13]. Next, we exploit the presented method to address an important physiological problem—analysis of the direction of the cardiorespiratory interaction.

Different aspects of interaction between cardiovascular and respiratory systems in humans have been the subject of interest of many researchers. In physiological terms, there are different levels where interaction between heart rate and respiratory rhythm might occur. Foremost, the central nervous interaction in the cardiorespiratory region in the brain stem plays an eminent role. A well-studied phenomenon is the modulation of the heart rate by respiration, known since 19th century as respiratory sinus arrhythmia [14]. Another possible effect of interaction is synchronization. So, $1:m$ locking between the cardiac and respiratory rhythms was investigated in Ref. [15]. Graphical tools and quantification measures allowing one to assess the general case of interaction with $n:m$ frequency relation were introduced in [8,10,11] and used in Ref. [16]. In our previous work [17], we analyzed cardiorespiratory interaction in a large group of healthy infants and we found that intensity of interaction increased with the age.

It is widely believed that coupling between the cardiovascular and respiratory system is unidirectional, i.e., the respiratory rhythm influences the heart rate via vagal stimulation and direct mechanical action on the primary cardiac pacemaker, the sinus node; this is called irradiation theory. Nevertheless, some evidence [18] conflicts with this theory suggesting that the respiratory oscillator in the central nervous system is not always dominant, i.e., the cardiorespiratory

*Electronic address: www.agnld.uni-potsdam.de

coupling is bidirectional. To obtain further insight into this controversy, we investigated the direction in cardiorespiratory interaction in healthy babies and its age dependence. We show that within the first 6 months of life there is a tendency to change from roughly symmetric interaction to a nearly unidirectional one (from respiration to heart rate). Furthermore, our directionality indices clearly demonstrate a dependence on breathing frequency. We explain this dependence by two classes of frequency response properties of the pathway transmitting information from the central nervous system to the heart.

The paper is organized as follows. In Sec. II, we present our techniques of data analysis and discuss their relation to other methods; in Sec. III, we illustrate the techniques by several model examples; in Sec. IV, we describe and discuss the analysis of experimental data; and in Sec. V, we summarize our results.

II. TECHNIQUES OF DATA ANALYSIS

Estimation of interdependence between two time series is a traditional problem of signal processing. Widely used tools such as cross spectra [19], mutual information [20] or maximal correlation [21] provide *symmetric* measures and are, therefore, not suitable for evaluation of *causality* in interrelation. The latter issue was addressed in recent studies, where one can outline two main approaches. One approach, based on the information theory, used entropy measures [22]. A second approach, arising from studies of generalized synchronization, exploited the idea of mutual predictability: it quantified the ability to predict the state of the first system from the knowledge of the second one [6]. While both approaches are rather complicated to implement and interpret, neither requires any assumptions on the systems under investigation. On the contrary, the approach to analysis of causality or directionality of interaction, introduced in Ref. [13] and further developed here, is explicitely based on the assumption that experimentalists deal with weakly interacting self-sustained oscillators. In this particular, but pretty often encountered case the direction of coupling can be efficiently quantified.

The main idea of Ref. [13] is to use the fact that weak coupling affects the phases of interacting oscillators, whereas the amplitudes remain practically unchanged [5,12]. Hence, the dynamics can be reduced to those of two phases $\phi_{1,2}$:

$$\dot{\phi}_{1,2}=\omega_{1,2}+\varepsilon_{1,2}f_{1,2}(\phi_{2,1},\phi_{1,2})+\xi_{1,2}(t). \tag{1}$$

Here, random terms $\xi_{1,2}$ describe noisy perturbations that are always present in real-world systems; small parameters $\varepsilon_{1,2} \ll \omega_{1,2}$ characterize the strength of the coupling. Equation (1) describes also the phase dynamics of coupled continuous-time chaotic systems; in this case $\xi_{1,2}$ are irregular terms that reflect the chaotic nature of amplitudes [3]. The fact that the regular component of the phase dynamics is two dimensional, essentially simplifies detection of the asymmetry in interaction. Functions $f_{1,2}$ are 2π periodic in both arguments and combine the description of the phase dynamics of autonomous (uncoupled) systems and the coupling between them. If the coupling is bidirectional, f_1 and f_2 depend on both ϕ_1 and ϕ_2. In case of unidirectional driving, say from system number 1 to system number 2, $f_1=f_1(\phi_1)$, whereas $f_2=f_2(\phi_1,\phi_2)$ is the function of two arguments.

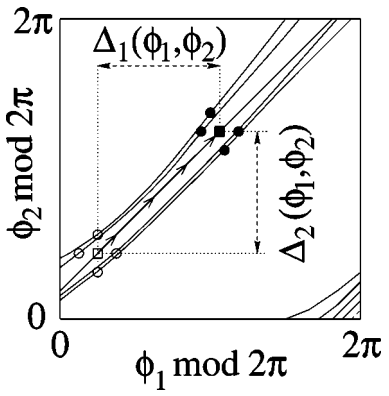

FIG. 1. Evolution of trajectories of system (1) on the torus (ϕ_1,ϕ_2) (schematically). Open symbols show some arbitrarily taken points, closed symbols show the positions of these points after time interval τ, where τ is a parameter; evolution of one point (boxes) is shown by arrows. Phase increment $\Delta_1=\phi_1(t+\tau)-\phi_1(t)$ depends on both ϕ_1,ϕ_2 if there is a driving from system 2 to system 1, and only on ϕ_1 if 2 does not act on 1 (similarly for Δ_2). Thus, analysis of dependences $\Delta_{1,2}=F_{1,2}(\phi_{1,2},\phi_{2,1})$ helps to reveal and quantify asymmetry in the coupling between two oscillators; smooth functions $F_{1,2}$ are obtained by an approximation. Note that $\Delta_{1,2}$ are computed with account of possible trajectory revolution around the torus, so that generally $\Delta_{1,2}>2\pi$.

In the following discussion of the algorithms, we assume that the time series of phases are known. Practically, the phases $\phi_{1,2}(t_k)$, $t_k=k\Delta t$, $k=1,2,\ldots$, where Δt is the sampling interval, can be estimated from the experimental data as discussed in Sec. IV.

A. Evolution map approach (EMA)

Here we briefly describe the technique introduced in Ref. [13], we call it the EMA. Let us consider increments of phases during some fixed time interval τ (Fig. 1):

$$\Delta_{1,2}(k)=\phi_{1,2}(t_k+\tau)-\phi_{1,2}(t_k), \tag{2}$$

the choice of the parameter τ is discussed below. Note that the phases are unwrapped, i.e., not reduced to the interval $[0,2\pi)$; hence $\Delta_{1,2}$ can be larger than 2π. These increments can be considered as generated by some unknown two-dimensional noisy map

$$\Delta_{1,2}(k)=\omega_{1,2}\tau+\mathcal{F}_{1,2}(\phi_{2,1}(t_k),\phi_{1,2}(t_k))+\eta_{1,2}(t_k). \tag{3}$$

The deterministic parts $\mathcal{F}_{1,2}$ of the map can be estimated from the time series $\Delta_{1,2}(k)$ and $\phi_{1,2}(k)$. For this purpose, we fit (in the least mean square sense) the dependences of Δ_1 and Δ_2 on ϕ_1,ϕ_2. As the phases are cyclic variables, the natural choice of the probe function is a finite Fourier series, $F_{1,2}=\Sigma_{m,l}A_{m,l}e^{im\phi_1+il\phi_2}$. Note that fitting also filters out the

noise. A similar procedure was used for noise reduction in discrete dynamical systems [23] and (with $\tau \to 0$) for extracting model equations from experimental noisy data [24].

From the smooth functions $F_{1,2}$ obtained via approximation one can compute the measures $c_{1,2}$ of the cross dependences of phase dynamics of two systems

$$c_{1,2}^2 = \int \int_0^{2\pi} \left(\frac{\partial F_{1,2}}{\partial \phi_{2,1}} \right)^2 d\phi_1 \, d\phi_2 . \tag{4}$$

Finally, the *directionality index* is introduced as

$$d^{(1,2)} = \frac{c_2 - c_1}{c_1 + c_2}. \tag{5}$$

Normalized in this way, the index varies from 1 in the case of unidirectional coupling $(1 \to 2)$ to -1 in the opposite case $(2 \to 1)$ with intermediate values $-1 < d^{(1,2)} < 1$ corresponding to bidirectional coupling. Note that the index is an integrated measure of how strong each system is driven and of how sensitive it is to the drive.

To understand exactly how the asymmetry in coupling is characterized by the index d, i.e., how d is related to the parameters of the model equation (1), we estimate the deterministic components $\Delta_{1,2}$ of the phase increase within the interval τ. As follows from Eq. (1), in the absence of noise, we obtain for small $\varepsilon_{1,2}$,

$$\begin{aligned} \Delta\phi_{1,2} &\approx \omega_{1,2}\tau + \varepsilon_{1,2} \int_0^{\tau} f_{1,2}(\phi_{2,1}, \phi_{1,2}) dt \\ &= \omega_{1,2}\tau + \mathcal{F}_{1,2}(\phi_{2,1}, \phi_{1,2}). \end{aligned} \tag{6}$$

So, for a particular (but rather common) case of antisymmetric coupling function $f_1(\phi_2, \phi_1) = -f_2(\phi_1, \phi_2)$, we obtain from Eq. (4) $c_{1,2} = a\varepsilon_{1,2}$, where the constant a is determined by the integral in Eq. (6). In general case the coefficients $c_{1,2} = a_{1,2}\varepsilon_{1,2}$, where $a_1 \neq a_2$ reflect also the difference in coupling functions $f_{1,2}$. Thus, the directionality index d characterizes the asymmetry in coupling but does not incorporate the difference in the frequencies of autonomous systems.

B. Instantaneous period approach (IPA)

Let us now compute the time needed for the phase $\phi_{1,2}(t_k)$ to increase by 2π; in other words, we compute the instantaneous periods or Poincaré return times, for all k [25]. Obviously, for uncoupled noisy and/or chaotic systems the return times fluctuate around a constant (mean period), $T_{1,2}(k) = T_{1,2}^0 + \eta_{1,2}(t_k)$, while for coupled systems $T_{1,2}(k) = T_{1,2}^0 + \Theta_{1,2}[\phi_{2,1}(t_k), \phi_{1,2}(t_k)] + \eta_{1,2}(t_k)$. The deterministic component $\Theta_{1,2}$ of this dependence can be again found by fitting a Fourier series, and the cross dependences of T_1 on ϕ_2 and of T_2 on ϕ_1 can be characterized in the same way as above, by computing coefficients $c_{1,2}$ from partial derivatives of $\Theta_{1,2}$ with respect to $\phi_{2,1}$, similar to Eq. (4). Then, the new directionality index $r^{(1,2)} = (c_2 - c_1)/(c_2 + c_1)$ is computed [cf. Eq. (5)]. An important advantage of the proposed algorithm is the absence of parameters.

Now we show that this algorithm provides different characterization of asymmetry than EMA. Indeed, for weak coupling, $\varepsilon_{1,2} \ll \omega_{1,2}$, the deterministic component of the instantaneous period T_1 can be estimated from Eq. (1) as

$$\begin{aligned} T_1(\phi_1, \phi_2) &= \int_{\phi_1}^{\phi_1 + 2\pi} \frac{d\phi'}{\omega_1 + \varepsilon_1 f_1(\phi_2, \phi')} \\ &= \frac{1}{\omega_1} \int_{\phi_1}^{\phi_1 + 2\pi} \frac{d\phi'}{1 + \frac{\varepsilon_1}{\omega_1} f(\phi_2, \phi')} \\ &= \frac{2\pi}{\omega_1} - \frac{\varepsilon_1}{\omega_1^2} \int_{\phi_1}^{\phi_1 + 2\pi} f(\phi_2, \phi') d\phi' \\ &= T_1^0 + \Theta_1(\phi_2, \phi_1), \end{aligned} \tag{7}$$

and similarly for T_2. Clearly, for coupling functions satisfying $f_1(\phi_2, \phi_1) = -f_2(\phi_1, \phi_2)$, this algorithm provides $c_{1,2} = a\varepsilon_{1,2}/\omega_{1,2}^2$. Hence, directionality index r reflects not only asymmetry in coupling coefficients $\varepsilon_{1,2}$ and asymmetry in coupling functions $f_{1,2}$, but also in natural frequencies $\omega_{1,2}$.

C. Mutual prediction approach (MPA)

As already mentioned, mutual prediction is used for estimation of causal relations in the methods based on the concept of generalized synchronization. These methods imply existence of a functional relationship between the (phase) states of two systems; such a relation arises due to a comparatively strong coupling. We exploit here a different understanding of mutual prediction, and this allows us to assess a weaker interaction. Namely, we look whether the predictability of, say, first time series can be improved by the knowledge of the second signal. A similar concept, initially introduced in Ref. [26] was very recently used by several groups [27,28]. The main distinction of our approach is that we work with phases, not with raw signals.

Thus, we take one series, say, $\phi_1(t_k)$ and use some scheme to predict a future of its points. For the kth point we compute the *univariate prediction error* $E_1(t_k) = |\phi_1'(t_k) - \phi_1(t_k + \tau)|$, where $\phi_1'(t_k)$ is the τ-step ahead prediction of the point $\phi_1(t_k)$; remember that phases are unwrapped. Next, we repeat the prediction for $\phi_1(t_k)$, but this time we use both signals ϕ_1, ϕ_2 for construction of the predictor. In this way we obtain the *bivariate prediction error* $E_{12}(t_k)$. If system 2 influences the dynamics of system 1 then we expect $E_{12}(t_k) < E_1(t_k)$, otherwise (for sufficient statistics) $E_{12}(t_k) = E_1(t_k)$. The root mean squared $E_1(t_k) - E_{12}(t_k)$, computed over all possible k and denoted by I_{12}, quantifies the *predictability improvement* for the first signal. This measure characterizes the degree of influence of the second system on the first one. Computing in the same way I_{21}, we end with the directionality index

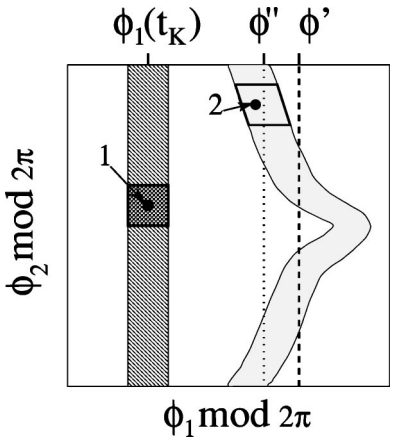

FIG. 2. Illustration of the mutual prediction approach. A chosen point, $\phi_1(t_K)$, evolves during the time interval τ from position 1 to position 2; the points that have close ϕ_1 coordinate (delineated vertical stripe) evolve to the dotted stripe. The average of these evolved states gives a univariate prediction ϕ'. A better prediction ϕ'' can be obtained using only the points that have close coordinates in both ϕ_1 and ϕ_2, i.e., points in a square neighborhood of point 1. Note that the stronger is the dotted stripe bent, the larger is the predictability improvement. As follows from Eq. (6), this bending is proportional to ε_1; hence, the index $p^{(1,2)}$ quantifies bidirectional coupling in the same way as the index $d^{(1,2)}$.

$$p^{(1,2)}=\frac{I_{21}-I_{12}}{I_{12}+I_{21}}. \tag{8}$$

Particularly, we use simple prediction scheme due to the low dimension of the phase dynamics. In constructing predictor, we exploit a common idea that similar states have similar future. So, we pick up one point of the signal $\phi_1(t_k)$, say at the time t_K and search for all points in the signal that have value close to the chosen point; important that here the phases are taken in $[0,2\pi)$ and the distances between points are defined on the unit circle. Namely, for a chosen point $\phi_1(t_K)$ we find all points $\phi_1(t_l)$ such that $|e^{i\phi_1(t_l)}-e^{i\phi_1(t_K)}|<\delta$, where δ is a constant; these points form a stripe on the (ϕ_1,ϕ_2) torus (see Fig. 2). Then we compute the predicted phase increment $\Delta_1'(K)=\langle\Delta_1(l)\rangle$, where $\Delta_1(l)$ are phase increments [see Eq. (2)], and $\langle\rangle$ denotes averaging. Univariate prediction error $E_1(K)$ is then $|\Delta_1'(K)-\Delta_1(K)|$. To make the bivariate prediction, we choose among t_l the subset of points t_m (mutual neighbors) satisfying $|e^{i\phi_2(t_m)}-e^{i\phi_2(t_K)}|<\delta$, and proceeding as described above, compute the error E_{12} [29]. The errors E_2,E_{21} corresponding to the signal $\phi_2(t_k)$ are obtained in a similar way.

Several remarks are in order. First, the described scheme can be understood as a kind of local (constant) approximation technique. Generally, different prediction schemes can be used to estimate directionality. Second, as we are interested in the predictability improvement, not in the predictability itself, it is not required to search for the optimal prediction scheme. Finally, we emphasize that the MPA does not directly use the assumption of weakly coupled oscillators; generally, it can be applied to arbitrary signals. If the assumption of weak coupling is correct, then the choice of phases is crucial as these variables are mostly sensitive to the coupling.

To summarize this section, we emphasize two points. First, it is clear that all methods fail if oscillators synchronize. Indeed, in this case $\phi_{1,2}$ are functionally related, and no information on the coupling direction can be obtained [30]. Practically it means that the points on the (ϕ_1,ϕ_2) torus collapse to a line, and the approximation procedure fails. Thus, the direction of interaction can be revealed if the coupling is too weak in order to induce mode locking (i.e., in the quasiperiodic state) or the noise in the system is strong enough to cause large deviations from the synchronous state. If the noisy systems are close to a synchronous state, the points on the torus form a band with some (rare) excursions from it. In this case the described global approximation procedures, i.e., EMA and IPA are not efficient and a scheme based on local approximation is required. Next, we emphasize that there is no unique way to quantify the directionality in case of bidirectional coupling; different methods can, therefore, give noncoinciding characteristics (e.g., d and r indices do not coincide). The choice of a quantification measure is to large extent a matter of taste.

III. TESTS OF ALGORITHMS WITH SIMULATED DATA

In this section we illustrate the introduced algorithms by application to simulated data and discuss the choice of parameters. Note that the IPA is parameter free, EMA has only one parameter τ, and MPA has two parameters τ and radius of the neighborhood δ. Next, we briefly discuss the case when the frequencies of two oscillators are essentially different and the case of more than two interacting systems. We especially pay attention to the case of short and noise contaminated data. The ability of the techniques to work with such records is particularly important for biomedical applications.

A. Two coupled phase oscillators

We start, following Ref. [13] with the model of coupled noisy phase oscillators:

$$\dot{\phi}_{1,2}=\omega_{1,2}+b\cos(\phi_{1,2})+\varepsilon_{1,2}\sin(\phi_{2,1}-\phi_{1,2})+\xi_{1,2}(t), \tag{9}$$

where $\phi_{1,2}$ are phase variables evolving on a two-dimensional torus, parameters $\omega_{1,2}$ govern the natural frequencies of oscillators (although do not coincide with them for $b\neq 0$), $\varepsilon_{1,2}$ are the coupling coefficients, and $\xi_{1,2}$ are noise terms. In the following simulations $\xi_{1,2}$ are Gaussian δ-correlated noise terms, $\langle\xi_i(t)\xi_j(t')\rangle=2D\delta(t-t')\delta_{i,j}$. The model (9) describes the phase dynamics in the general case of weakly coupled noisy limit cycle oscillators [12]; it also appears in the description of interacting continuous-time chaotic systems, Josephson junction arrays [31], and phase-locked loops [32].

First, we consider the effect of noise on the estimates of directionality (Fig. 3). The parameters of the system (9) are

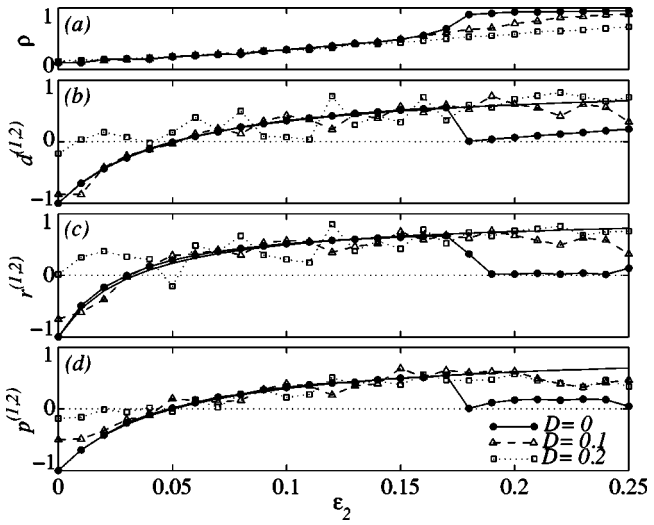

FIG. 3. Effect of noise on the estimation of directionality indices. One coupling coefficient is kept constant, $\varepsilon_1=0.05$, whereas the second coefficient is gradually varied. The indices are shown in (b)–(d) for different values of noise intensity. The solid curves show the dependence $y=(\varepsilon_2-\varepsilon_1)/(\varepsilon_2+\varepsilon_1)$ in (b),(d) and $y=(\varepsilon_2\omega_1^2-\varepsilon_1\omega_2^2)/(\varepsilon_2\omega_1^2+\varepsilon_1\omega_2^2)$ in (c). The degree of synchronization can be traced by the synchronization index ρ (a). In the absence of noise, all indices correctly reflect the asymmetry in interaction as long as the system remains in the quasiperiodic state (for $\varepsilon_2<\approx 0.17$); noise helps to estimate the indices for $\varepsilon_2>0.17$, causing deviations from the synchronous regime.

$\omega_{1,2}=1\pm 0.1$, $b=0.5$. Coupling coefficient ε_1 is fixed at 0.05 while ε_2 is varied in the interval [0,0.25] and three directionality indices $d^{(1,2)}$, $r^{(1,2)}$, and $p^{(1,2)}$ are computed for different values of the noise intensity D. For the noise-free case, all indices correctly recover the information on the asymmetry of coupling as long as the system remains in a quasiperiodic state (for $\varepsilon_2<\approx 0.17$). The estimated indices $d^{(1,2)}$ and $p^{(1,2)}$ closely follow the theoretical curve

$$\frac{\varepsilon_2-\varepsilon_1}{\varepsilon_1+\varepsilon_2}, \tag{10}$$

whereas the index $r^{(1,2)}$ follows

$$\frac{\varepsilon_2\omega_1^2-\varepsilon_1\omega_2^2}{\varepsilon_1\omega_2^2+\varepsilon_2\omega_1^2}. \tag{11}$$

The performance of all algorithms degrade rapidly with the synchronization transition (traced by means of the synchronization index ρ [33]). Indeed, direction of interaction cannot be estimated in case of synchronization, when phases $\phi_{1,2}$ are functionally related. The influence of noise is twofold. On one hand, it naturally makes the estimation less precise, especially for very weak coupling [clearly, correct estimation is not possible if the noise term in Eq. (9) is in average larger than the coupling]. On the other hand, noise facilitates estimation of the indices for larger coupling values (correspondent for the synchronized regimes in the noise-free system). Note that the records used for estimation of indices contain only ≈ 100 periods of oscillations; with such short records, the MPA approach works better in the noisy case. Increase of the data length allows for better estimation of directionality from noisy data, the corresponding results are shown in Fig. 4.

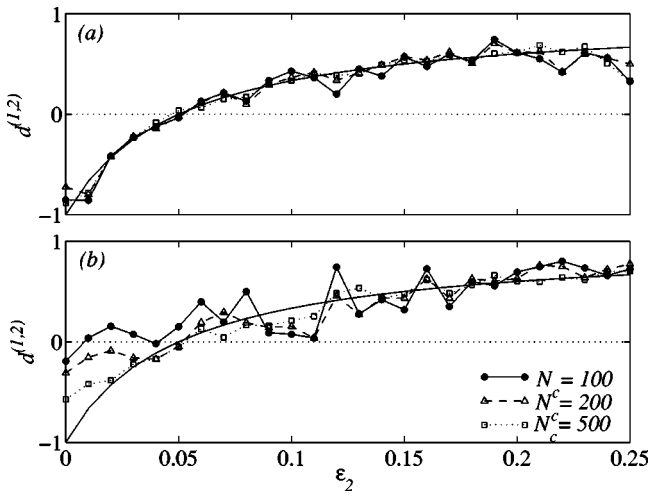

FIG. 4. Effect of data length on the estimation of directionality index d for noise intensity $D=0.1$ (a) and $D=0.2$ (b). The estimates are shown for different numbers of cycles N_c in the data; the solid line shows the dependence $y=(\varepsilon_2-\varepsilon_1)/(\varepsilon_2+\varepsilon_1)$.

Now we discuss the selection of parameters for EMA and MPA, starting with the parameter τ. Clearly, the value of τ should be related to the periods of oscillation $\tau=T_{1,2}$. Indeed, the influence on the own dynamics of an oscillator [note the $b\cos(\phi_{1,2})$ term in Eq. (9)] averages out during each cycle. As the frequencies of two oscillators are differ-

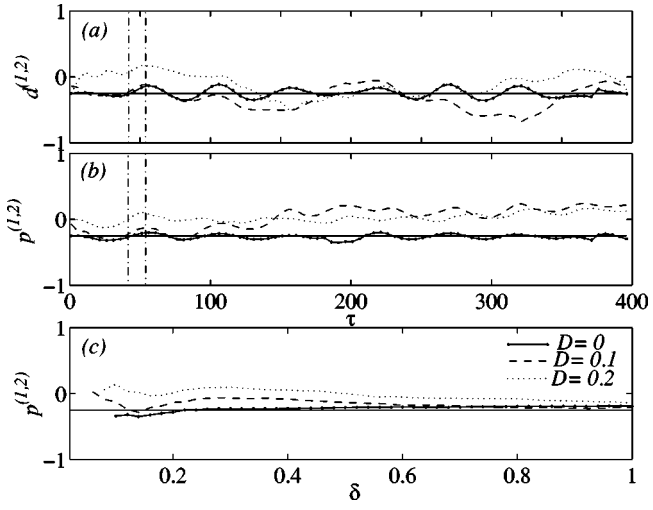

FIG. 5. Dependence of d and p indices on parameters for one coupling configuration ($\varepsilon_1=0.05,\varepsilon_2=0.03$) and different levels of noise. (a) d vs τ, (b) p vs τ for $\delta=0.3$, and (c) p vs δ for $\tau=(T_1+T_2)/2$. The vertical dashed lines in (a),(b) show the values corresponding to mean oscillation periods of both systems.

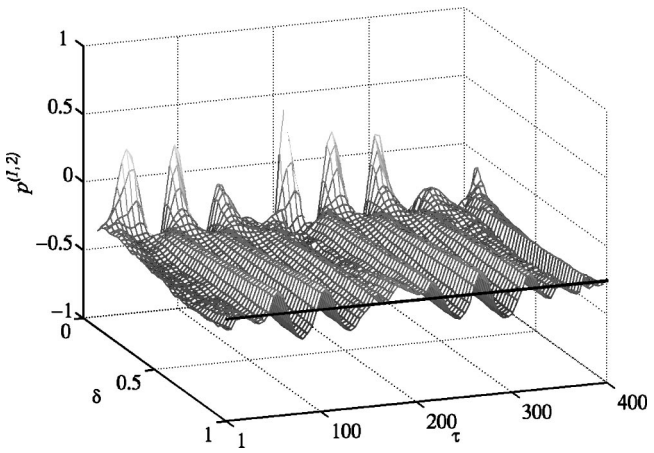

FIG. 6. Dependence of p index on parameters δ and τ for one coupling configuration ($\varepsilon_1=0.05, \varepsilon_2=0.03$) in the absence of noise.

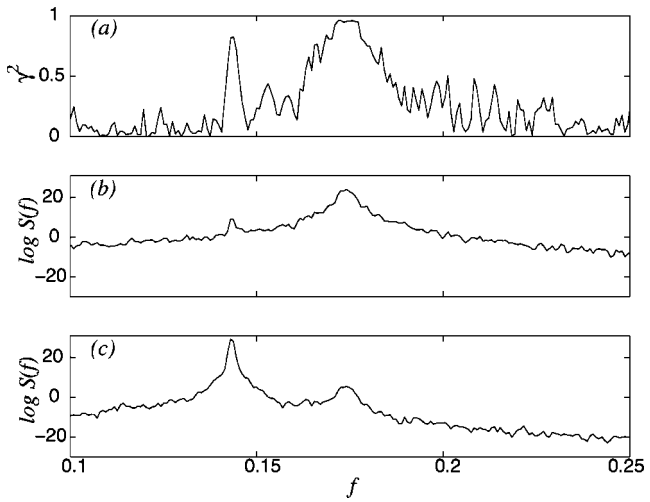

FIG. 7. Coherence function (a) and power spectra (b),(c) for two coupled oscillators. High coherence is seen around the natural frequencies of oscillators $\omega_{1,2}/2\pi$.

ent, we have to find a compromise. Our tests suggest the following choice: $\tau=\min(T_1,T_2)$ and $\tau=(T_1+T_2)/2$ for EMA and MPA, respectively. The computed dependences of d and p indices on τ are shown in Figs. 5(a), 5(b) for different levels of noise. Regarding the parameter δ, we emphasize two counteracting tendencies: δ should be small enough to resolve the influence of coupling and large enough in order to cope with the noise contamination dominating at small scales; the computed dependences are shown in Fig. 5(c) and Fig. 6. Clearly, short records require larger δ. Note that by definition $0<\delta<2$.

We have also tested the algorithms in case when the natural frequencies of coupled oscillators are essentially different, $\omega_1\approx 0.4$, $\omega_2\approx 1.2$, $b=0$. The computations show that the indices follow the theoretical curves (10) and (11) in this case as well. Note, that these curves are now essentially different due to the factor ω_1/ω_2. In conclusion, tests with the data generated by two coupled phase oscillators demonstrate that all indices allow reliable estimate of the asymmetry in coupling from short noisy data.

B. Asymmetric coupling

We discuss now the case of asymmetric coupling. For the sake of definiteness, we consider $f_1=\sin(\phi_2-3\phi_1)$, $f_2=\sin(3\phi_1-\phi_2)$. Clearly, in computation of the coefficient c_2 according to Eq. (4) we obtain, due to derivation, an additional factor of 3. Hence, the indices $d^{(1,2)}$ and $r^{(1,2)}$ follow now the dependences $(3\varepsilon_2-\varepsilon_1)/(\varepsilon_1+3\varepsilon_2)$ and $(3\varepsilon_2\omega_1^2-\varepsilon_1\omega_2^2)/(\varepsilon_1\omega_2^2+3\varepsilon_2\omega_1^2)$, respectively. Important, for this case the results of the MPA differ from the results of EPA: index $p^{(1,2)}$ follows the curve $(\varepsilon_2-\varepsilon_1)/(\varepsilon_1+\varepsilon_2)$. Indeed, the predictability improvement is proportional to the amplitude of the coupling function and does not depend on its period (see caption to Fig. 2). Thus, MPA fails to reveal the asymmetry in coupling functions $f_{1,2}$. We note that the difference in estimates obtained by EMA and MPA may be used to extract information about the coupling function.

The above considerations were tested with the model (9), for which parameter values are $\omega_1\approx 0.4$, $\omega_2\approx 1.2$, $b=0$, $\varepsilon_1=0.01$, and ε_1 varied in the range from 0 to 0.018.

C. A note on more complex cases

In our tests of the techniques we always assumed that we deal with two coupled oscillators. In real-world applications we nevertheless can encounter more complex situations, e.g., when two systems are a part of a complex oscillatory network. Here, we comment on several important cases.

Uncoupled systems. Our algorithms cannot properly treat this situation. Hence, one should check whether both $c_{1,2}$ are close to zero and, if the presence of interaction is not obvious *a priori*, it is recommended to conduct first standard cross correlation (or other) analysis to check whether the two signals are inter-related.

Two coupled oscillators versus two uncoupled oscillators under common forcing. Two noninteracting systems can be driven by a common force. Certainly, in this case estimation of directionality indices is senseless. In order to exclude this case, we can exploit the cross-spectrum analysis, as illustrated by the following example. We simulate the output $x_{1,2}$ of two coupled noisy van der Pol oscillators

$$\ddot{x}_{1,2}-0.2(1-x_{1,2}^2)\dot{x}_{1,2}+\omega_{1,2}^2x_{1,2}+\varepsilon_{1,2}(\dot{x}_{2,1}-\dot{x}_{1,2})+\xi_{1,2}=0,$$

to be compared with the output of two uncoupled systems under common driving

$$\ddot{x}_{1,2}-0.2(1-x_{1,2}^2)\dot{x}_{1,2}+\omega_{1,2}^2x_{1,2}+\varepsilon_{1,2}\dot{x}_3+\xi_{1,2}=0,$$

where

$$\ddot{x}_3-0.2(1-x_3^2)\dot{x}_3+\omega_3^2x_3+\xi_3=0$$

and $\omega_1=0.9$, $\omega_2=1.1$, $\omega_3=1$, $\varepsilon_{1,2}=0.05$, and intensities of noise $\sigma_{1,2}=0.1$, $\sigma_3=0.5$. From the result of the cross-spectrum analysis shown in Figs. 7 and 8 we definitely can

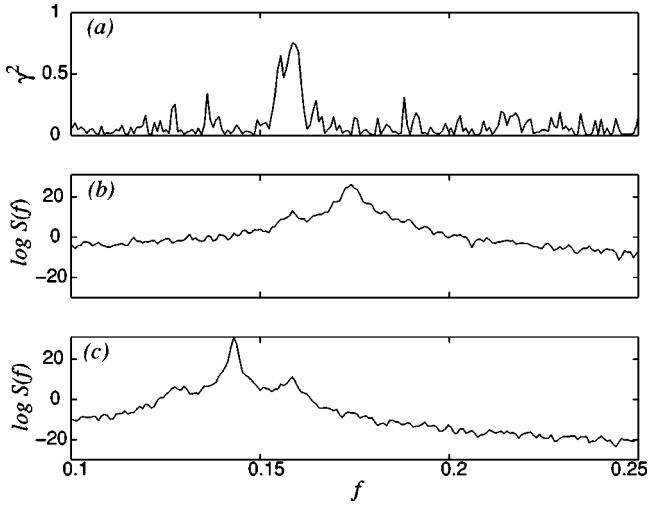

FIG. 8. Coherence function (a) and power spectra (b),(c) for two uncoupled oscillators driven by a common force. High coherence is observed at the frequency of that drive, but there is no coherence at the frequencies of oscillators. (Note that the frequency peak corresponding to the drive is barely seen in power spectra because the drive is very noisy.)

distinguish these two cases.

Three oscillators in a ring. Finally, we perform a frequently used test and consider three noisy van der Pol oscillators with unidirectional coupling, arranged in a ring (Fig. 9):

$$\ddot{x}_i - 0.2(1-x_i^2)\dot{x}_i + \omega_i^2 x_i = \varepsilon \dot{x}_{(i+2)\bmod 3} + \xi_i .$$

Computing a directionality index for, say, oscillators 1 and 2, we expect this index to be between 0 and 1. Indeed, oscillator 2 acts on the oscillator 1 indirectly, via the system 3, and this action should be weaker than direct forcing of 2 by 1. To check this, we take the parameters $\omega_1 = 0.95$, $\omega_2 = 1.05$, $\omega_3 = 1$, $\varepsilon = 0.05$, a noise intensity 0.1, and estimate the d index from ≈ 500 oscillation periods; $\varepsilon = 0.05$, τ is of the order of the period. The results (see also Fig. 9) $d^{(1,2)} = 0.41$, $d^{(1,3)} = -0.7$, and $d^{(2,3)} = 0.57$ correctly reveal the direction of interaction in the ring structure. Next, we take identical systems, $\omega_1 = \omega_2 = \omega_3 = 1$, so that in the absence of noise the systems synchronize. With a sufficiently strong noise (with intensity 0.2), direction of coupling can be nevertheless detected: $d^{(1,2)} = 0.12$, $d^{(1,3)} = -0.19$, and $d^{(1,3)} = 0.27$.

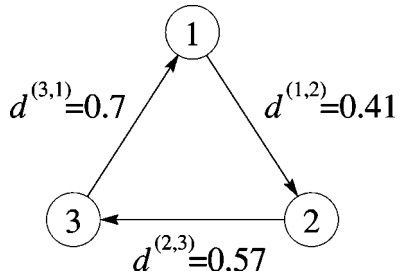

FIG. 9. Three oscillators arranged in a ring. The unidirectional (clockwise) coupling is revealed by pairwise estimation of the directionality index.

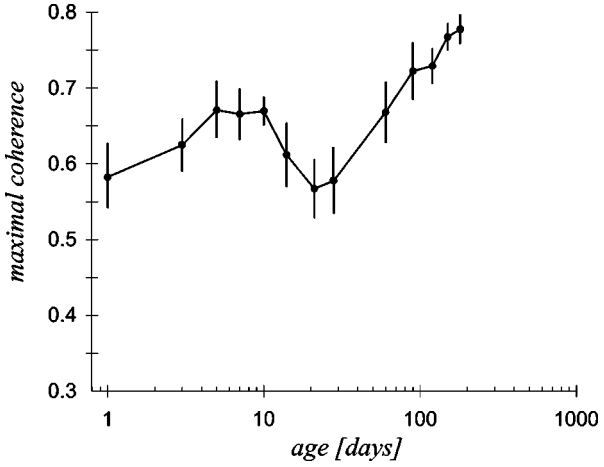

FIG. 10. Cross-spectral analysis demonstrates the presence of interaction between heart rate and respiration. For each of 16 subjects the maximal value of the coherence function was determined; the line and vertical bars show the mean and the standard error, respectively.

IV. DIRECTIONALITY OF CARDIORESPIRATORY INTERACTION IN HEALTHY NEWBORNS

The goal of our experimental study is to clear the controversy concerning the direction of cardiorespiratory interaction. For this purpose we analyze bivariate data, namely, heart rate and respiration obtained from healthy newborns. The presence of interaction is indicated by the presence of respiratory sinus arrhythmia as well as the results of cross-spectral (Fig. 10) and synchronization [17] analysis performed on the same group of subjects. On the other hand, synchronous epochs are rather rare, so that the coupling can be considered weak. Next, we study the dependence of directionality indices on age as well as on heart rate and respiratory frequency.

A. Measurements and data analysis

We measured the electrocardiograms (ECG) using a bipolar limb lead (Biomonitor 501, Meßgerätewerk Zwönitz, Germany) and obtained thoracic respiration with the inductive plethysmographic method (Respitrace, Studley Data Systems, Oxford, UK) in 25 newborn infants; data sets from five newborns are used in the present paper. Measurements were performed on each of the first 5 days of life, then every week and later monthly up to the 6th month of life. Data acquisition began 30–60 min after feeding, in the evening hours between 8 p.m. to 11 p.m., and took approximately 1 h. Data were stored on a digital audio tape (DAT) multichannel recorder (DAT, DTR-1800, biologic, France) for further analysis. The data were off-line digitized with a computer based monitoring system (XmAD, ftp://sunsite.unc.edu/pub/Linux/science/lab/) with a sampling rate of 1000 Hz.

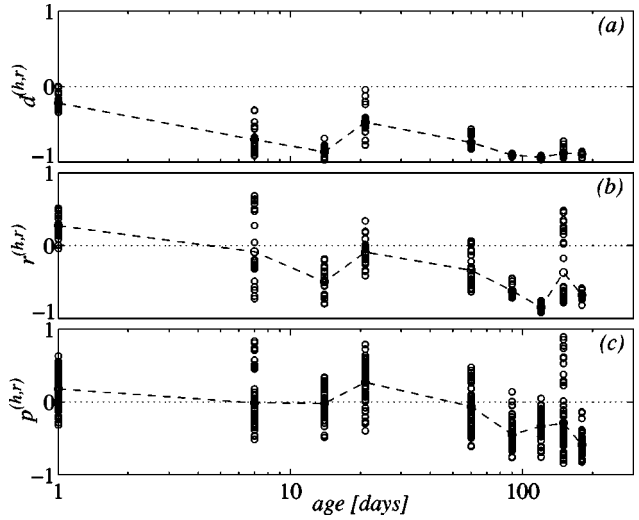

FIG. 11. Three directionality indices as a function of age for one subject. Each symbol shows the estimate of the respective index computed in a running window, the dashed lines connect the mean value for a particular day. Note the smaller variability of the d index.

An artifact free, $\approx$10-min-long segment of each measurement was chosen for the further analysis; these segments correspond to the stage of quiet sleep. R waves were detected with the precision of 1 ms by means of a convolution technique applied to a fifth-order high-pass filtered ECG (20 ms moving average) and a typical QRS template. The instantaneous phase of the cardiac signal has been estimated according to

$$\phi_h(t) = 2\pi k + 2\pi \frac{t - t_k}{t_{k+1} - t_k}, \tag{12}$$

where t_k are the times of appearance of a kth R peak in the ECG. Phase of the respiratory signal has been obtained by means of Hilbert transform applied on the whole segment. Prior to phase derivation, the respiratory signal has been detrended (linear or polynomial, up to fourth order, trend was removed with manual check of all records), and smoothed using a second-order Savitzky-Golay filter of 501 data points length. See Refs. [5,11] for discussion of phase estimation techniques.

In order to trace the variation in the direction of coupling due to nonstationarity in the system, the corresponding indices were computed in a sliding window (with 3/4 overlap) and the average for each day was obtained. We found that all three methods provide consistent results (Fig. 11), supporting our assumption of weak coupling. Next, the stability of EMA and MPA with respect to parameter variation was checked. Comparing EMA and MPA we found that the d index is more stable with respect to parameter(s) variation than the p index; we remind that IPA has no parameters. In order to illustrate the robustness of EMA towards parameter variation, we focus on two distinct data sets from the same subject, corresponding to the first and the last (180th) recording day. An

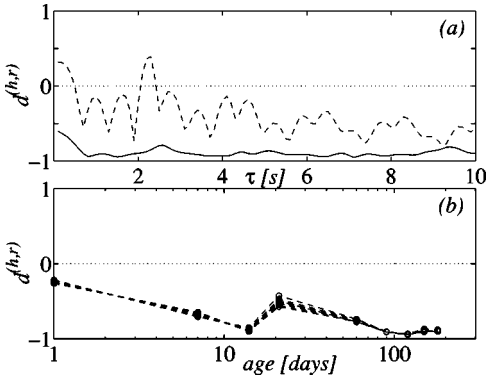

FIG. 12. Robustness of the estimates of the directionality index $d^{(hr)}$ with respect to parameters. (a) $d^{(h,r)}$ vs τ for the first (dash-dotted line) and 180th (solid line) day of life; each estimate was computed from a data segment containing 200 heartbeats. (b) Influence of the window length. Open circles show the average of estimates of $d^{(h,r)}$ computed with different window size (100,200, . . . ,800 heartbeats).

$\approx$100-s-long segment was extracted from each of these two records, then $d^{(hr)}$ was computed for $\tau \leqslant 10$ s [see Fig. 12(a)]; the average interbeat interval was, respectively, $\langle T_h \rangle = 0.46$ s and $\langle T_h \rangle = 0.54$ s. A good stability of directionality index estimates with respect to the window size is reflected in Fig. 12(b). Further, data sets for five babies have been analyzed, with the window length corresponding to 200 heartbeats and τ taken as the average cardiac cycle within a window.

B. Results and discussion

Below we present only the results of the EMA approach (d index). This choice is motivated by our interest in the

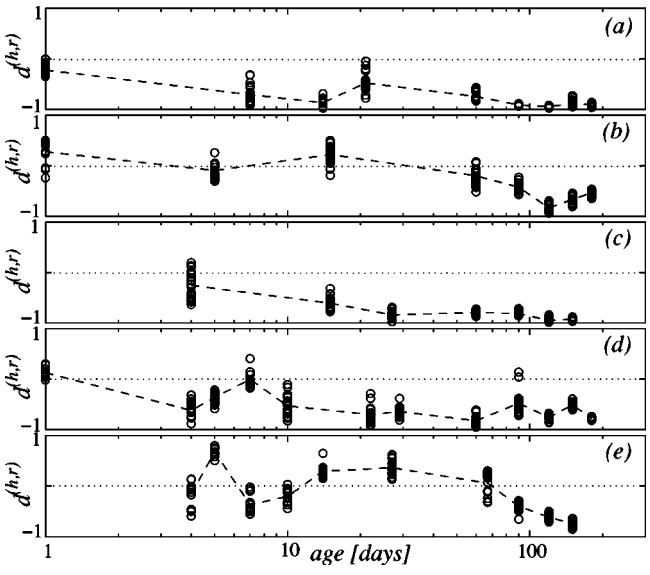

FIG. 13. Directionality index $d^{(hr)}$ versus age (log scale) for five newborns. Symbols show the values obtained from different windows; dashed lines show the average (for a certain day) values. All subjects demonstrate tendency towards unidirectional coupling (respiration drives heartbeat) with maturation.

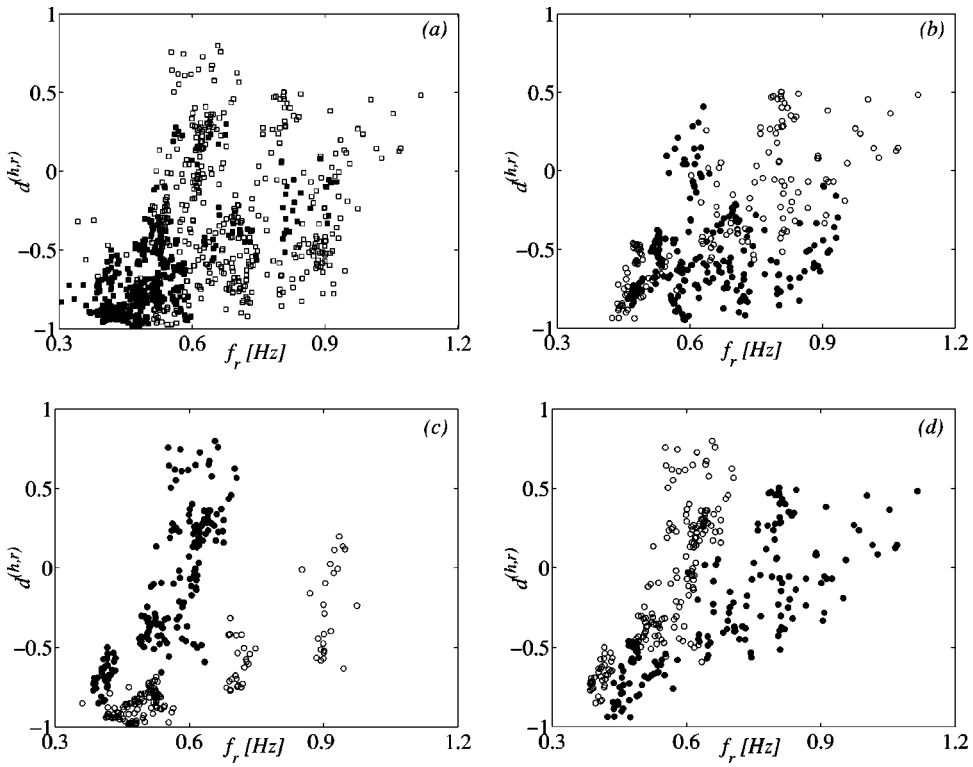

FIG. 14. Scatter plots of the $d^{(hr)}$ index versus breathing frequency (f_r) have a characteristic ν shape. (a) All five subjects together. Opened and filled squares denote the estimates during the first month and 2–6 months, respectively. (b), (c), and (d) show the results for two subjects (denoted by different symbols). One can see that the points from some subjects fall only onto one branch of the ν curve (c), while the estimates from other subjects fall onto both branches (b). In one subject the first days fall onto one, others fall onto the second stripe (d).

dependence of the directionality on both respiratory frequency and heart rate. We remind also that d index does not directly include oscillator frequencies [cf. Eqs. (10),(11)] what results in a smaller variability of its estimates (cf. Fig. 11).

The main results are summarized in Fig. 13 clearly indicating the evolution from an approximately symmetric interaction during the first days of life to a dominant unidirectional coupling (respiration drives the heart rate) at the age of 6 months. Next, we analyzed the dependence of the directionality index $d^{(h,r)}$ on the frequency of respiration f_r and on heart rate f_h. No dependence between $d^{(h,r)}$ and f_h was seen, whereas the plot of $d^{(h,r)}$ vs f_r displays a characteristic ν shape [Fig. 14(a)]. It can be seen that, for all measurements with $f_r<0.5$ Hz the interaction occurs dominantly in one direction, from respiration to heart rate. We suggest the following explanation. The cardiac influence on respiration is weak and frequency independent, while the coupling from the respiration to heart rate is similar to a low-pass filter. Then, for low frequencies ($f_r<\approx 0.5$ Hz in our case) the respiratory driving effect is relatively strong compared with the strength of the cardiac influence; correspondingly, the directionality index is close to -1. For higher frequencies, the signal from the respiratory center [35] is attenuated and therefore the interaction appears as nearly symmetrical. This explanation is supported by the fact that variability of d index estimates is larger for higher frequencies (influence of noise on the estimate of an index is stronger for weak coupling, see discussion in the Sec. III).

The basis of the low-pass behavior of the information transmission channel can be found in the physiological mechanisms of the coupling. Indeed, signals from the vagal nerve to the sinus node are transmitted by means of the neurotransmitter acetylcholine. The release and the enzymatic degradation of the acetylcholine is frequency limited [37]. Note also, that respiratory sinus arrhythmia is a frequency-dependent phenomenon as well [14].

The presence of two branches in the ν-shaped plot of d index vs f_r indicates two possible modes of interaction, characterized by different characteristics of the low-pass filter (see Fig. 14). At very young ages (first week of life), the value of the cutoff frequency appears to be lower. Maturation of the functions of the central nervous system as well as cardiovascular adaptation processes to extrauterine conditions such as closure of fetal shunts may account for this finding. Correlation to hemodynamic data could give further insight into this hypothesis. Another possible explanation of the existence of two modes of interaction may be related to different substages of quiet sleep [38].

In summary, our results support the ''irradiation theory'' in the sense that there is a clear effect of respiration on heart rate. However, at physiological conditions, characterized by high breathing rates, this unidirectional action is abolished. The reason for this abolishment is explained by the well-known neurotransmitter kinetics of acetylcholine at the vagal-atrial junction. To reveal mechanisms responsible for the ν shape of the dependence of the directional index on breathing frequency further investigations are necessary.

V. CONCLUSIONS

We have proposed and analyzed approaches for identification of direction of weak coupling between two self-sustained oscillators. We have compared the efficiency of three algorithms and have shown that they can be used for analysis of real-world data. One algorithm EMA requires

only one parameter, is generally more stable towards its variation and easier to use than the algorithm based on the idea of mutual predictability. The essential advantage of the proposed method IPA is that it has no parameters. More important, all methods work with rather short and noisy records, that makes them suitable for applications to biological, geophysical, astrophysical, and other real-world signals.

Application of the considered methods to a particular problem, analysis of cardiorespiratory coupling, revealed that this interaction is age dependent: it evolves from approximately symmetric coupling during the first days of life to unidirectional after 6 months of age. Moreover, the dependence of the directionality index on the respiratory frequency indicates the possible existence of two regimes of interaction.

ACKNOWLEDGMENTS

We are indebted to A. Pikovsky for constant help and valuable comments and to P. Ivanov and F. Starmer for a careful reading of the manuscript and useful remarks. We gratefully acknowledge discussions with R. Friedrich, J. Kurths, U. Parlitz, G. Osipov, T. Schreiber, P. Tass, and M. Zaks. M.R. was supported by EU Network COSYS of SENS.

[1] H.D.I. Abarbanel, *Analysis of Observed Chaotic Data* (Springer-Verlag, New York, 1996); H. Kantz and T. Schreiber, *Nonlinear Time Series Analysis* (Cambridge University Press, Cambridge, U.K., 1997).

[2] N.F. Rulkov, M.M. Sushchik, L.S. Tsimring, and H.D.I. Abarbanel, Phys. Rev. E **51**, 980 (1995); L. Kocarev and U. Parlitz, Phys. Rev. Lett. **76**, 1816 (1996).

[3] M.G. Rosenblum, A.S. Pikovsky, and J. Kurths, Phys. Rev. Lett. **76**, 1804 (1996).

[4] A.S. Pikovsky, M.G. Rosenblum, G.V. Osipov, and J. Kurths, Physica D **104**, 219 (1997); A. Pikovsky, M. Rosenblum, and J. Kurths, Int. J. Bifurcation Chaos Appl. Sci. Eng. **10**, 2291 (2000).

[5] A. Pikovsky, M. Rosenblum, and J. Kurths, *Synchronization, A Universal Concept in Nonlinear Sciences* (Cambridge University Press, Cambridge, 2001).

[6] S.J. Schiff, P. So, T. Chang, R.E. Burke, and T. Sauer, Phys. Rev. E **54**, 6708 (1996); M. Le van Quyen, C. Adam, M. Baulac, J. Martinerie, and F. Varela, Brain Res. **792**, 24 (1998); J. Arnhold, P. Grassberger, K. Lehnertz, and C. Elger, Physica D **134**, 419 (1999); R. Quian Quiroga, J. Arnhold, and P. Grassberger, Phys. Rev. E **61**, 5142 (2000); A. Schmitz, *ibid.* **62**, 7508 (2000); F. Drepper, *ibid.* **62**, 6376 (2000).

[7] M. Rosenblum, A. Pikovsky, and J. Kurths, IEEE Trans. Circuits Syst., I: Fundam. Theory Appl. **44**, 874 (1997).

[8] C. Schäfer, M.G. Rosenblum, J. Kurths, and H.-H. Abel, Nature (London) **392**, 239 (1998).

[9] P. Tass, M. Rosenblum, J. Weule, J. Kurths, A. Pikovsky, J. Volkmann, A. Schnitzler, and H.-J. Freund, Phys. Rev. Lett. **81**, 3291 (1998).

[10] C. Schäfer, M. Rosenblum, H.-H. Abel, and J. Kurths, Phys. Rev. E **60**, 857 (1999).

[11] M.G. Rosenblum, A.S. Pikovsky, J. Kurths, C. Schäfer, and P. A. Tass, in *Neuro-informatics*, edited by F. Moss and S. Gielen, Handbook of Biological Physics, Vol. 4 (Elsevier, New York, 2001), pp. 279–321.

[12] Y. Kuramoto, *Chemical Oscillations, Waves, and Turbulence* (Springer, Berlin, 1984).

[13] M.G. Rosenblum and A.S. Pikovsky, Phys. Rev. E **64**, 045202 (2001).

[14] A. Angelone and N. Coulter, J. Appl. Physiol. **19**, 479 (1964).

[15] H. Pessenhofer and T. Kenner, Pfluegers Arch. **355**, 77 (1975); T. Kenner, H. Pessenhofer, and G. Schwaberger, *ibid.* **363**, 263 (1976); K.H. Stutte and G. Hildebrandt, *ibid.* **289**, R47 (1966); F. Raschke, in *Temporal Disorder in Human Oscillatory Systems*, edited by L. Rensing, U. an der Heiden, and M. Mackey, Springer Series in Synergetics Vol. 36 (Springer-Verlag, Berlin, 1987), pp. 152–158; F. Raschke, in *Rhythms in Physiological Systems*, edited by H. Haken and H.P. Koepchen, Springer Series in Synergetics Vol. 55 (Springer-Verlag, Berlin, 1991), pp. 155–164; D. Hoyer, O. Hader, and U. Zwiener, IEEE Eng. Med. Biol. Mag. **16**, 97 (1997); M. Schiek, F.R. Drepper, R. Engbert, H.-H. Abel, and K. Suder, in *Nonlinear Analysis of Physiological Data*, edited by H. Kantz, J. Kurths, and G. Mayer-Kress (Springer, Berlin, 1998), pp. 191–209; H. Seidel and H.-P. Herzel, IEEE Eng. Med. Biol. Mag. **17**, 54 (1998).

[16] M. Bračič and A. Stefanovska, Physica A **283**, 451 (2000).

[17] R. Mrowka, A. Patzak, and M.G. Rosenblum, Int. J. Bifurcation Chaos Appl. Sci. Eng. **10**, 2479 (2000).

[18] H.P. Koepchen, *Die Blutdruckrhythmik* (Dr. Dietrich Steinkopff Verlag, Darmstadt, 1962).

[19] R.K. Otnes and L. Enochson, *Digital Time Series Analysis* (Wiley, New York, 1972).

[20] B. Pompe, J. Stat. Phys. **73**, 587 (1993).

[21] H. Voss and J. Kurths, Phys. Lett. A **234**, 336 (1997).

[22] T. Schreiber, Phys. Rev. Lett. **85**, 461 (2000); M. Paluŝ, V. Komárek, Z. Hrnčiř, and K. Štěrbová, Phys. Rev. E **63**, 046211 (2001).

[23] A.S. Pikovsky, Sov. J. Commun. Technol. Electron. **31**, 81 (1986).

[24] R. Friedrich, S. Siegert, J. Peinke, S. Lück, M. Siefert, M. Lindemann, J. Raethjen, G. Deuschl, and G. Pfister, Phys. Lett. A **271**, 217 (2000).

[25] Practically, for discrete data, this can be done in the following way. For any t_k we find t_j such that $\phi(t_j) \leqslant \phi(t_k) + 2\pi$ and $\phi(t_{j+1}) > \phi(t_k) + 2\pi$. Then t' correspondent to $\phi = \phi(t_k) + 2\pi$ is obtained via interpolation between t_j and t_{j+1}. If the sampling rate is high, simple linear interpolation suffices, otherwise spline interpolation (using several points around t_j) is recommended; this procedure also reduces the effect of noise.

[26] C. Granger, Econometrica **37**, 424 (1969).

[27] M. Wiesenfeldt, U. Parlitz, and W. Lauterborn, Int. J. Bifurcation Chaos Appl. Sci. Eng. **11**, 2217 (2001).

[28] U. Feldmann and J. Bhattacharya (unpublished); B. Schack and M. Arnold (private communication).

[29] We emphasize that the phases are considered unwrapped when

we compute the phase increase Δ, and wrapped when we search for close neighbors. Considering the averaging, we note that for short records the number of mutual neighbors is small, and the statistics is therefore poor, and the predictability improvement is reduced. To compensate this, we used only *m* out of *l* points in averaging involved in computation of the univariate prediction error.

[30] Indeed, for the simplest case of sine coupling function, $f_{1,2}=\sin(\phi_{2,1}-\phi_{1,2})$, in the synchronous regime the constant phase difference is $\phi_2-\phi_1=\arcsin(\omega_2-\omega_1)/(\varepsilon_2+\varepsilon_1)$, and we cannot extract information on $\varepsilon_{1,2}$ separately.

[31] K.K. Likharev, *Dynamics of Josephson Junctions and Circuits* (Gordon and Breach, Philadelphia, 1991).

[32] V.S. Afraimovich, V.I. Nekorkin, G.V. Osipov, and V.D. Shalfeev, *Stability, Structures, and Chaos in Nonlinear Synchronization Networks* (World Scientific, Singapore, 1994).

[33] We use the index $\rho^2=\langle\cos[\phi_1(t)-\phi_2(t)]\rangle^2+\langle\sin[\phi_1(t)-\phi_2(t)]\rangle^2$, where $\langle\rangle$ denote time average, see Refs. [11,34].

[34] E. Rodriguez, N. George, J.-P. Lachaux, J. Martinerie, B. Renault, and F.J. Varela, Nature (London) **397**, 430 (1999).

[35] Current models of respiration imply that the respiratory rhythm is generated in the brain stem, in a network, which includes also neurons modulating heart rate [36].

[36] D.W. Richter and K.M. Spyer, in *Central Regulation of Autonomic Functions*, edited by A.D. Loewy and K.M. Spyer (Oxford University Press, New York, 1990), pp. 189–207.

[37] W. Osterrieder, Q.F. Yang, and W. Trautwein, Pfluegers Arch. **389**, 283 (1981); M.R. Boyett and A. Roberts, J. Physiol. (London) **393**, 171 (1987); M.H. Chen, R.D. Berger, J.P. Saul, K. Stevenson, and R.J. Cohen, Comput. Cardiol. **13**, 149 (1987); F. Dexter, Y. Rudy, and G.M. Saidel, Am. J. Physiol. **266**, H298 (1994).

[38] Quiet sleep in young infants is usually not further classified into substages in clinical practice.